ornl

**OAK
RIDGE
NATIONAL
LABORATORY**

UNION
CARBIDE

Heavy-Section Steel Technology Program Quarterly Progress Report for April–June 1979

G. D. Whitman
R. H. Bryan

1439 217

7911300631

**OPERATED BY
UNION CARBIDE CORPORATION
FOR THE UNITED STATES
DEPARTMENT OF ENERGY**

1439 218

Contract No. W-7405-eng-26

Engineering Technology Division

HEAVY-SECTION STEEL TECHNOLOGY PROGRAM QUARTERLY PROGRESS REPORT FOR APRIL—JUNE 1979

G. D. Whitman   R. H. Bryan

Manuscript Completed — September 26, 1979
Date Published — October 1979

1439 219

CONTENTS

1439 221

PREFACE

The Heavy-Section Steel Technology (HSST) Program, which is sponsored by the Nuclear Regulatory Commission (NRC), is an engineering research activity devoted to extending and developing the technology for assessing the margin of safety against fracture of the thick-walled steel pressure vessels used in light-water-cooled nuclear power reactors. The program is being carried out in close cooperation with the nuclear power industry. This report covers HSST work performed in April through June 1979, except for subcontractor contributions which may cover the three-month period ending in May. The work performed by Oak Ridge National Laboratory (ORNL) and by subcontractors is managed by the Engineering Technology Division. Major tasks at ORNL are carried out by the Engineering Technology Division and the Metals and Ceramics Division. Prior progress reports on this program are ORNL-4176, ORNL-4315, ORNL-4377, ORNL-4463, ORNL-4512, ORNL-4590, ORNL-4653, ORNL-4681, ORNL-4764, ORNL-4816, ORNL-4855, ORNL-4918, ORNL-4971, ORNL/TM-4655 (Vol. II), ORNL/TM-4729 (Vol. II), ORNL/TM-4805 (Vol. II), ORNL/TM-4914 (Vol. II), ORNL/TM-5021 (Vol. II), ORNL/TM-5170, ORNL/NUREG/TM-3, ORNL/NUREG/TM-28, ORNL/NUREG/TM-49, ORNL/NUREG/TM-64, ORNL/NUREG/TM-94, ORNL/NUREG/TM-120, ORNL/NUREG/TM-147, ORNL/NUREG/TM-166, ORNL/NUREG/TM-194, ORNL/NUREG/TM-209, ORNL/NUREG/TM-239, NUREG/CR-0476 (ORNL/NUREG/TM-275), NUREG/CR-0656 (ORNL/NUREG/TM-298), and NUREG/CR-0818 (ORNL/NUREG/TM-324).

1439 222

SUMMARY*

1. PROGRAM ADMINISTRATION AND PROCUREMENT

The Heavy-Section Steel Technology (HSST) Program is an engineering research activity conducted by the Oak Ridge National Laboratory (ORNL) for the Nuclear Regulatory Commission (NRC) in coordination with other research sponsored by the federal government and private organizations. The program comprises studies relating to all areas of the technology of the materials fabricated into thick-section primary-coolant containment systems of light-water-cooled nuclear power reactors. The principal area of investigation is the behavior and structural integrity of steel pressure vessels containing cracklike flaws. Current work is organized into the following tasks: (1) program administration and procurement, (2) fracture mechanics analyses and investigations, (3) effect of high-temperature primary reactor water on the subcritical crack growth of reactor vessel steels, (4) investigations of irradiated materials, (5) pressure vessel investigations, and (6) thermal shock investigations.

The work performed under the existing research and development subcontracts is included in this report.

Thirteen program briefings, reviews, or presentations were made during the quarter.

2. FRACTURE MECHANICS ANALYSES AND INVESTIGATIONS

Work on the mesh generation feature of the finite-element computer program (NOZ-FLAW) for analyzing nozzle-corner flaws was essentially completed. Stress-intensity factor (K_I) distributions were calculated for four geometries for which measurements were previously made photoelastically. The K_I distributions were also calculated by the BIGIF computer program, which gave results in reasonable agreement with

---

*Conversions from SI to English units for all SI quantities are listed on a foldout page at the end of this report.

NOZ-FLAW. However, there are some discrepancies between results of calculations and experiments.

3. EFFECT OF HIGH-TEMPERATURE PRIMARY REACTOR WATER ON THE SUBCRITICAL CRACK GROWTH OF REACTOR VESSEL STEELS

Fatigue testing of four specimens was completed. Weld metal specimens tested at a low R ratio with a saw-tooth wave form gave nearly identical results to those tested with sinusoidal loading. The heat-affected-zone (HAZ) specimen also gave similar results.

The last test in the ramp- and hold-time study was completed. It was generally shown that the hold time does not affect crack growth rate in the pressurized-water reactor (PWR) environment. As previously reported, decreasing the ramp rate enhances the crack growth rate. The results of this study have been summarized in Chap. 3.

4. INVESTIGATIONS OF IRRADIATED MATERIALS

Final design of the capsules for the fourth irradiation series was completed, and preparation of the facility and specimens is in progress.

The a/W-sidegroove test matrix initiated in the previous quarter and utilizing 1T compact specimens was completed and analyzed. Analyses included that agreed upon by the HSST contractors in September 1978 and several others pursued in an attempt to improve the analysis procedures.

5. PRESSURE VESSEL INVESTIGATIONS

Preliminary studies of the feasibility of further fracture tests in thick-section vessels were initiated. Two concepts of interest are (1) a critical evaluation of the capability of elastic-plastic fracture mechanics to characterize upper-shelf behavior and (2) an experimental investigation of crack growth in a structure under cyclic thermal and pressure loadings.

6. THERMAL SHOCK INVESTIGATIONS

Preliminary three-dimensional finite-element linear elastic fracture mechanics analysis results were obtained for the flaws associated with test TSE-2. As before, the results of less precise methods of analysis indicate that warm prestressing may have been involved; but there is still too much uncertainty to be reasonably sure.

Two thermal-hydraulic experiments were conducted with test cylinder TSC-1 in the liquid nitrogen thermal shock test facility, and the results indicate that satisfactory quench rates and symmetry in quenching can be obtained for test TSE-5. Subsequently, final preparations for TSE-5 were commenced.

Development of the electron-beam (EB)-weld flawing technique was completed, a full-length EB-weld flaw was generated successfully in the TSC-1 prolongation, and final preparations were made for generating the flaw in TSC-1.

The fracture toughness vs tempering temperature study for TSC-1 material was completed, and a tempering temperature of 613°C was selected for TSC-1. Both TSC-1 and its prolongation were tempered at this temperature prior to generation of the EB-weld flaws.

1439 225

HEAVY-SECTION STEEL TECHNOLOGY PROGRAM QUARTERLY
PROGRESS REPORT FOR APRIL—JUNE 1979

G. D. Whitman   R. H. Bryan

ABSTRACT

The Heavy-Section Steel Technology (HSST) Program is an
engineering research activity conducted by the Oak Ridge Na-
tional Laboratory (ORNL) for the Nuclear Regulatory Commission
(NRC). The program comprises studies related to all areas of
the technology of the materials fabricated into thick-section
primary-coolant containment systems of light-water-cooled nu-
clear power reactors. The principal area of investigation is
the behavior and structural integrity of steel pressure ves-
sels containing cracklike flaws. Current work is organized
into six tasks: (1) program administration and procurement,
(2) fracture mechanics analyses and investigations, (3) effect
of high-temperature primary reactor water on the subcritical
crack growth of reactor vessel steels, (4) investigations of
irradiated materials, (5) pressure vessel investigations, and
(6) thermal shock investigations.
    A user-oriented finite-element computer program for
calculating mixed-mode stress-intensity factors for nozzle-
corner flaws of arbitrary shape is being developed. Ramp-and-
hold fatigue tests have been completed. Procedures for un-
loading compliance J tests of irradiated fracture specimens
were prepared. Studies of additional intermediate-vessel test
concepts were initiated. Preparations were continued for the
first thermal shock test in the liquid nitrogen facility.

---

1. PROGRAM ADMINISTRATION AND PROCUREMENT

G. D. Whitman

The Heavy-Section Steel Technology (HSST) Program, a major safety

program sponsored by the Nuclear Regulatory Commission (NRC), is con-

cerned with the structural integrity of the primary systems (particularly

the reactor pressure vessels) of light-water-cooled nuclear power reactor

stations. The structural integrity of these vessels is ensured by de-

signing and fabricating them according to the standards set by the code

for nuclear pressure vessels, by detecting flaws of significant size that

occur during fabrication and in service, and by developing methods ca-

pable of producing quantitative estimates of conditions under which frac-

tures could occur. The program is concerned mainly with developing

pertinent fracture technology, including knowledge of the material used in these thick-walled vessels, the flaw growth rate, and the combination of flaw size and load that would cause fracture and thus limit the life and/or operating conditions for this type of reactor plant.

The program is coordinated with other government agencies and the manufacturing and utility sectors of the nuclear power industry in the United States and abroad. The overall objective is a quantification of safety assessments for regulatory agencies, professional code-writing bodies, and the nuclear power industry. Several of the activities are conducted under subcontracts by research facilities in the United States and through informal cooperative efforts on an international basis. Four research and development subcontracts are currently in force.

Administratively, the program is organized into six tasks, as reflected in this report: (1) program administration and procurement, (2) fracture mechanics analyses and investigations, (3) effect of high-temperature primary water on the subcritical crack growth of reactor vessel steels, (4) investigations of irradiated material, (5) pressure vessel investigations, and (6) thermal shock investigations.

During this quarter, 13 program briefings, reviews, or presentations were made by the HSST staff at technical meetings and at program reviews for the NRC staff or visitors.

1439 227

2. FRACTURE MECHANICS ANALYSES AND INVESTIGATIONS — A COMPUTER PROGRAM FOR DIRECT EVALUATION OF K FACTORS FOR ARBITRARILY SHAPED FLAWS AT PRESSURE-VESSEL NOZZLE CORNERS*[†]

Satya N. Atluri[‡] K. Kathiresan[‡] J. W. Bryson

Work on the mesh generation feature of the finite-element computer program NOZ-FLAW was essentially completed during the current reporting period. Final examination and debugging of all of the various options available in the mesh generator are currently under way.

Stress-intensity factor distributions were calculated for four nozzle-corner flaws in a pressurized boiling-water reactor (BWR) vessel employing the fully automatic mesh generation mode. These same flaws were investigated by C. W. Smith et al.[1] using the frozen-stress photo-elastic technique. Figure 2.1 shows the four flaw geometries considered. In addition, K_I distributions were calculated at Oak Ridge National Laboratory (ORNL) for the four flaw shapes using the BIGIF[2] (Boundary Integral Generated Influence Functions) computer program. This program was developed by Failure Analysis Associates under Electric Power Research Institute (EPRI) sponsorship and is based on an influence function approach that requires a prior stress analysis of the uncracked structure. The stress analysis was obtained at ORNL from the finite-element computer program CORTES-EP.[3] Figure 2.2 shows the junction region of the mesh generated by CORTES-EP.

Comparisons of calculated results from NOZ-FLAW with both photo-elastic and BIGIF results are shown in Figs. 2.3 through 2.6. A Poisson's ratio of 0.45 was used in NOZ-FLAW, whereas the photoelastic results are for $\nu = 0.5$. In BIGIF, the four flaw shapes were idealized as quarter-circular flaws having a radius equal to the depth of the flaw at

---

*Conversions from SI to English units for all SI quantities are listed on a foldout page at the end of this report.

[†]Work sponsored by HSST program under UCCND Subcontract 7565 between Union Carbide Corporation Nuclear Division and Georgia Institute of Technology.

[‡]School of Engineering Science and Mechanics, Georgia Institute of Technology, Atlanta, Ga. 30332.

ORNL-DWG 79-8580R

VESSEL WALL

——— ACTUAL CRACK SHAPE
– – – FITTED QUARTER ELLIPSE

III-A
$(a/T = 0.81)$

II-B
(0.53)

IV-B
(0.23)

I-AV
(0.14)
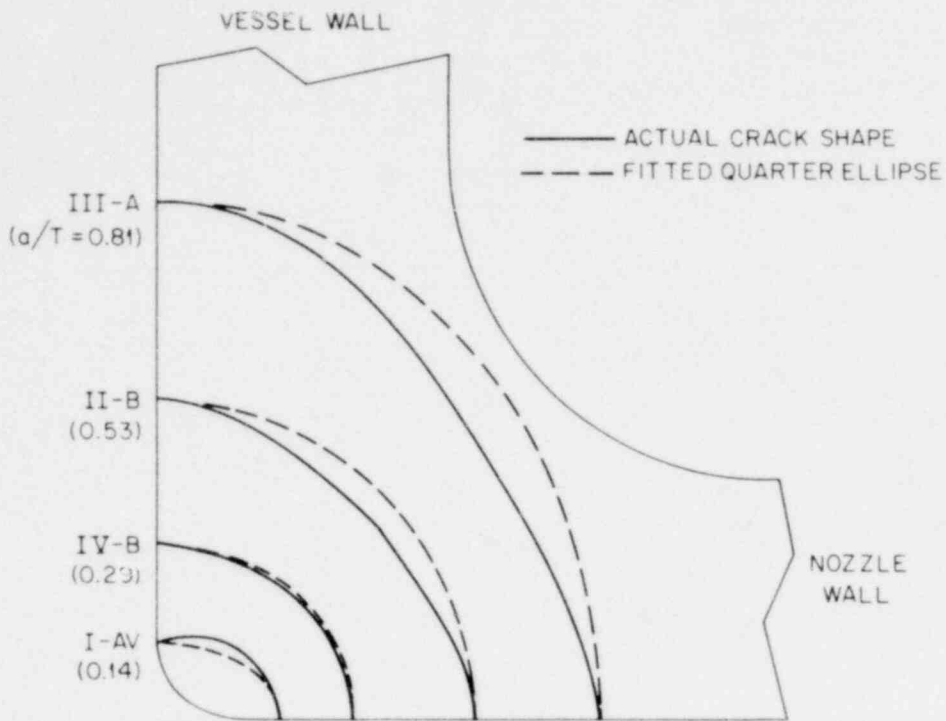
NOZZLE
WALL

Fig. 2.1. Nozzle-corner flaws investigated photoelastically by Smith et al. (Ref. 1).

ORNL-DWG 79-13898

ISOMETRIC VIEW

CROSS-SECTIONAL VIEW
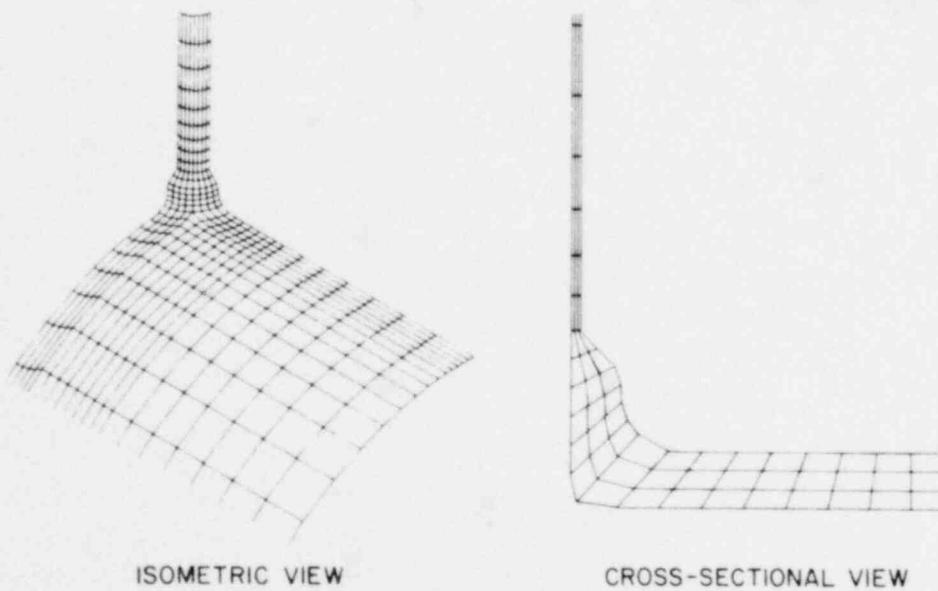
Fig. 2.2. Finite-element mesh generated by CORTES-EP for nozzle-vessel junction region of a BWR vessel.

5
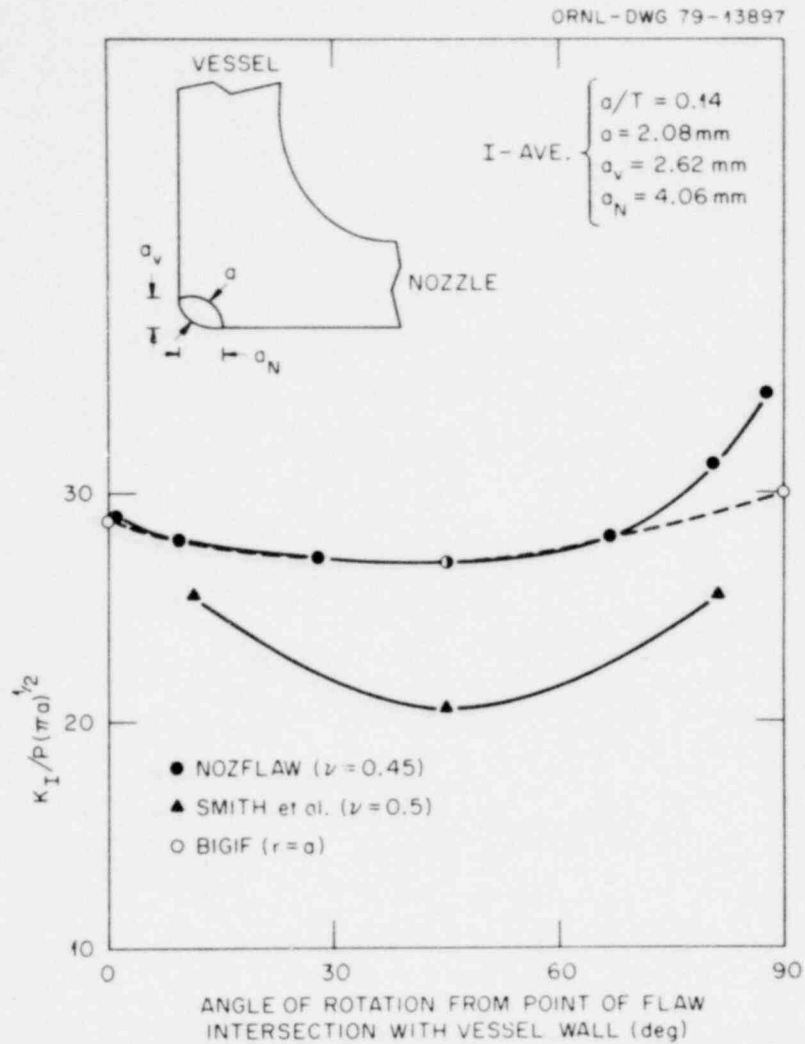
Fig. 2.3. Variation of normalized K_I along flaw front for a pressurized BWR model (a/T = 0.14).
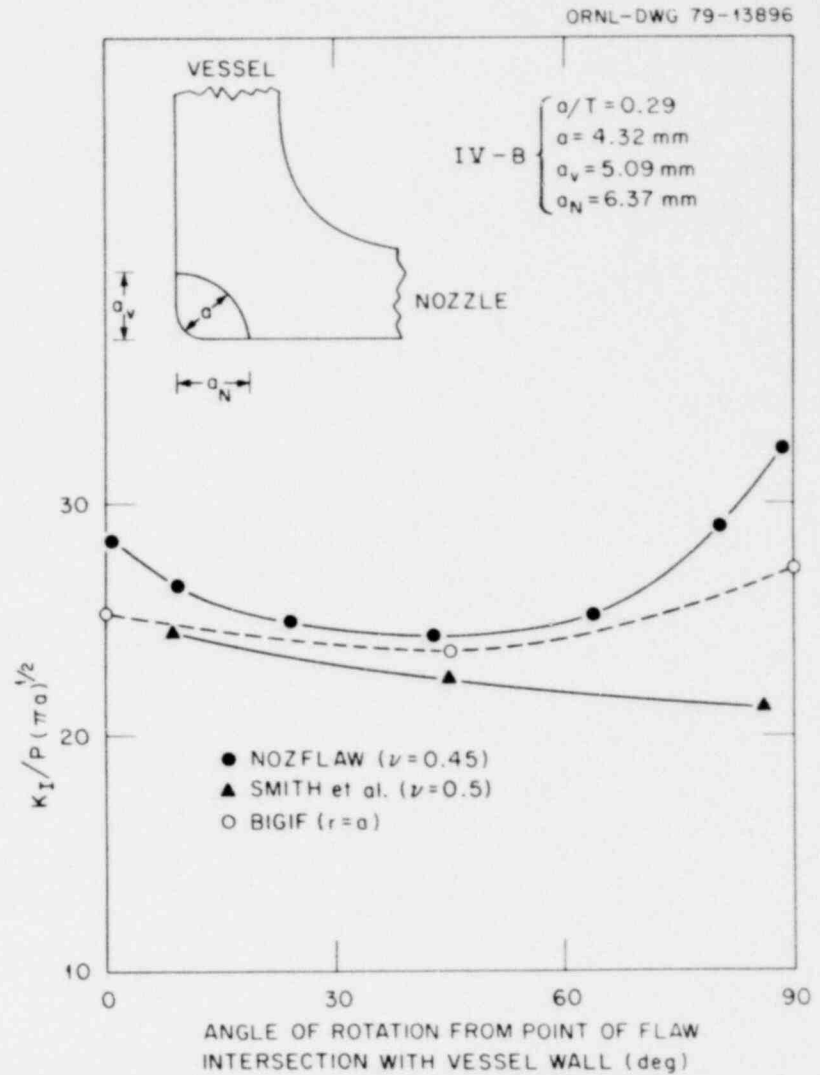
Fig. 2.4. Variation of normalized K_I along flaw front for a pressurized BWR model (a/T = 0.29).

6
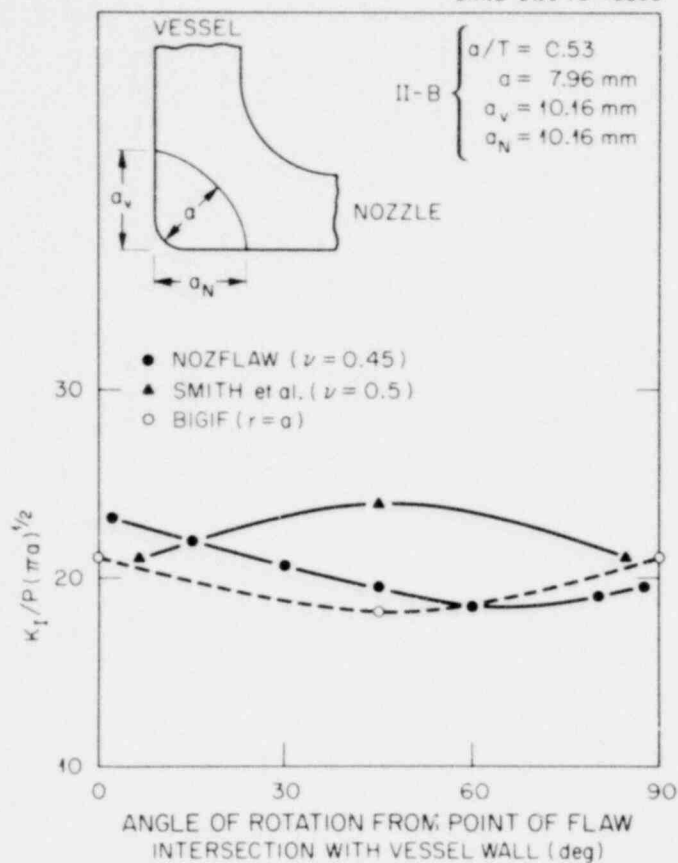
Fig. 2.5. Variation of normalized K_I along flaw front for a pressurized BWR model (a/T = 0.53).
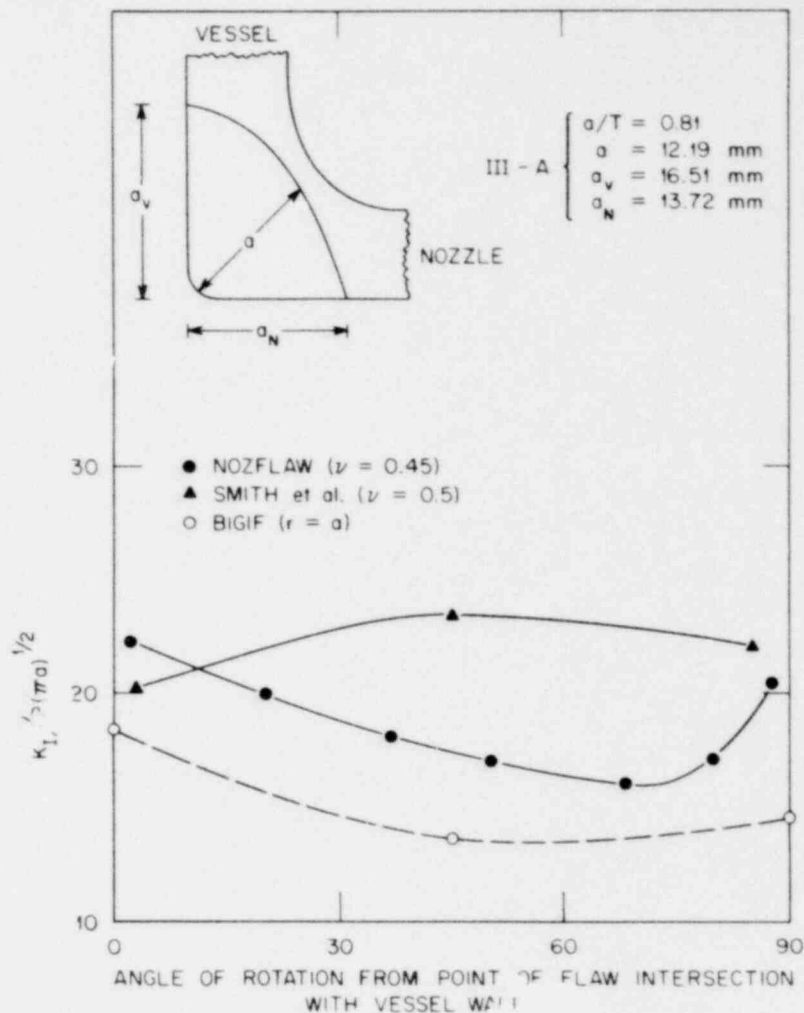
Fig. 2.6. Variation of normalized K_I along flaw front for a pressurized BWR model (a/T = 0.81).

45° from the point of flaw intersection with the vessel wall (r = a). Also, the influence functions employed in BIGIF are derived for solid infinite bodies and do not fully consider the effects of certain finite nozzle dimensions (i.e., the back-free-surface effect and out-of-plane nozzle curvature). Recent studies, however, indicate that the BIGIF idealized nozzle-corner flaw model will give accurate results for a/T ≤ 0.5 for nozzle dimensions typical of a BWR feedwater nozzle.[2]

NOZ-FLAW and BIGIF give reasonably good agreement for three of the four nozzle corner flaws. As might be expected from the above discussion, less satisfactory agreement was obtained between the two for the deep flaw (Fig. 2.6) where a/T = 0.81 > 0.5. Comparisons between NOZ-FLAW and the photoelastic results (Smith et al.[1]) indicate opposite trends for the K_I distribution for moderately deep (a/T = 0.53, Fig. 2.5) to deep (a/T = 0.81, Fig. 2.6) nozzle-corner flaws. NOZ-FLAW calculates a K_I distribution along the flaw front having an increasing slope with respect to the angle of rotation measured from the point of flaw intersection with vessel wall, but the photoelastic results display the opposite trend for these two flaws. Attempts are presently being made to understand and explain the above discrepancies between calculated and photoelastic results. Both the calculated and photoelastic results are planned to be presented at the forthcoming Fifth Structural Mechanics in Reactor Technology (SMIRT) Conference.[4,5]

References

1. C. W. Smith et al., *Stress Intensity Distributions in Nozzle Corner Cracks of Complex Geometry*, NUREG/CR-0640, VPI-E-79-2 (January 1979).

2. P. M. Besuner, D. C. Peters, and R. C. Cipolla, *BIGIF — Fracture Mechanics Code for Structures*. Failure Analysis Associates (July 1978).

3. G. H. Powell, *Finite Element Analysis of Elasto-Plastic Tee Joints*, ORNL/Sub-319 -2, UC-SES 74-14 (September 1974).

4. S. N. Atluri and K. Kathiresan, "Stress Intensity Factor Solutions for Arbitrarily Shaped Flaws in Reactor Pressure Vessel Nozzle Corners," Paper G4/6 to be presented at *Fifth Conference on Structural Mechanics in Reactor Technology*, West Berlin, Federal Republic of Germany, August 1979.

5. C. W. Smith et al., "Stress Intensity Distributions in Nozzle Corner Cracks of Complex Geometry," Paper G4/4 to be presented at *Fifth Conference on Structural Mechanics in Reactor Technology*, West Berlin, Federal Republic of Germany, August 1979.

1439 233

3. EFFECT OF HIGH-TEMPERATURE PRIMARY REACTOR WATER ON THE SUBCRITICAL CRACK GROWTH OF REACTOR VESEL STEELS[*][†]

W. H. Bamford[‡]
D. M. Moon[‡]   L. J. Ceschini[‡]

The objective of this continuing program is to characterize the fatigue-crack-growth rate properties of ferritic vessel steels exposed to PWR primary-coolant environments. Four environmental chambers are being used, and the following areas are being investigated:

Weld and heat-affected-zone materials, starting conditions (2T-WOL, 2T CT specimens)	3 chambers (14 MPa, 288°C)
Crack growth rate at high K (4T-WOL, 4T CT specimens)	1 chamber (14 MPa, 288°C)

During this report period, four specimens were completed, including two welds and one heat-affected-zone specimen and the last of the specimens to be tested under the ramp- and hold-time matrix. This report will present a summary report on all the ramp- and hold-time tests, as well as the results of the weld specimens tested to date.

3.1 Crack Growth Rate Behavior of Welds and Heat-Affected Zones

Three additional specimens of the same submerged arc weld tested previously were completed during the report period. Two were from the weld itself, with the crack propagating along the welding direction, and the third specimen had a crack propagating in the heat-affected zone (HAZ).

---

[*] Conversions from SI to English units for all SI quantities are listed on a foldout page at the end of this report.

[†] Work sponsored by HSST program under UCCND Subcontract 3290 between Union Carbide Corporation Nuclear Division and Westinghouse Electric Corporation.

[‡] Westinghouse Electric Corporation.

The results of these individual specimens are shown in Figs. 3.1 through 3.3. All the specimens were tested with R ratio = 0.2 and showed equivalent results. Results of these recent tests are compared with those of previous tests on the same weldment in Fig. 3.4.

Specimens C-7 and C-9 were tested to complete the characterization of this weld at low R ratio, using a positive saw-tooth wave form to compare with the previous results obtained with a sinusoidal wave form. As may be seen in Fig. 3.4, the results were entirely equivalent to the previous results, and, in fact, the results from specimen C-9 were nearly identical with those of specimen C-2 (tested at one cycle per min), even including a sizable arrest event that occurred about halfway through the test. All the tests were started at precisely the same value of ΔK, that is, 22 MPa$\sqrt{in}$., to allow for a good comparison.

The specimen from the HAZ performed no differently than the specimens where the crack propagated entirely in the weld. The crack propagated entirely in one plane throughout the test, which was not entirely expected, because some earlier tests of Charpy specimens showed that the crack jumped out of the HAZ and propagated in the base metal immediately adjacent to it.[1] Apparently, fatigue loadings of less intensity and at slower rates allow the crack to remain in the HAZ. The fatigue-crack-growth rates obtained were approximately in the middle of the data for the weld specimens, so it appears that no special treatment is necessary for the HAZ material. This conclusion was also reached for a BWR environment by Hale et al.[2]

A series of tests is being conducted on this weld and HAZ under the positive saw-tooth loadings at high R ratio, and results will be reported next quarter.

3.2 Effects of Ramp and Hold Time

The completion of testing for specimen R-9 during this report period marks the completion of the series of tests to study ramp- and hold-time effects. Results of this test are shown in Fig. 3.5 and are typical of other results obtained with a 1-min ramp. Because the study of ramp and hold times extended over more than two years, it is important to summarize

ORNL–DWG 79–6108 ETD
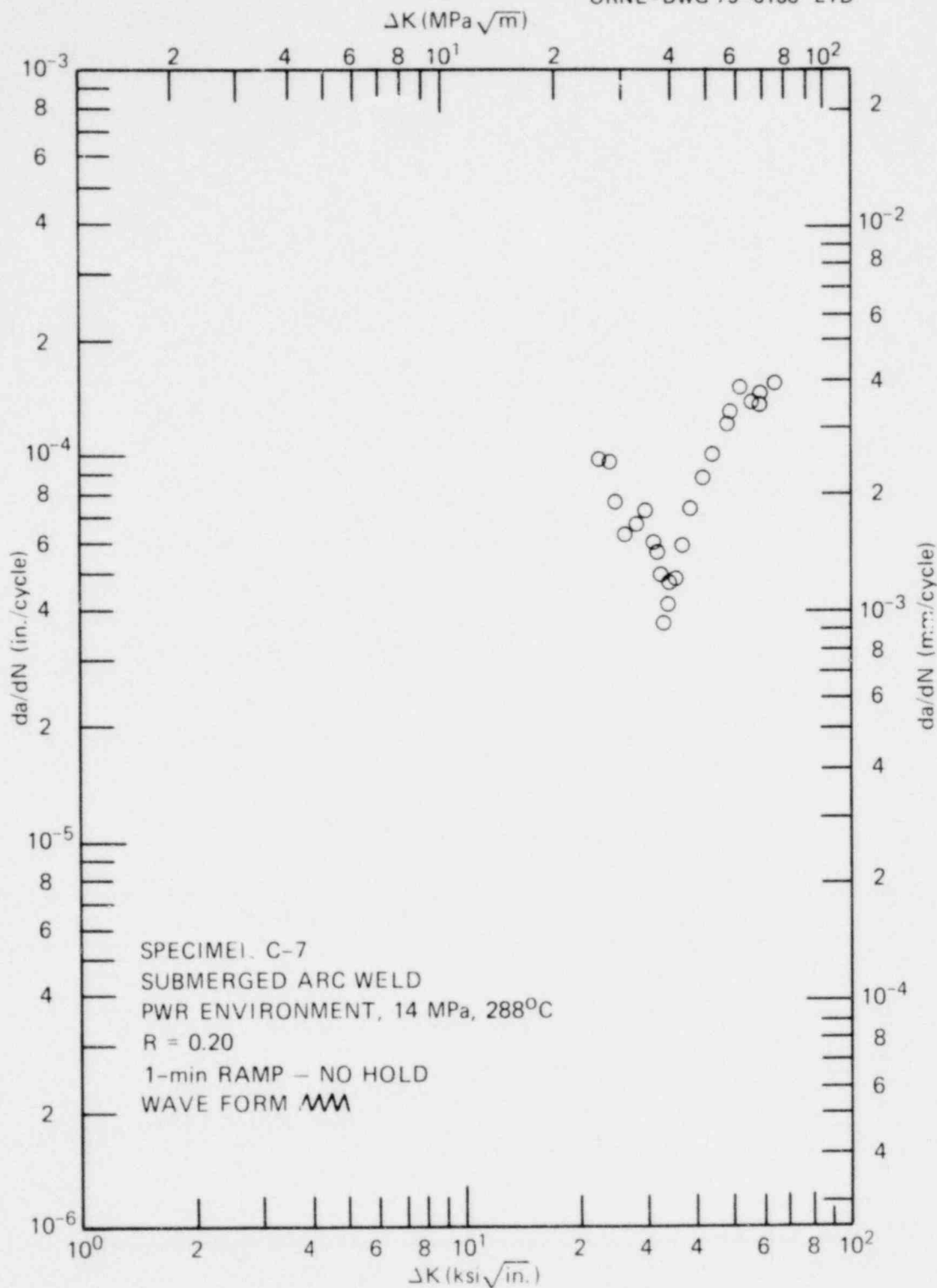

Fig. 3.1. Fatigue-crack-growth rate test results — specimen C-7.

1439 236
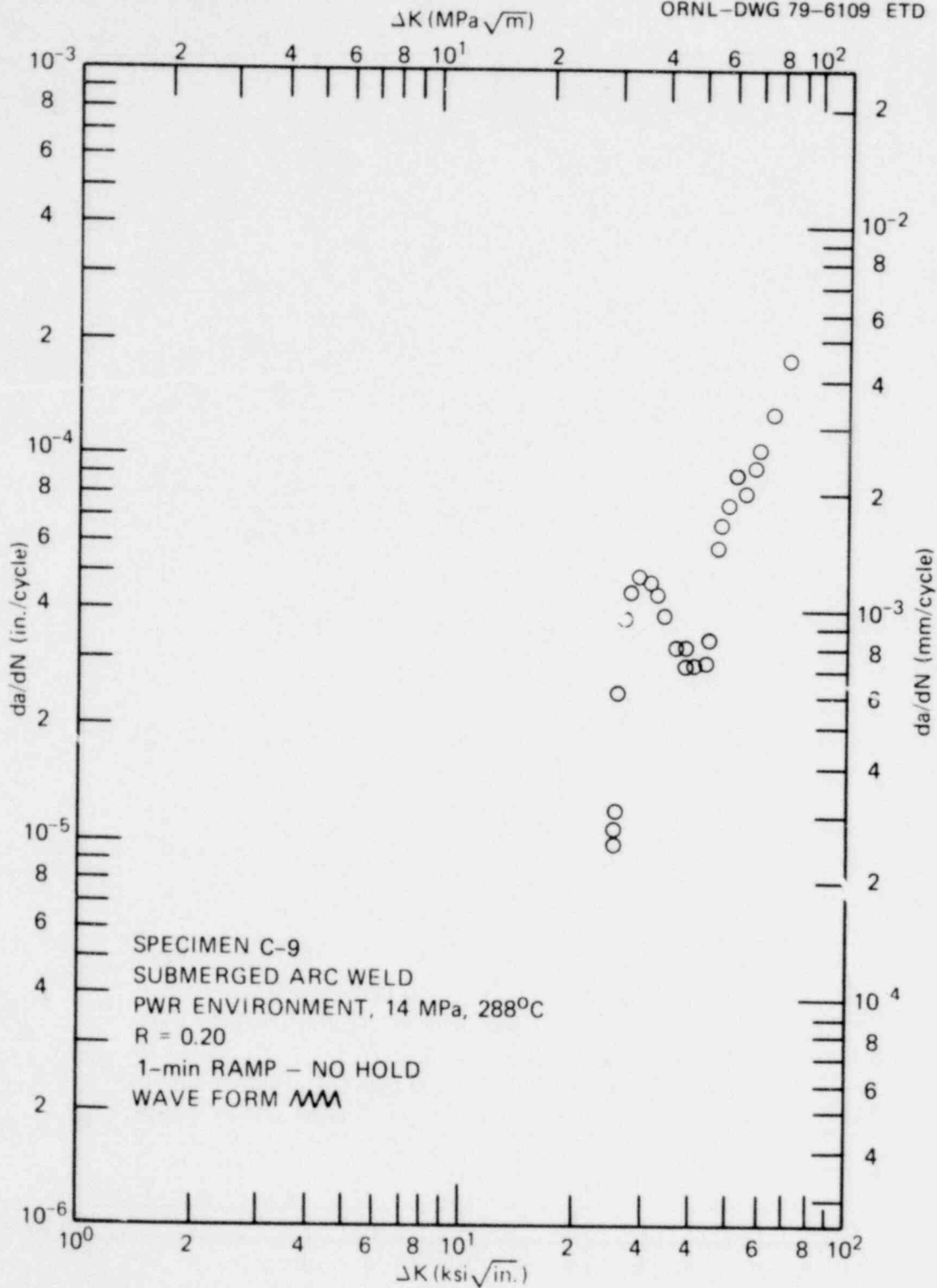
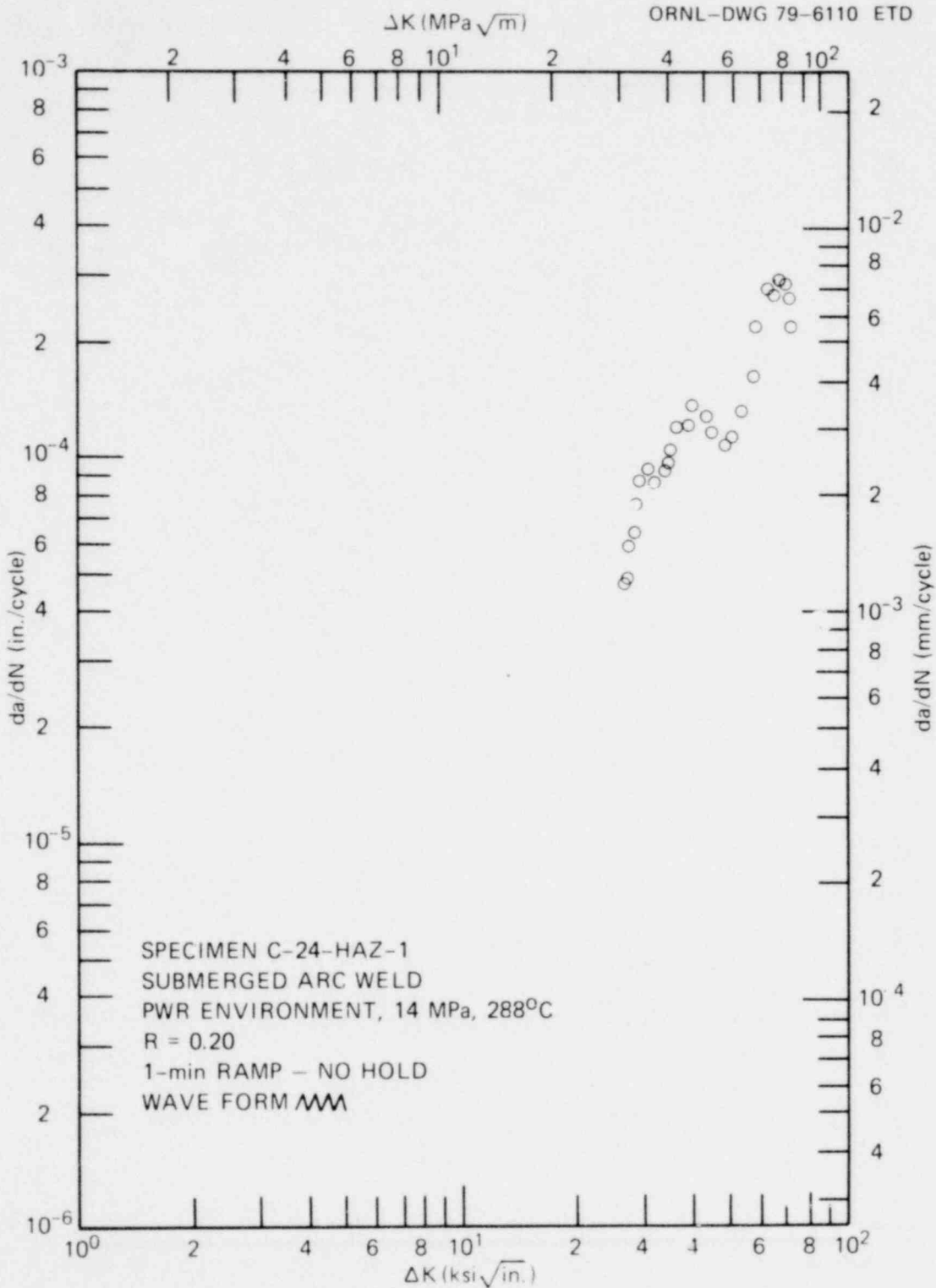Fig. 3.2. Fatigue-crack-growth rate test results — specimen C-9.

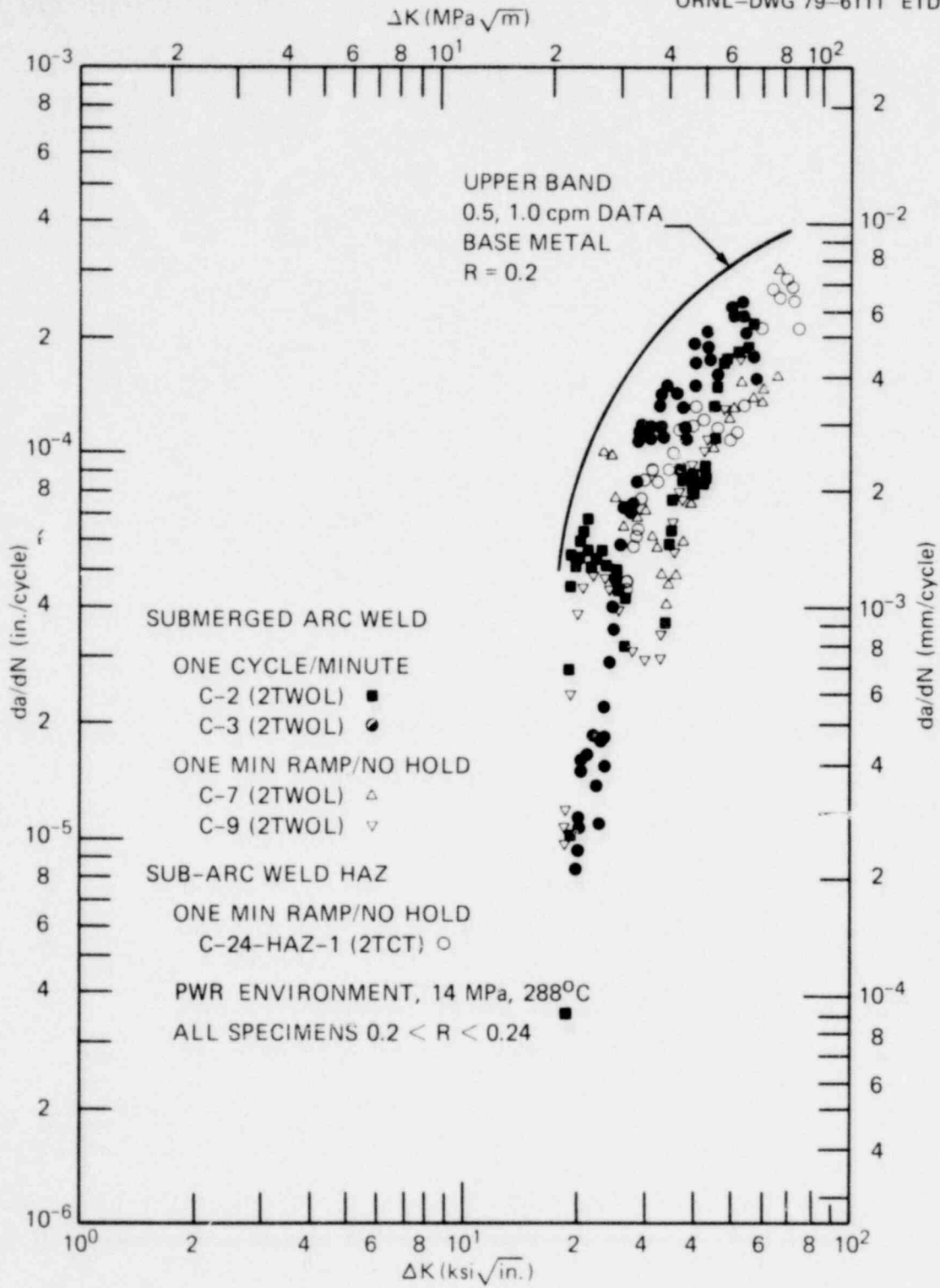Fig. 3.3. Fatigue-crack-growth rate test results — specimen C-24-HAZ-1.

Fig. 3.4. Summary of fatigue-crack-growth rate test results —
Linde 124 welds tested at low R ratio.
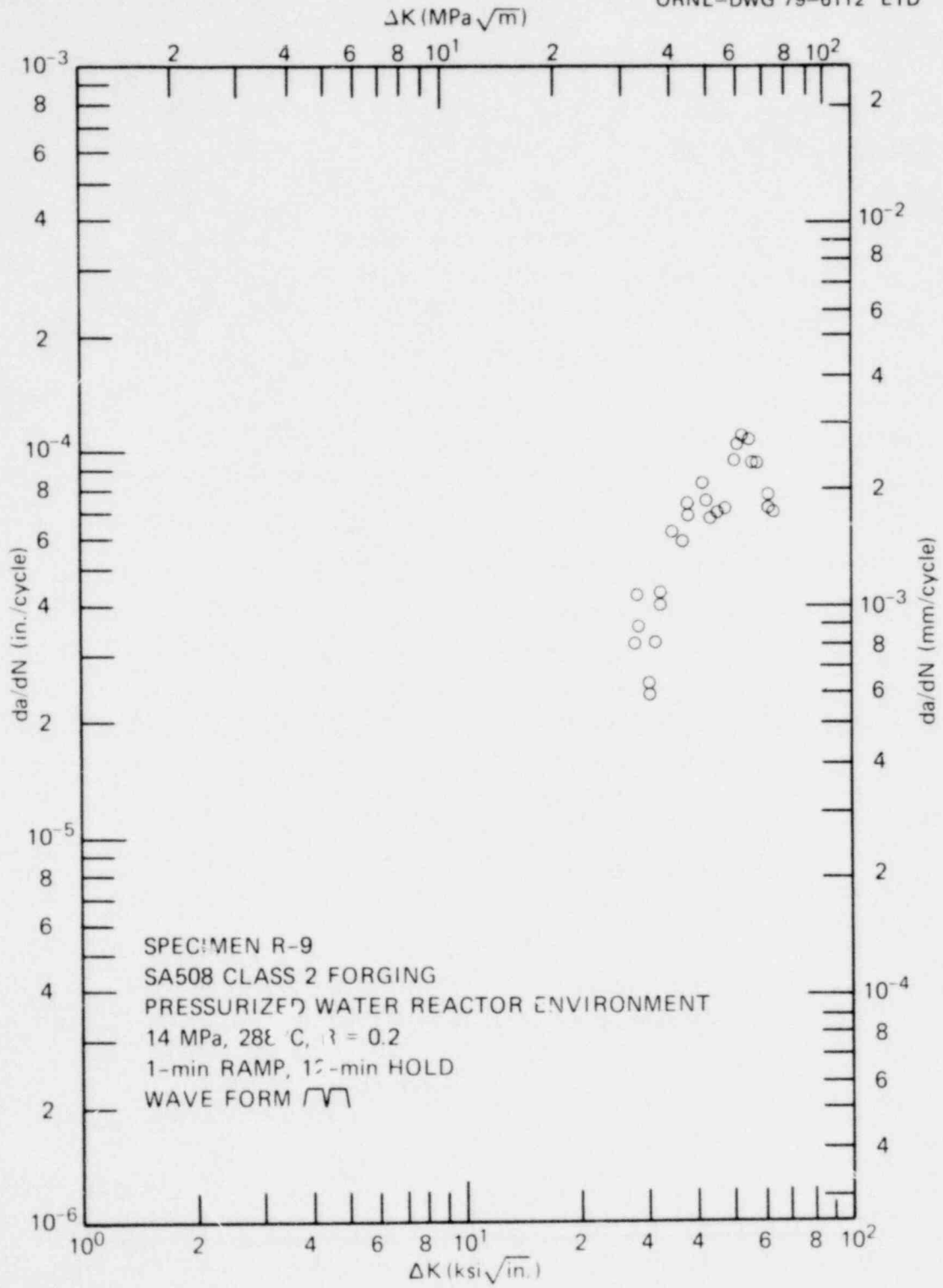
Fig. 3.5. Fatigue-crack-growth rate test results — specimen R-9.

the results of the entire program, even though many of the individual specimen results have been previously reported.

The study was conducted on specimens taken from two heats of SA508 Class 2 forging steel, machined into 50.8-mm-thick specimens, both wedge-opening loading (WOL) and compact (CT) type. Tests were conducted by both Westinghouse and the Naval Research Laboratory (NRL) using a test matrix designed to allow comparison between laboratories and to optimize the use of available facilities. Ramp times included were 1 sec and 1, 5, and 30 min, and hold times were 1 sec and 1, 3, and 12 min. Tests were conducted at both 93 and 288°C. Results are now available for all the ramp times listed except the 30-min ramp-time tests, which are continuing at NRL. The test results indicate that ramp time is more important than hold time in affecting fatigue-crack-growth rates; thus, the summary to follow is presented in figures that show different hold-time tests having a common ramp time.

A summary of results obtained with a 1-sec ramp time is found in Fig. 3.6, which shows that, at such a fast ramp rate, the environment did not have time to enhance the crack growth rate significantly. Several different hold times were tried, but they had no effect on the data, which show growth rates only slightly higher than results obtained in air. Data of Cullen et al.[3] from the NRL are included and show good agreement with these data, even though the R ratio was slightly lower. Two test temperatures have been included in this data summary and show that essentially the same data were produced at 288 and 93°C.

Increasing the ramp time to 1 min results in considerably enhanced crack growth rates, and results of the tests conducted at 93°C are summarized in Fig. 3.7. Growth rates increase very quickly at the beginning of the test and then begin to increase at a slower rate, causing the logarithmic portrayal of growth rate vs range of applied stress-intensity factor to bend over somewhat, in this case trending back toward the air growth rates at ΔK equal to 77 to 99 MPa$\sqrt{in}$. The data presented in Fig. 3.7 show a relatively tight scatter band and again reveal excellent agreement with those of Cullen et al.[3] There is no perceptible effect of hold time on the data and no effect of specimen type, because the "F" specimens were WOL type and the specimens of Ref. 3 were CT specimens.
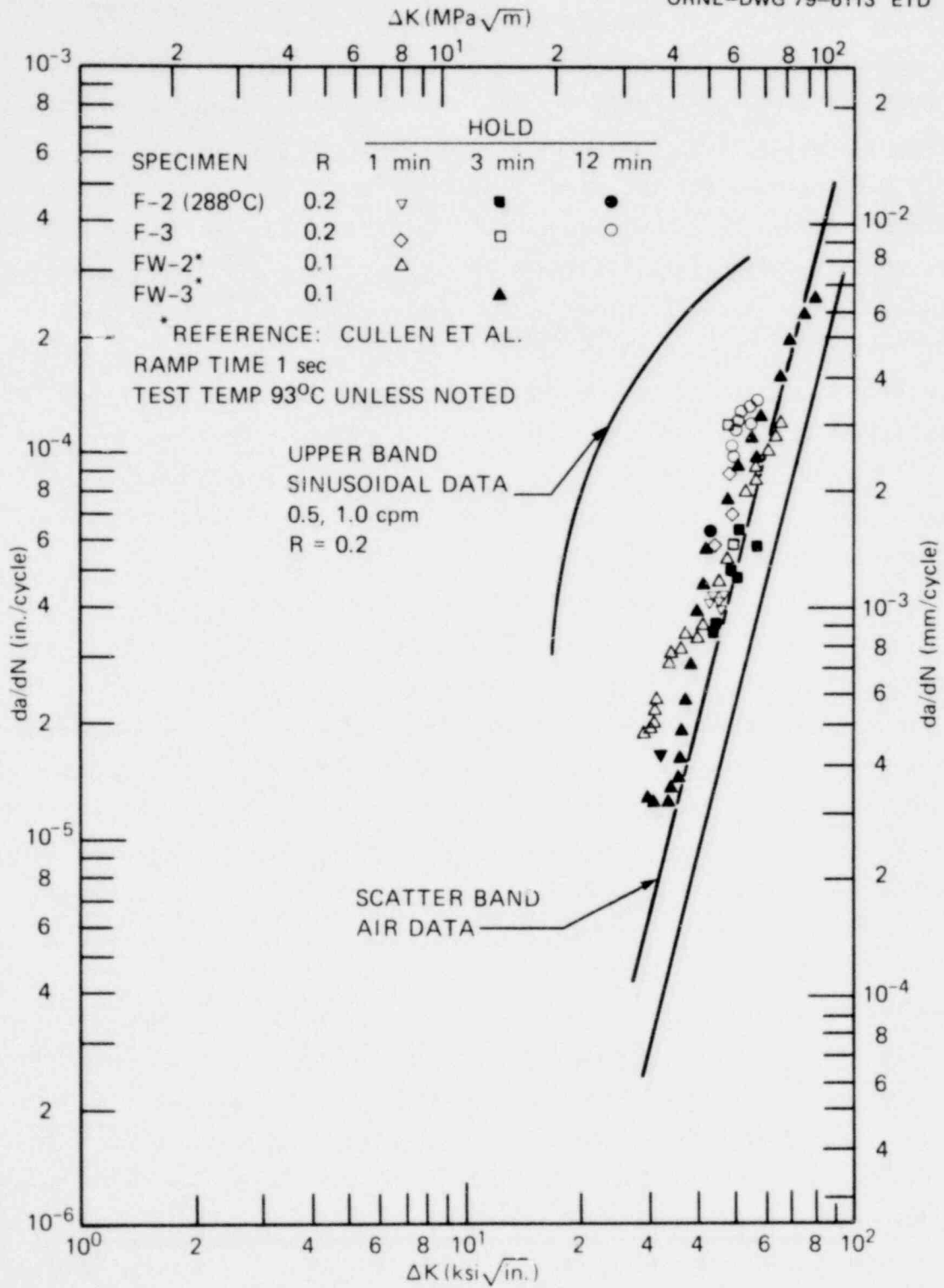
ORNL–DWG 79–6113 ETD

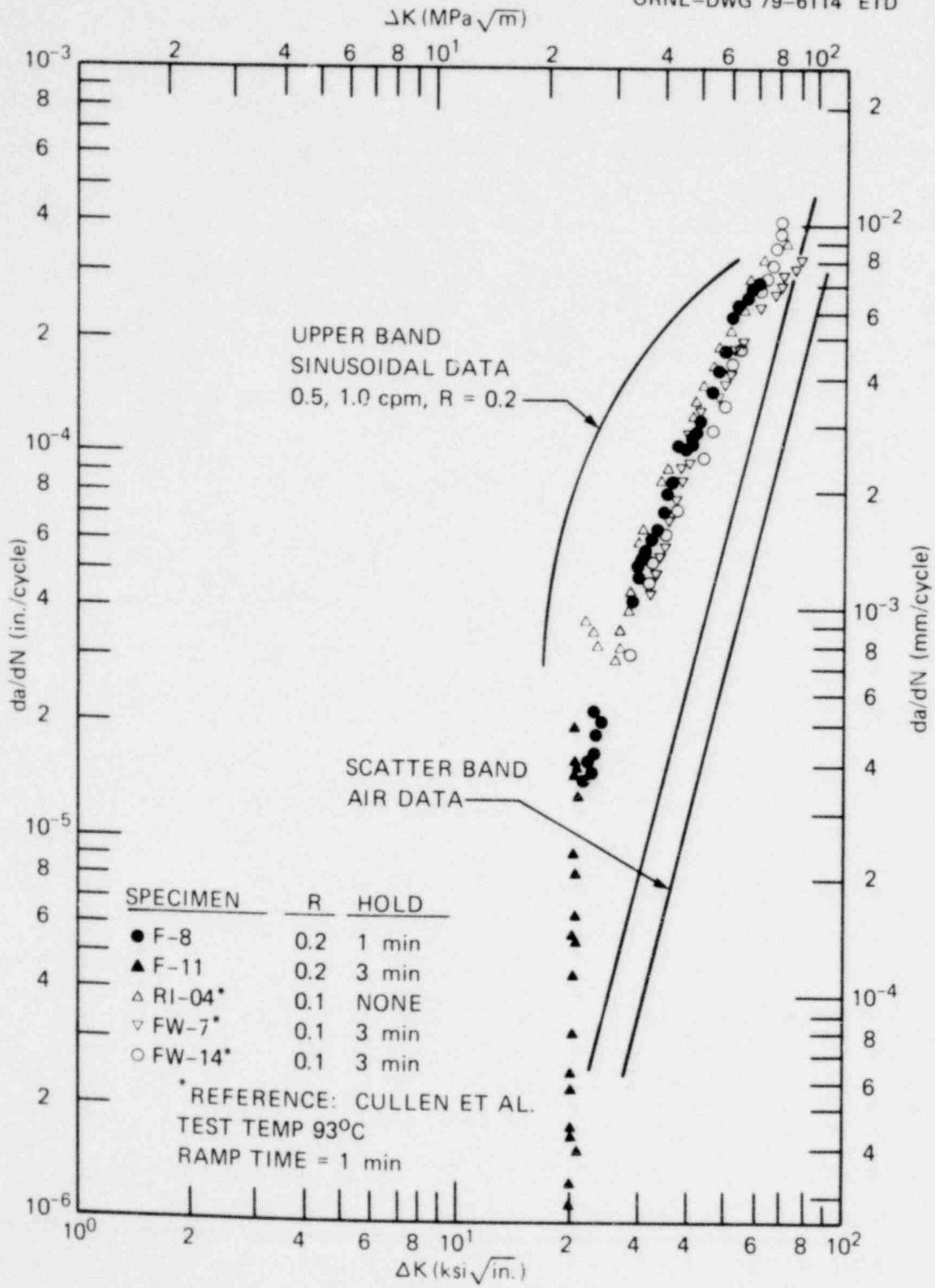Fig. 3.6. Summary of results, 1-sec ramp tests.

1439 242

Fig. 3.7. Summary of results, 1-min ramp tests at 93°C.

Results of 1-min ramp-time tests conducted in higher-temperature water environment of 288°C show considerably more scatter than those at the lower temperature. Again, the growth rate increases steeply at the beginning of the test, and the environmental enhancement is clearly evident. The crack growth rate has been found to be difficult to sustain in the region where it is increasing so rapidly, and it has a strong tendency to revert back to the air behavior. This tendency is further enhanced when test interruptions occur, such as shutdowns caused by hardware problems or electrical outages.

There were several specimens in this series that showed large decreases in growth rate following such interruptions; therefore, the data were ignored after the interruption. Examples are F-10 and F-9, where the retarded data have been discarded. This behavior has been verified with striation measurements and is discussed in some depth in Ref. 4. In several cases, these arrests in crack growth have occurred early in a test and have been so severe that the specimens were abandoned.

The imposition of hold times also tends to encourage this behavior, as can be seen in Fig. 3.8. The ramp time of 1 min corresponds to a sinusoidal frequency of 0.5 cycles per min, and the data fall well short of the upper band of the sinusoidal data. Thus, the conclusion is that 1-min ramp data with various hold times are somewhat less severe than sinusoidal data for an equivalent loading rate.

Behavior of the pressure vessel steels in the light-water reactor (LWR) environment at ramp times longer than 1 min has not been studied extensively, because the tests require long periods to perform. The available data for a 5-min ramp time and the equivalent 0.1 cycle per min data are summarized in Fig. 3.9. Again the same general behavior is obtained as with the 1-min ramp, but two specimens tested at 288°C show data that exceed the upper scatter band of the sinusoidal data obtained at 0.5 and 1.0 cycles per min. The previously believed saturation in the growth rates at sinusoidal frequencies of between 0.5 and 1.0 cycles per min is somewhat refuted by these data, but a strong conclusion is not possible because of the lack of sufficient data. Results from a test conducted at 93°C fall near the middle of the data.[3]
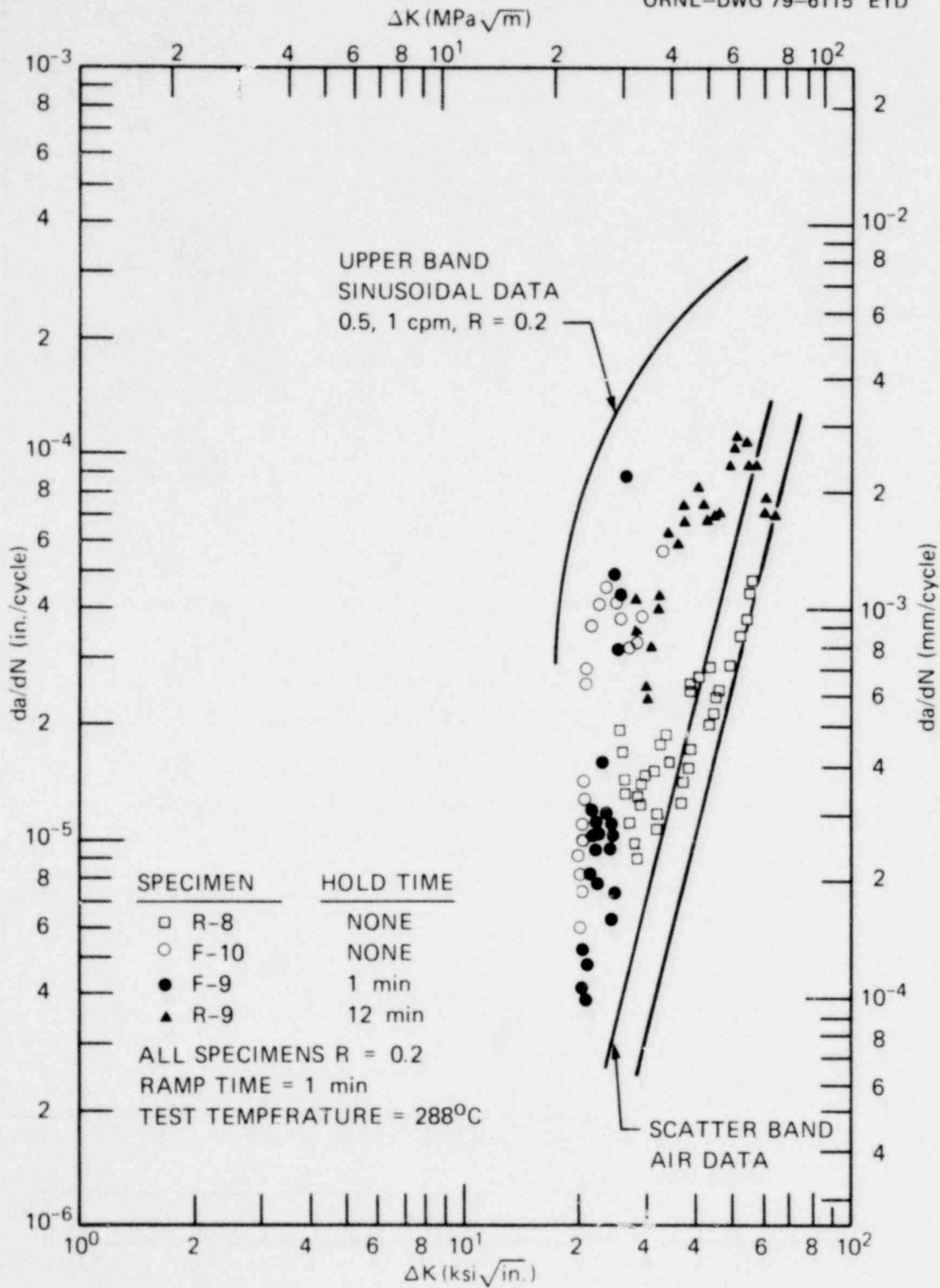
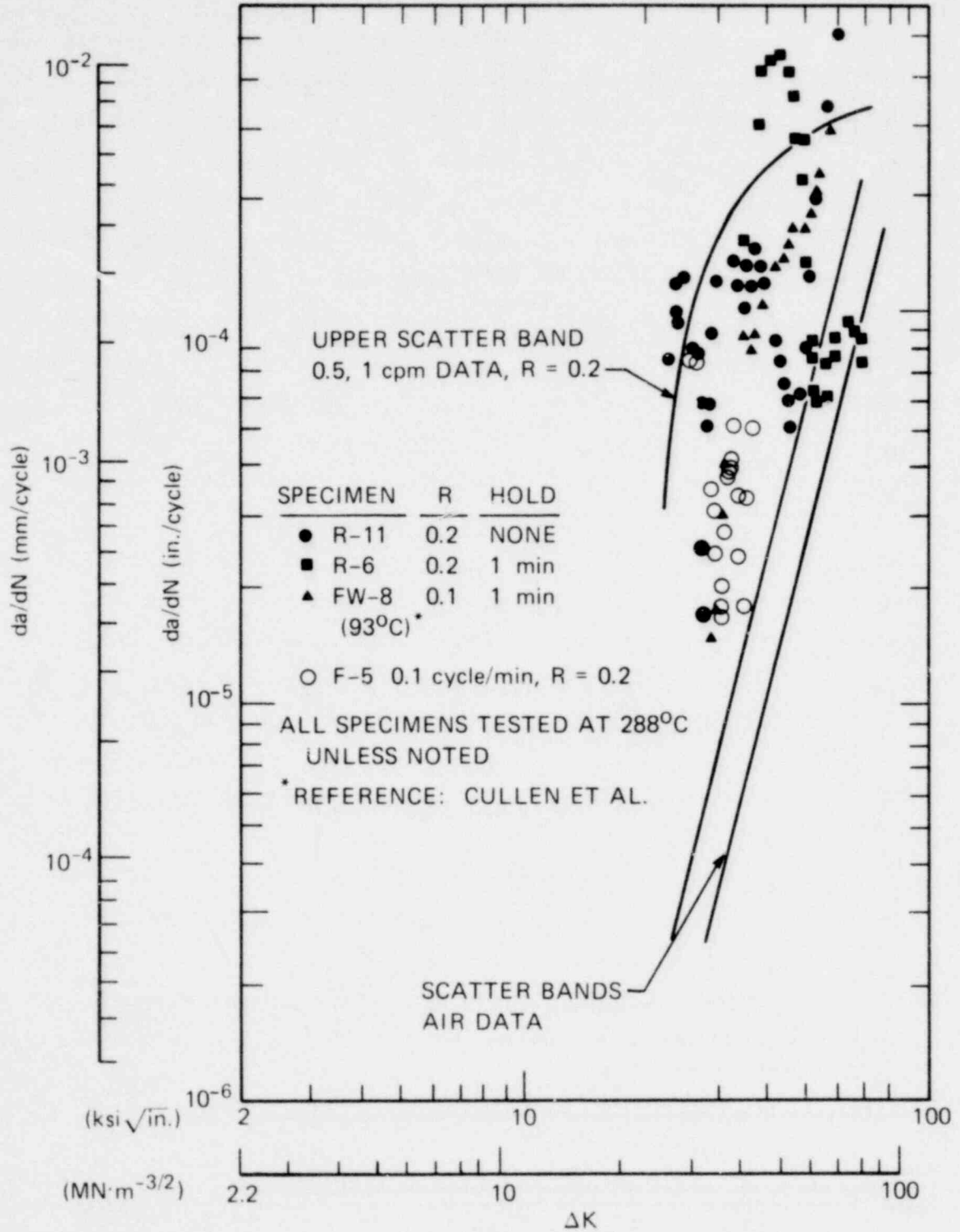Fig. 3.8. Summary of the effect of hold time for 1-min ramp tests conducted at 288°C.

ORNL—DWG 79—6116 ETD

Fig. 3.9. Summary of fatigue-crack-growth rate test results —
5-min ramp and equivalent sinusoidal tests.

The growth rates of specimens R-6 and R-11, which exceeded the upper band of the sinusoidal data, were subjected to considerable fractographic study to verify the macroscopically observed rates. The results of these studies are shown in Figs. 3.10 and 3.11 and verify the macroscopic rates in general. For specimen R-6, the striation measurements follow the specimen behavior even through a sizable arrest event. The striation measurements for specimen R-11 are in agreement with the macroscopic data at the beginning and the end of the test, but they do not reflect the apparent arrest that occurred near the middle of the test. This "arrest" may have been caused by the fact that the crack front was very uneven during the middle of the test, as shown in Fig. 3.12. Certainly the striation measurements on both specimens confirm that the growth rates were indeed higher than the upper band of the sinusoidal data.

Specimen R-11 displayed a character in its fracture surface that had not been observed before — an alternating light- and dark-banded appearance that was visible to the naked eye. This is shown in Figs. 3.12 and 3.13, where magnifications of both the light and dark bands are provided. The reason for this banded behavioi is currently unknown, but striations are clearly visible in both regions and give comparable growth rate measurements. The only real difference between the two types of regions is that the dark regions appear to have a rougher texture with more crack branching, as seen in Fig. 3.13.

A number of other specimens were studied fractographically to confirm the macroscopic growth rates, and the resulting measurements are shown in Table 3.1. The striation measurements matched the macroscopic growth in all cases for tests conducted at 288°C, as shown further for specimen F-9 in Fig. 3.14. Tests conducted at 93°C produced striations that did not match the macroscopic growth, however, as shown in Fig. 3.15 for specimen F-8. This is particularly interesting because the macroscopic growth rates of the specimens tested at the two temperatures are comparable. This indicates the presence of a corrosion component that adds to the mechanical growth in the lower-temperature specimen.

The fracture surfaces of specimens tested at the two temperatures are considerably different, however, and this at least partially explains

Fig. 3.10. Striation spacing measurements for specimen R-6.

ORNL–DWG 79–6118 ETD
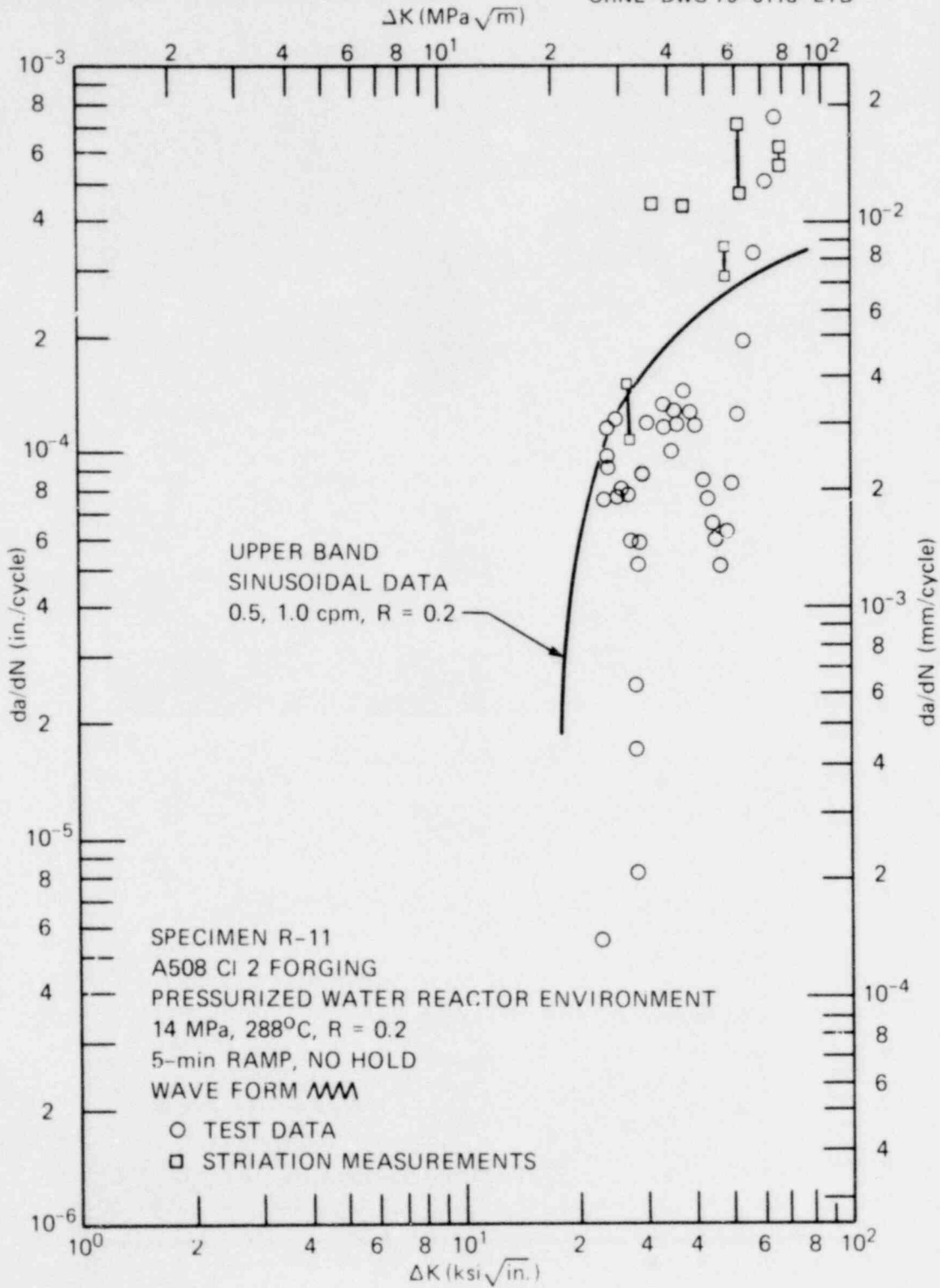
Fig. 3.11. Striation spacing measurements for specimen R-11.

Fig. 3.12. Fracture surface of specimen R-11.

ORNL–PHOTO 3012–79R
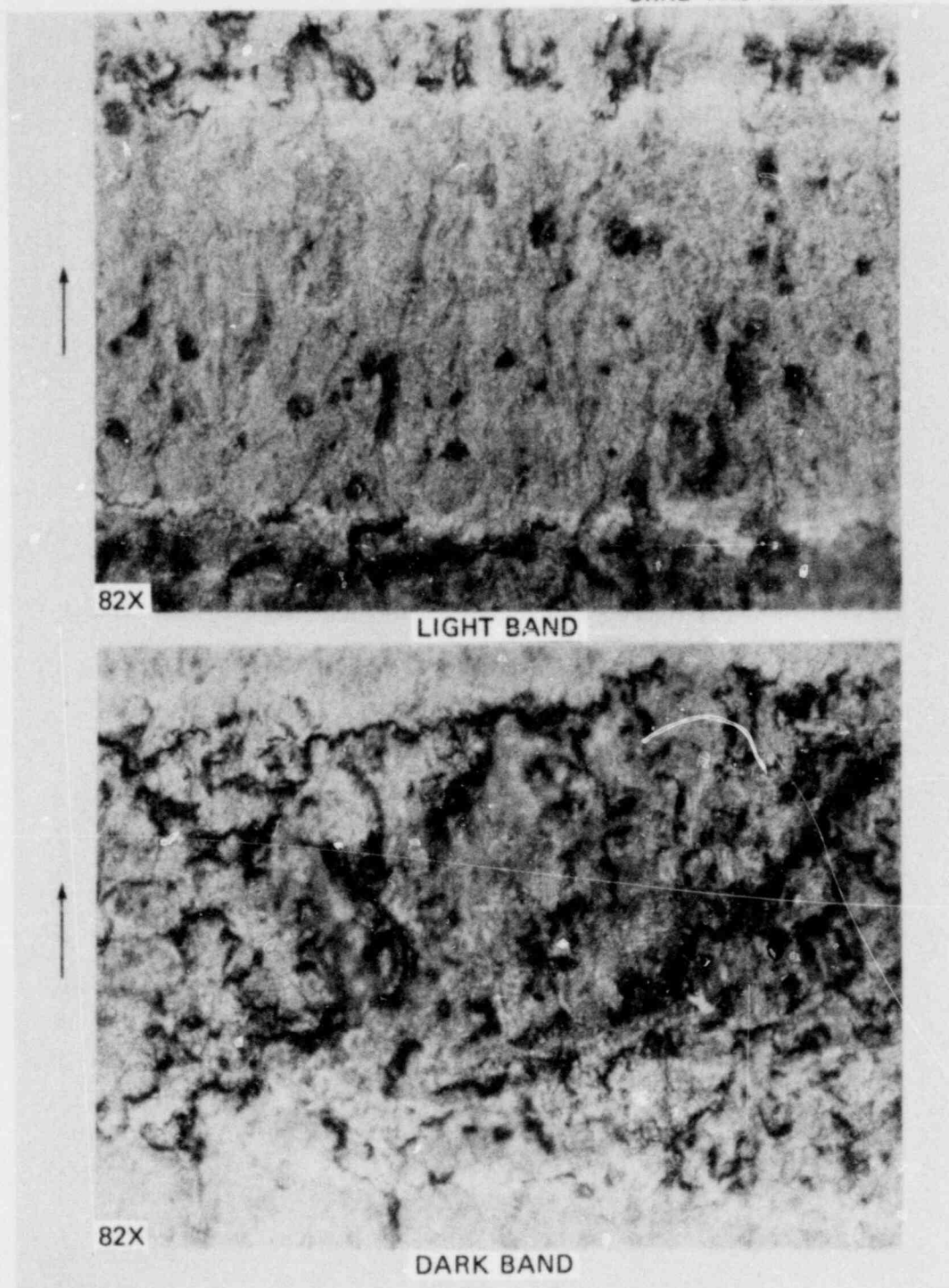
Fig. 3.13. Close-up photograph of banded regions of specimen R-11.

1439 251
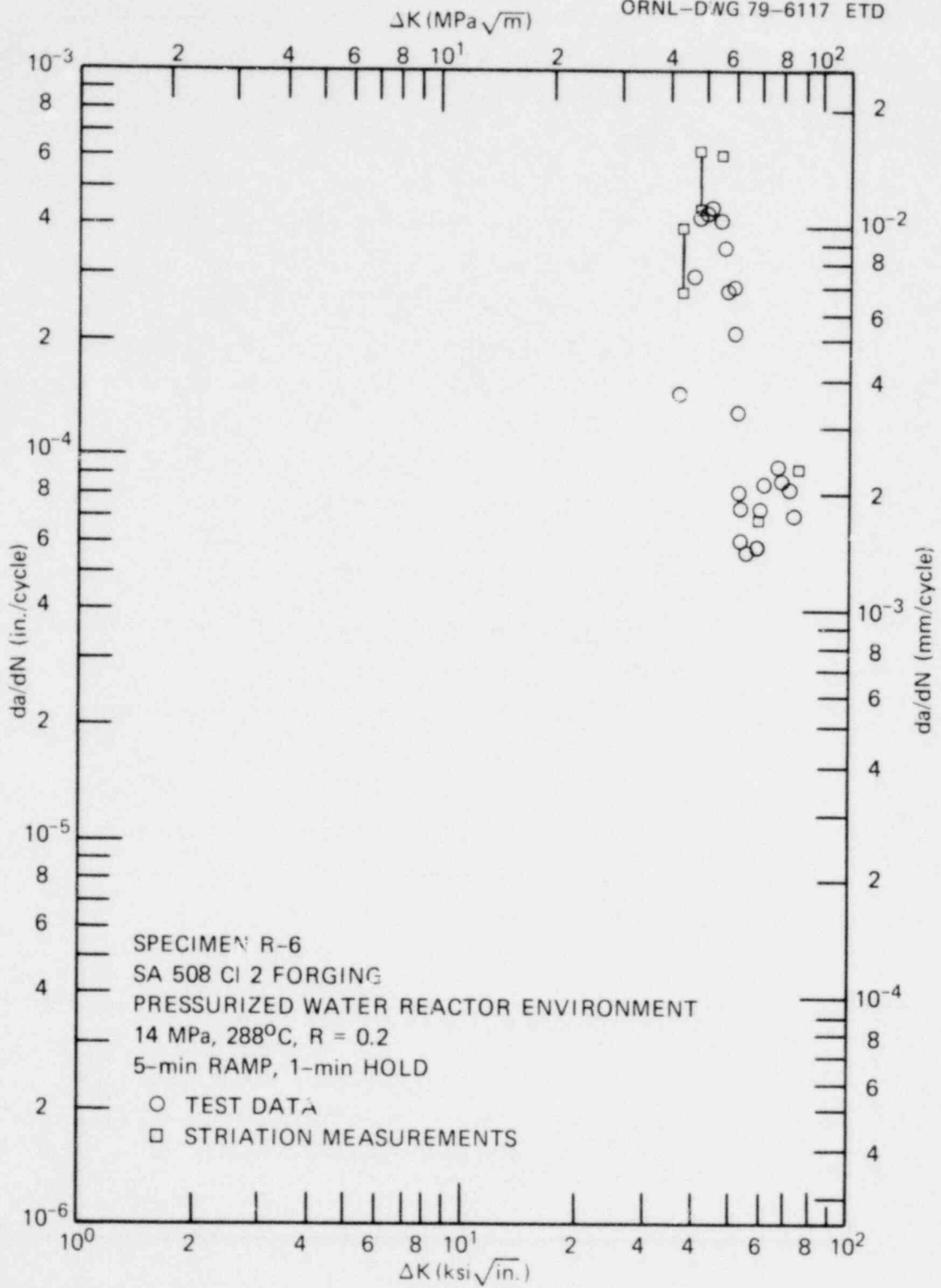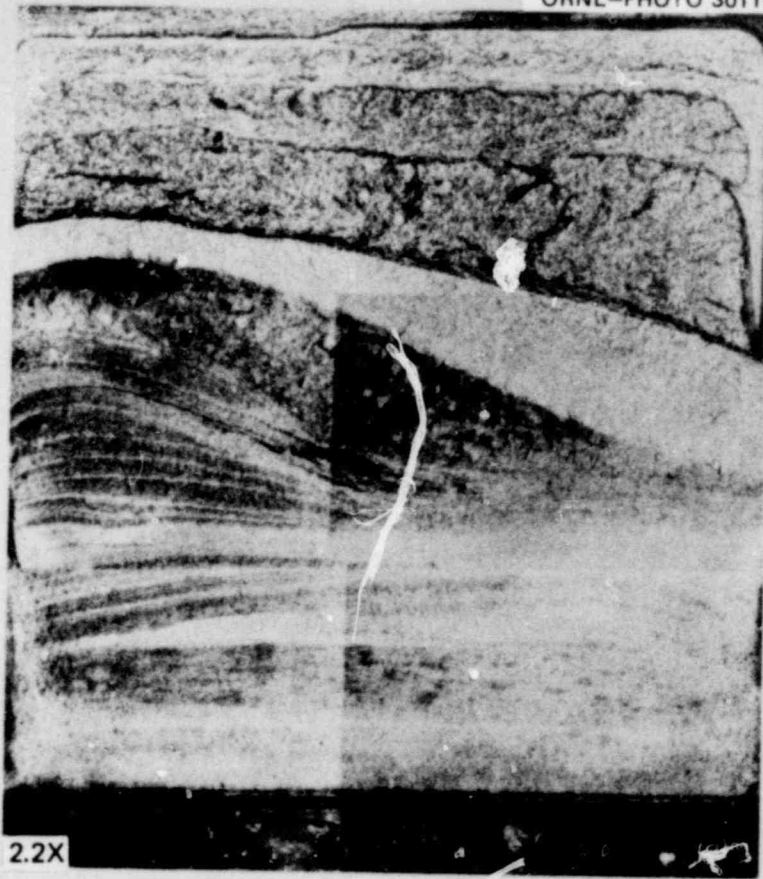
Fig. 3.14. Striation spacing measurements for specimen F-9.
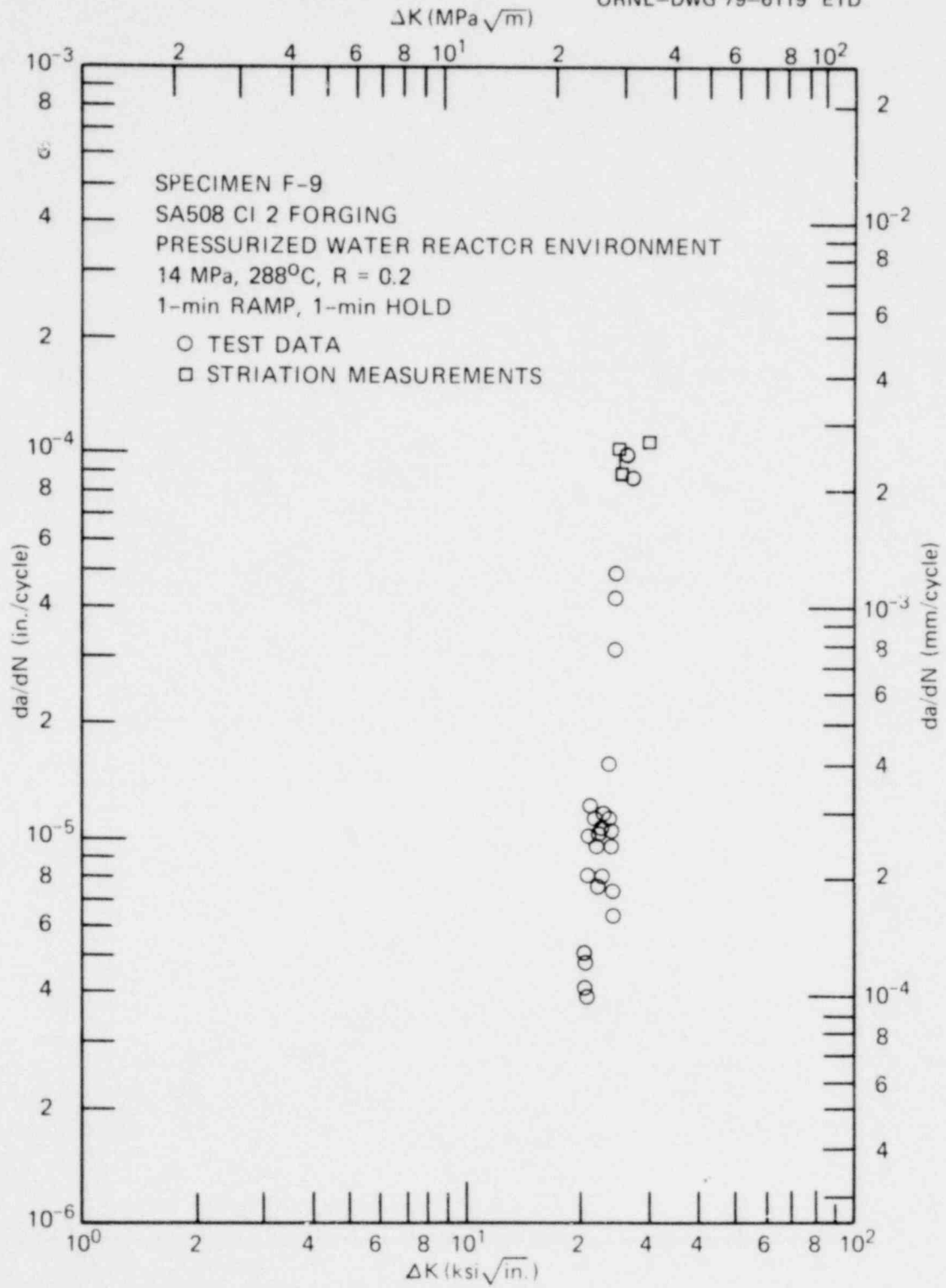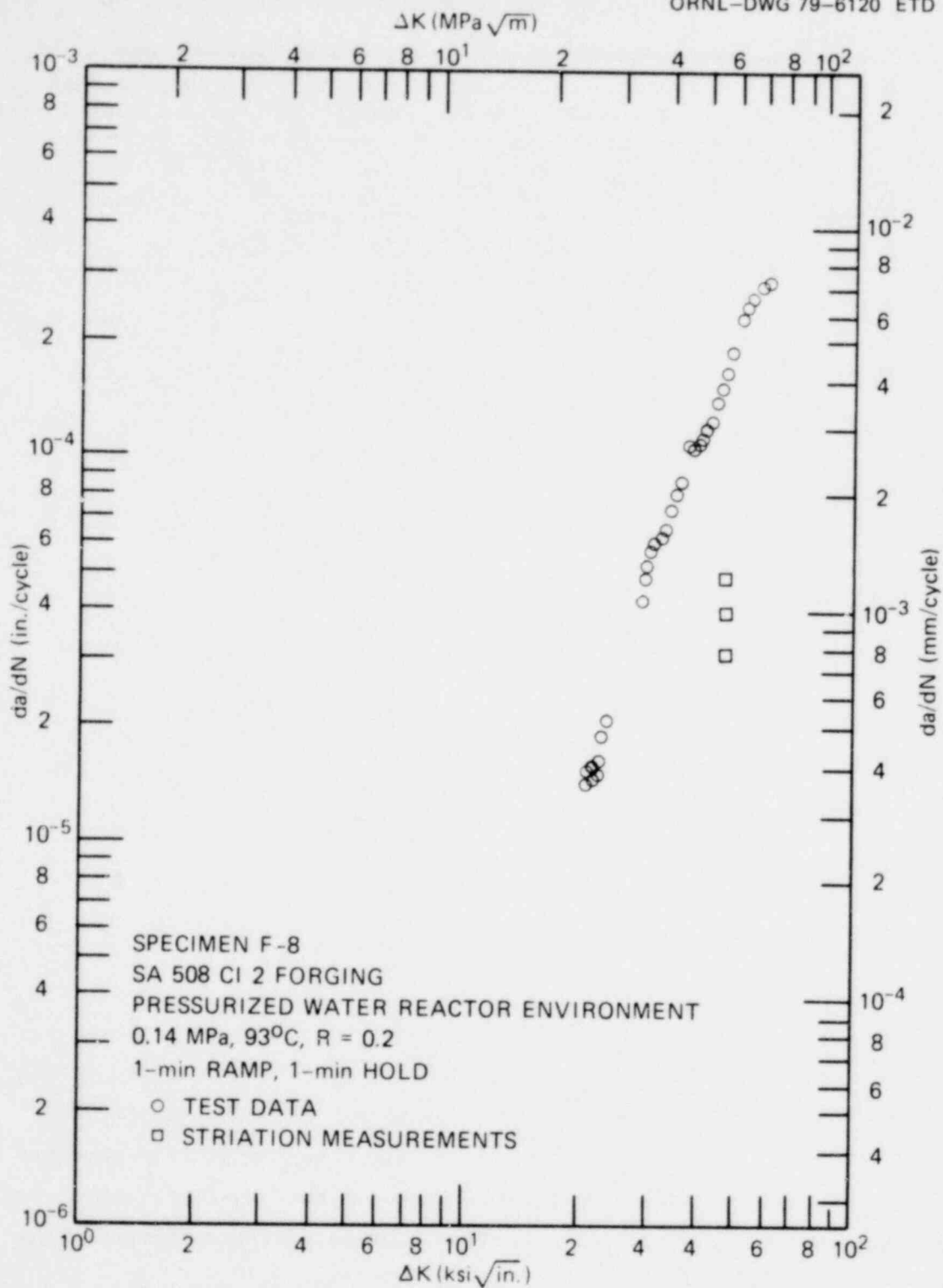
Fig. 3.15. Striation spacing measurements for specimen F-8.

Table 3.1. Crack growth rate determinations from striation
spacing measurements for ramp- and hold-time specimens

Specimen	Applied ΔK (MPa$\sqrt{m}$)	Striation spacing (mm per cycle)	Macroscopic data (mm per cycle)
F-2	56.2	7.6×10^{-4}	
	56.4	1.0×10^{-3}	1.7×10^{-3}
	57.0	1.3×10^{-3}	
F-9	28.4	2.3×10^{-3}	2.5×10^{-3}
	28.4	2.5×10^{-3}	
	33.0	2.8×10^{-3}	2.2×10^{-3}
R-6	38	6.9×10^{-3}	3.66×10^{-3}
	38	9.7×10^{-3}	
	44	1.1×10^{-2}	1.0×10^{-2}
	44.6	1.5×10^{-2}	
	47.7	1.5×10^{-2}	1.10×10^{-2}
	63.4	1.7×10^{-3}	1.48×10^{-2}
	78.0	2.3×10^{-3}	1.77×10^{-3}
R-11	29	2.8×10^{-3}	2.0×10^{-3}
	29	4.1×10^{-3}	
	33	1.1×10^{-2}	2.8×10^{-3}
	38	1.0×10^{-2}	3.0×10^{-3}
	48	7.4×10^{-3}	
	48	8.6×10^{-3}	1.5×10^{-2}
	55	1.2×10^{-2}	3.12×10^{-3}
	55	1.9×10^{-2}	
	85	1.4×10^{-2}	
	85	1.5×10^{-2}	3.15×10^{-2}
F-8 (93°C)	52	7.6×10^{-4}	
	52	1.0×10^{-3}	4.11×10^{-3}
	52	1.3×10^{-3}	

the inconsistencies between macroscopic and striation measured growth
rates. The fracture surfaces of specimens F-9 and F-8 are shown in Figs.
3.16 and 3.17. The fracture surface of the high-temperature specimen
shows entirely striated growth, while that of the low-temperature speci-
men displays a mixture of cleavage and ductile striated growth. This is
shown very clearly in the bottom picture of Fig. 3.17.

Besides the intended assessment of the effects of ramp and hold
time and temperature on fatigue crack growth, a number of other things

ORNL PHOTO 4194-78
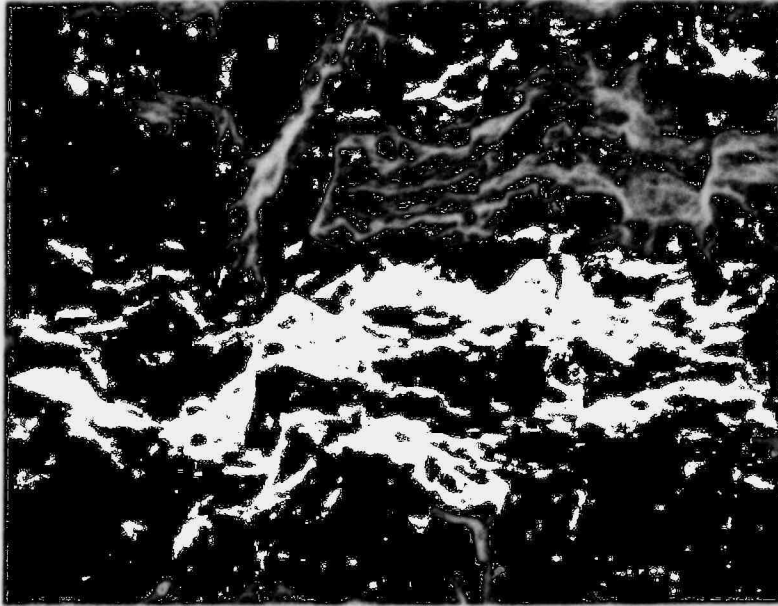
500X
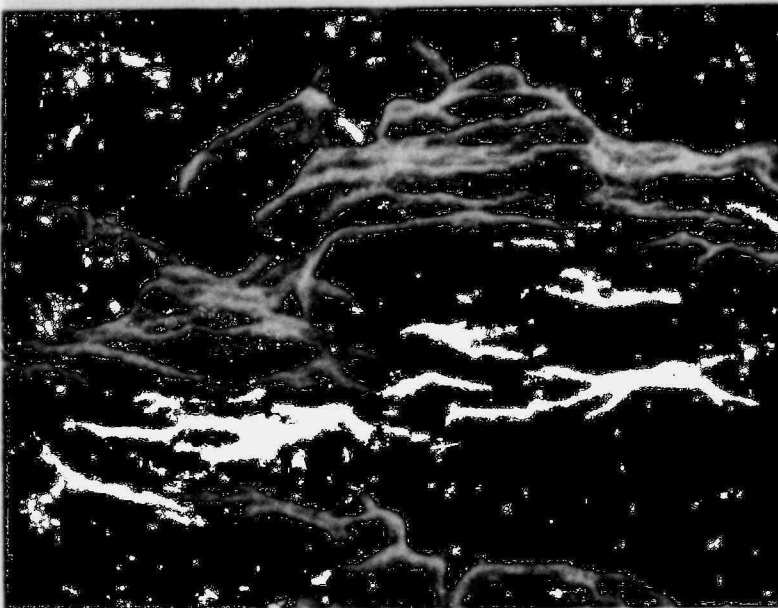
2000X

Fig. 3.16. Fracture surfaces of specimen F-9 — 1-min ramp- and 1-min hold-time, R = 0.2, temperature = 288°C.
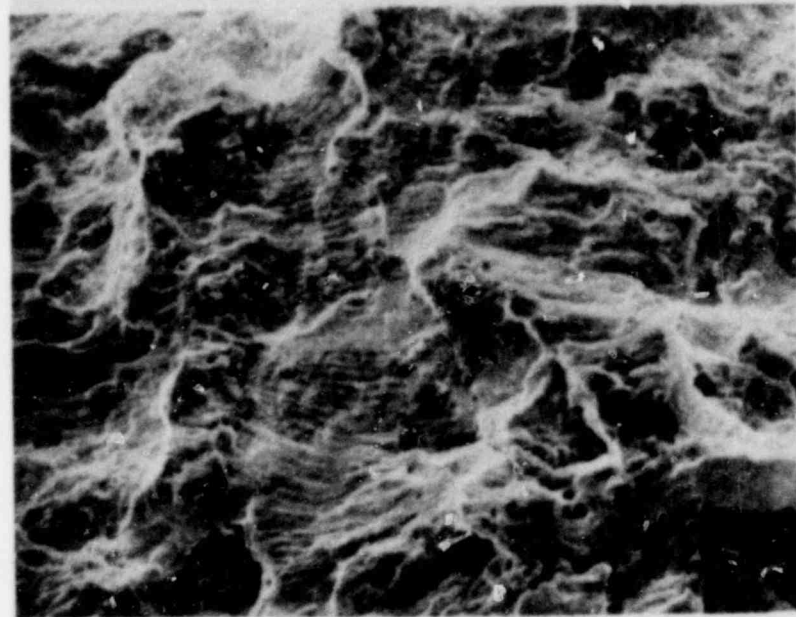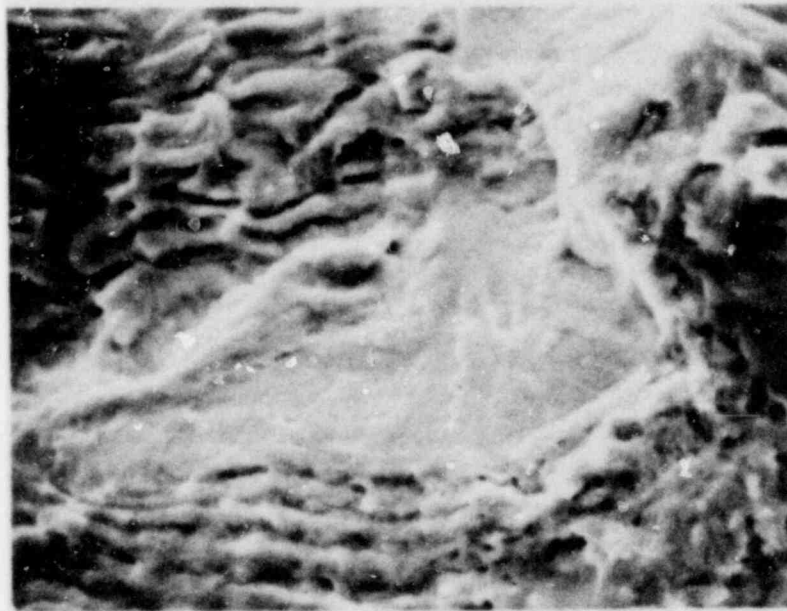
Fig. 3.17. Fracture surfaces of specimen F-8 — 1-min ramp- and 1-min hold-time, R = 0.2, temperature = 93°C.

were learned in the study. One of the most interesting and most diffi-
cult to explain is the tendency of the accelerated growth to revert back
to the unaccelerated air behavior when interruptions occur in the test,
as has been previously discussed. Another very important point is that
the accelerated growth is never attained if the specimen is begun at too
high a value of applied ΔK or K_{max}. This effect is shown, for example,
in Fig. 3.18 and is believed to be related to the mechanisms of crack
growth rate acceleration in the water environment. There is likely a
definite relationship between this starting effect and the effect of in-
terruptions in causing the growth rates to revert to a nonaccelerated be-
havior.

The process of fatigue crack growth in a water environment is com-
plicated indeed, and it is believed to be accelerated by the effects of
hydrogen produced in the crack-tip water-steel reaction. If the mechani-
cal loading rate on the cracked geometry exceeds the rate that hydrogen
is produced and diffuses to the region ahead of the crack, the growth
will not be accelerated by the water environment. The rate at which
hydrogen is produced is affected by many things, only some of which are
well understood. On the basis of present evidence, the electrochemical
cell set up at the crack tip that supplies hydrogen to the crack-tip
region during a test is apparently easily affected by changes in the
specimen loadings. Hydrogen is probably produced most efficiently dur-
ing slow regular loadings, of which the sinusoid is a good example.
Irregular loadings — for example, those that include hold times or tests
that are interrupted — cause this cell to operate less efficiently; thus,
the acceleration is not as pronounced. There must be a very fine balance
between the mechanically induced loading rate and the environmentally
produced hydrogen to result in highly accelerated growth. If the me-
chanical loading, as measured by the stress-intensity factor K, occurs
at too fast a rate, the crack will tend to propagate mechanically faster
than the environment can influence it, and no enhancement will be ob-
served. This effect has been observed before and is exemplified by com-
paring 1-sec and 1-min ramp test results, but the same mechanism may be
the cause of the starting conditions effect shown in Fig. 3.18. If the
specimen is initially loaded at a relatively high ΔK (or K_{max}), the
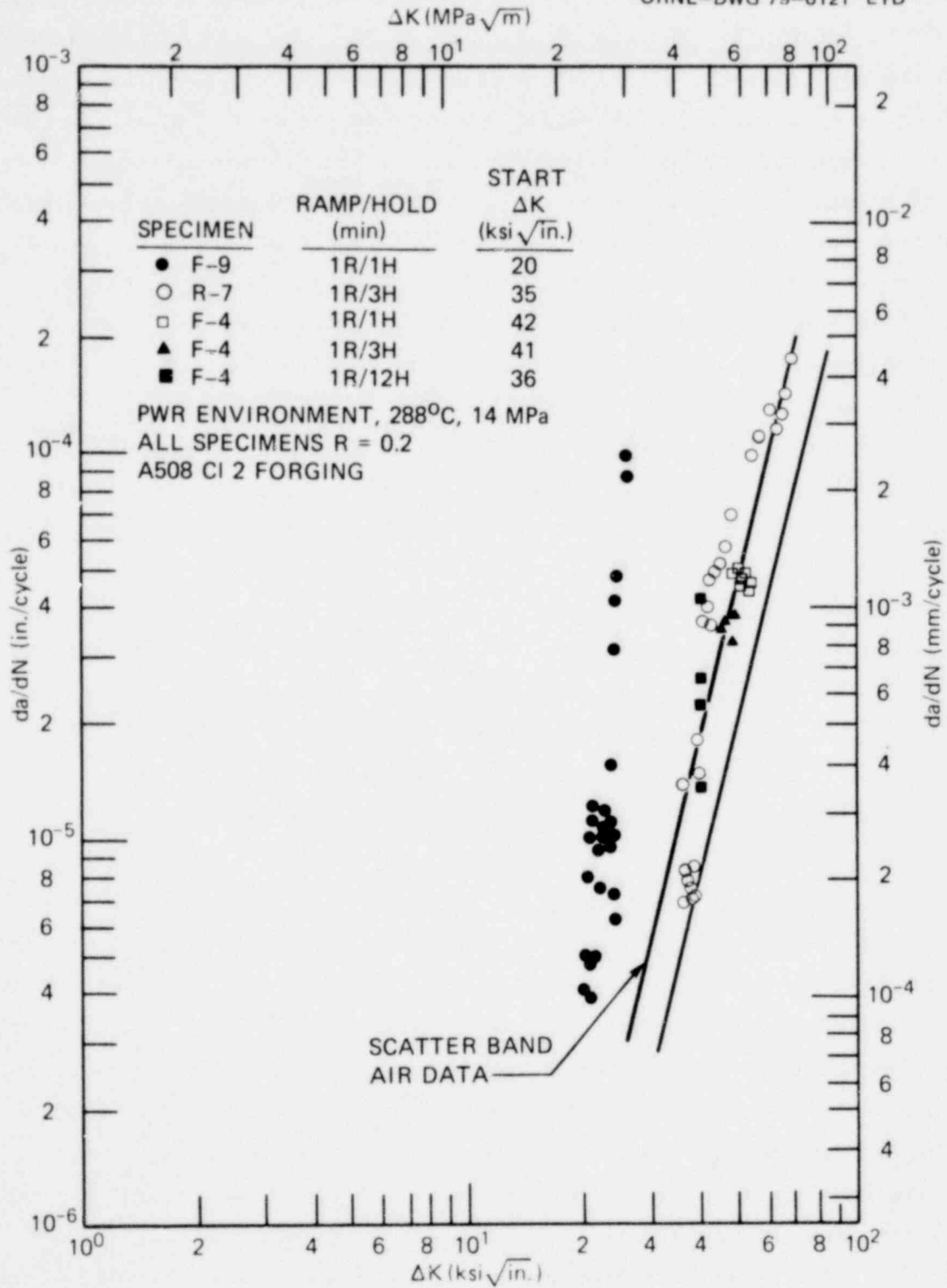
Fig. 3.18. Examples of starting condition effects.

mechanically induced crack growth rate is faster than the environment can influence it, and no enhancement is observed. In the reactor water environment, this lack of environmental influence is continued throughout the test, while in other steel-environment combinations, the environment will gradually catch up to the moving crack, and the enhancement will intensify until a steady-state behavior of full enhancement is obtained.[5] Further evidence that this effect is strongly dependent on the material and environment combination is provided by a series of tests conducted in hydrogen sulfide gas, as shown in Fig. 3.19. In this environment,
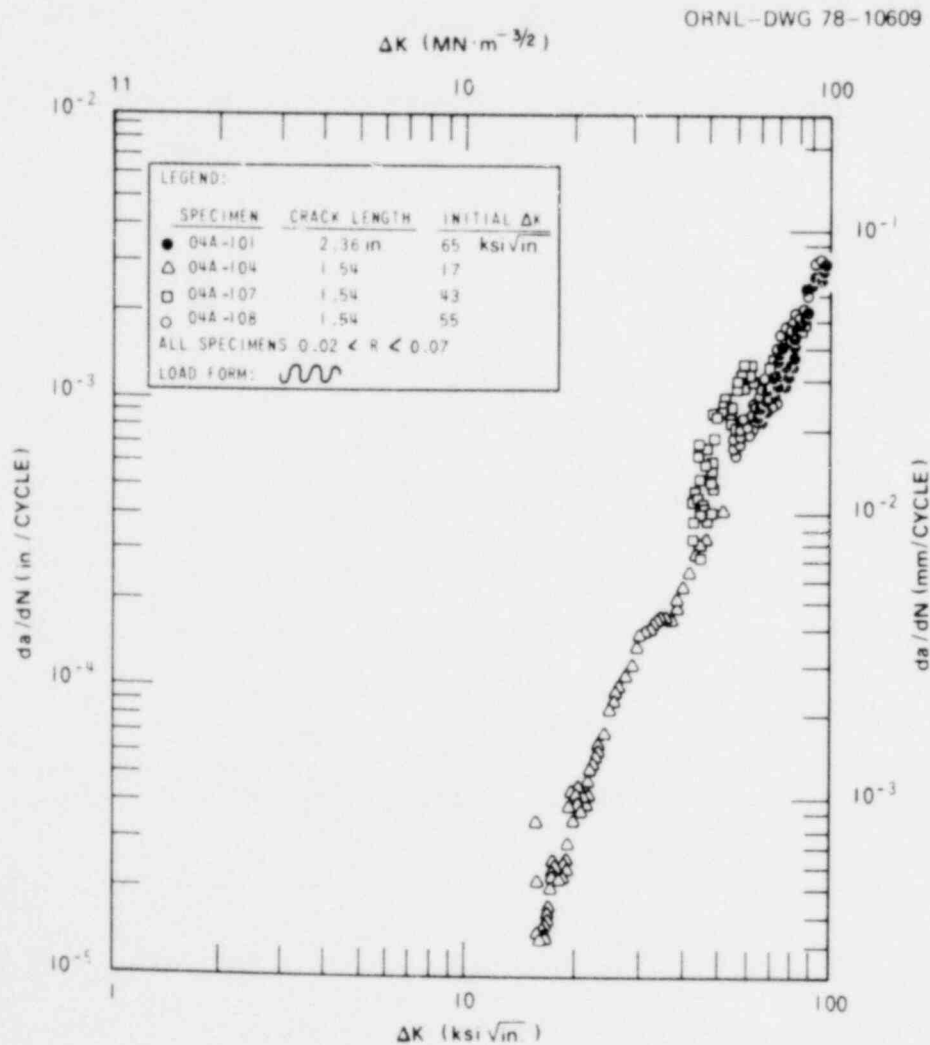
Fig. 3.19. Effect of starting conditions on fatigue-crack-growth rates in reactor pressure vessel steel in hydrogen sulfide at room temperature.

there is no effect of starting conditions, presumably because the environmental kinetics are so fast that the hydrogen can keep up with the crack no matter how fast it is growing.

Clearly there is much more to be done to fully understand this element of the environmental crack growth rate behavior, but, for the present, it must be emphasized that crack growth rate tests should not be started at high values of applied stress-intensity factor. Based on present evidence, to avoid this effect, a test should not be started at an applied K_{max} greater than 33 MPa$\sqrt{m}$.

3.3 Crack Growth Rates at High ΔK

Testing is continuing on specimen 04AE1, a 101.6-mm-thick specimen of HSST Plate 04, being tested at R = 0.7.

References

1. R. H. Bryan et al., *Test of 6-in.-Thick Pressure Vessels, Series 3: Intermediate Test Vessel V-7B*, ORNL/NUREG-38 (October 1978).

2. D. A. Hale, J. Yuen, and T. Gerber, *Fatigue Crack Growth in Piping and Reactor Pressure Vessel Steels in Simulated PWR Environment*, General Electric Company, GEAP 24098/NRC-5 (January 1978).

3. W. H. Cullen et al., *Fatigue Crack Growth of A508 Steel in High Temperature Pressurized Reactor Grade Water*, NUREG/CR-0942, NRL Memorandum Report 4063 (July 1979).

4. G. D. Whitman and R. H. Bryan, *Heavy-Section Steel Technology Program Quart. Prog. Rep. October—December 1978*, ORNL/NUREG/TM-298 (April 1979).

5. R. P. Wei, "On Understanding Environment Enhancement Fatigue Crack Growth — A Fundamental Approach," *Fatigue Mechanisms*, ASTM STP 675, to be published in 1979.

4. INVESTIGATIONS OF IRRADIATED MATERIALS*

4.1 Toughness Investigations of Irradiated
Materials — Fourth HSST
Irradiation Series

R. G. Berggren   J. W. Woods
T. N. Jones   D. A. Canonico

Final detailed design of the capsules for the Fourth HSST Irradiation Series is complete. Fabrication of capsule parts, preparation of neutron dosimeters, specimen preparation, and control system modifications for the first capsule are all in progress.

Four weldments are now on hand, and two additional materials are being obtained for irradiation in the other three capsules planned for this irradiation series.

4.2 Ductile Fracture Toughness from the J-R Curve
Method Using Computerized Unloading
Compliance Testing†

J. A. Williams‡   K. W. Carlson‡

Based on the results reported in the previous quarterly progress report, a set of procedures for conducting unloading compliance J-R curve tests using the interactive computer data acquisition and processing system was developed. Contained in these procedures are numerous checks on the systems and test conditions. Having established these guidelines, the "a/W-sidegroove test matrix" was completed and analyzed; these results are summarized in this progress report. Also during this quarter, preliminary work leading to the testing of 0.5T irradiated CT specimens was initiated.

---

*Conversions from SI to English units for all SI quantities are listed on a foldout page at the end of this report.

†Research performed under Purchase Order 11Y-50917V for the Oak Ridge National Laboratory, operated by Union Carbide Corporation.

‡Hanford Engineering Development Laboratory.

4.2.1 Scope

In light of the needs of the J-integral fracture toughness testing criteria, the objective of this investigation was to determine the effects of relative crack length, a/W, and sidegrooving of the remaining ligament section on the J-R curve. Sidegrooving is of interest because it increases the degree of stress-state triaxiality ahead of the crack tip, thus imposing a larger degree of plane strain behavior. Because of the desirability of a single specimen test for nuclear reactor applications, the unloading compliance technique was employed to generate the J-R curve. Therefore, a second objective of this study was to explore and establish analytical procedures for unloading compliance J-R curve tests.

4.2.2 Procedure

The material used in this investigation was ASTM A533 Grade B Class 1 (A533-B1) steel; the composition and mechanical properties are reported elsewhere.[1-4] In an attempt to encourage comparable data, a set of guidelines for testing and analysis was agreed upon by a group of HSST contractors at a meeting in Annapolis, Maryland, in September 1978. These guidelines served as a basis for this investigation and are described in this section.

To systematically assess the effect of a/W and sidegrooving on the J-R curve, a test matrix was established varying a/W and depth of sidegrooving. All specimens were 1T compact specimens (CSs) with varying notch depths so that, after fatigue precracking, there were three specimen groups each having a/W values of 0.5, 0.6, 0.7, and 0.8. In each of these groups, one specimen was left with a smooth surface (0% sidegrooving), one was given 45° V-shaped sidegrooves to a total depth of 10% (5% on each side) of the thickness, and the third was given sidegrooves to a total depth of 20% of the thickness.

The fracture toughness tests were conducted at 149°C, where uppershelf behavior was observed. The temperature was controlled to ~±2 K in an air-circulating electrically heated furnace. The specimen temperature was sensed with a thermocouple attached to the specimen surface.

The tests, which were performed on an 89.0-kN-capacity (20,000-lb), closed-loop, servo-controlled, hydraulic test system, were conducted in stroke control at a rate of 0.5 mm/min. Loading clevises with flat bottom holes were used to test the compact specimens, and the load was monitored by the system load cell. Two independent extensometer systems were used to measure displacement. A dual linear variable differential transformer (LVDT) system described elsewhere[5] was mounted on the front face straddling the load points on each side of the specimen. The signals from the LVDTs were added to give average displacement measurements. An electrical resistance clip gauge (CG) was also mounted on razor blades affixed to the crack notch at the load line.

To compute J for the compact specimens, the formula developed by Rice et al.,[6] modified for the tensile component of load after Merkle and Corten,[7] and shortened by the ASTM Task Group E24.01.09,[8] was used:

$$J = \frac{2A}{Bb} \frac{(1 + \alpha)}{(1 + \alpha^2)} , \tag{1}$$

where

$$\alpha = \left[\left(\frac{2a_o}{b}\right)^2 + \frac{4a_o}{b} + 2 \right]^{1/2} - \left(\frac{2a_o}{b} + 1\right) , \tag{2}$$

and

A = area (energy) under the load-deflection record,

B = thickness (net section thickness for sidegrooved specimens),

b = remaining uncracked ligament,

a_o = initial crack length.

To compute crack length from the measured compliance, the compliance equation developed by Saxena and Hudak[9] was used:

$$a/W = 1.000196 - 4.06319\ U + 11.242\ U^2$$
$$- 106.043\ U^3 + 465.335\ U^4 - 650.677\ U^5 , \tag{3}$$

where

$U = 1/(\sqrt{ECB} + 1)$,

E = elastic modulus,

C = compliance.

The initial crack length was computed from the mean of ten compliance measurements at very low load levels. Crack extension was computed by subtracting this value from subsequent computed crack lengths.

To determine the J_{Ic} value, representation of the crack-tip blunting behavior and crack extension behavior was necessary. The intersection of the lines representing these two phenomena was taken as the J_{Ic} value. The analysis agreed on was based on the recommended procedures.[8] The blunting line was taken as following the theoretical relationship

$$\Delta a = J/2\sigma_o , \tag{4}$$

where

σ_o = flow stress = $(\sigma_y + \sigma_{ts})/2$,

σ_y = yield stress (0.2% offset),

σ_{ts} = ultimate tensile stress.

The crack extension data points used were contained in the interval defined by two lines parallel to the blunting line, Eq. (4), displaced 0.754 and 1.397 mm along the crack extension (Δa) axis. The crack extension portion of the R curve was a least-squares linear regression through these points.

After completion of the test, the specimen was heat-tinted in a furnace at 649°C and then broken after cooling in liquid nitrogen. The blue oxide coating clearly delineates both the fatigue precrack and the crack extension from the fracture toughness test; these quantities were measured under a microscope with a vernier calibrated traveling stage. To measure crack extension on curved crack fronts, crack extension measurements were made at nine equally spaced points along the crack front. The crack extension was taken as the mean of eight points: the seven interior measurements plus the average of the two surface measurements.

The initial crack length, as measured on the specimen fracture surface, was used to recompute the J values.

A minicomputer system described in previous quarterly progress reports was used for data acquisition and computation. During an unloading compliance J-integral test, the specimen is unloaded about 10% at frequent intervals and the compliance measured. The system was programmed to accurately measure load and displacements, compute the compliance, and assess the accuracy of compliance measurements. Real-time computations of the crack length, the compliance, and the estimated J values were made and printed at the time of each unloading; all data were stored on a magnetic disk. While performing these tasks, the x-y recorder was auto-graphically producing the load-deflection record. On completion of the test, the data from all the unloadings were assembled and plotted as a temporary J-R curve. After subsequent crack length measurements were made from the broken specimen, the data were recalled from the magnetic disk, and new J and Δa data were computed and plotted as a final J-R curve; these new data were also stored on the magnetic disk. With all data permanently stored on the magnetic disks, the data were easily retrievable for subsequent analyses or replay.

4.2.3 Results and discussion

The analysis agreed on for use in this investigation utilized the blunting line approximation given in Eq. (4). The data points included for analysis of the crack extension line of the R curve were those between the two offset lines described. The intersection of the blunting and crack extension line was defined as the onset of crack extension, and the J value at this point was attributed to the J_{Ic} designation. Paris et al.[10] have suggested that the slope of the crack extension line is related to a parameter that describes stable crack extension; the "tearing modulus," T, is given by

$$T = (dJ/da)(E/\sigma_o^2) \ , \tag{4.5}$$

where

> dJ/da = slope of the crack extension line,
>
> E = modulus of elasticity,
>
> σ_o = flow stress.

The J_{Ic}, dJ/da, and T results for this matrix of tests will be presented in detail in a topical report that is in preparation. Some of the important observations derived from these results include the following.

1. The R curves developed from crack extension computed from the LVDT and clip gauge compliances are different from one another for the same test. In some specimens, particularly those with smaller a/W and no sidegrooving, the difference was large. For deeper cracks and side-grooves, the differences were essentially negligible. The disparity between the R curves developed from the clip gauge and LVDT compliance is the subject of an ongoing investigation.

2. The two extensometers are attached at physically different locations and give different compliance values on a given specimen. Thus, it was deemed expedient to model the compliance behavior of each extensometer separately by employing different compliance relationships. The Saxena-Hudak relationship was found to work quite satisfactorily for the clip gauge location at the load line on the crack plane. A tenth-order polynomial was developed to model the LVDT behavior for its location mounted on the front face straddling the load line.

3. The compliance equations were accurate for predicting the initial crack lengths where the crack fronts were relatively straight. Final crack lengths were consistently underestimated, because crack front tunneling produced a deviation between the measured average crack length and that predicted by the compliance relationships. Therefore, the crack extension was consistently underestimated.

4. As both a/W and the depth of sidegrooving increase, the degree of triaxiality through the thickness of the specimen at the crack tip increases. The resulting higher constraint tends to give straighter crack fronts with tunneling reduced or eliminated.

5. Another consequence of the increased constraint is that J_{Ic} decreases, in general, as a/W and depth of sidegrooving increase. J_{Ic} seems to approach some minimum plane strain value.

6. It was also noted that the slope of the crack extension line on the R curve decreased as a/W and depth of sidegrooving increased.

7. Further work is needed to obtain an understanding of the relationship between compliance behavior of each of the extensometers and the crack-tip blunting and crack extension phenomena at the crack tip. To accomplish this, multiple-specimen heat-tint R curves should be developed for a number of specimen sizes in the test matrix studied in this investigation.

References

1. C. E. Childress, *Fabrication History of the First Two 12-Inch Thick ASTM A533 Grade B Class 1 Steel Plates of the Heavy Section Steel Technology Program, Documentary Report 1,* ORNL-4313 (February 1969).

2. J. A. Williams, *Heavy Section Steel Technology Program Technical Report No. 31 — The Irradiation and Temperature Dependence of Tensile and Fracture Properties of ASTM A533 Grade B Class 1 Steel Plate and Weldment,* HEDL-TME 73-75 (August 1973).

3. J. M. Steichen and J. A. Williams, *Heavy Section Steel Technology Program Technical Report No. 32 — High Strain Rate Tensile Properties of Irradiated ASTM A533-B Pressure Vessel Steel,* HEDL-TME 73-74 (July 1973).

4. W. J. Stelzman and R. G. Berggren, *Radiation Strengthening and Embrittlement in Heavy Section Steel Plates and Welds,* ORNL-4871 (June 1973).

5. W. J. Mills, L. A. James, and J. A. Williams, "A Technique for Measuring Load-Line Displacements of Compact Ductile Fracture Toughness Specimens at Elevated Temperatures," *J. Test. Evaluation* 5(6), 446—51 (November 1977).

6. J. R. Rice, P. C. Paris, and J. G. Merkle, "Some Further Results of J-Integral Analysis and Estimates," *Progress in Flaw Growth and Fracture Toughness Testing,* ASTM STP 536, pp. 231—45 (1973).

7. J. G. Merkle and H. T. Corten, "A J-Integral Analysis for the Compact Specimen, Considering Axial Force as Well as Bending Effects," *J. Pressure Vessel Technol.,* American Society of Mechanical Engineers (1974).

8. G. A. Clarke et al., "A Procedure for the Determination of Ductile Fracture Toughness Values Using J Integral Techniques," *J. Test. Evaluation* 7(1), 49—56 (January 1979).

9. A. Saxena and S. J. Hudak, Jr., *Review and Extension of Compliance Information for Common Crack Growth Specimens*, Westinghouse Scientific Paper 77-9E7-AFCGR-P1 (May 1977).

10. P. C. Paris et al., "Instability of the Tearing Mode of Elastic-Plastic Crack Growth," *Elastic Plastic Fracture*, ASTM STP 668, p. 1 (1979).

1439 268

5. PRESSURE VESSEL INVESTIGATIONS

R. H. Bryan

The feasibility of a number of types of tests utilizing intermediate-scale vessels is under consideration. Two types of experimental investigations of particular interest are conceptually possible. One type of test would demonstrate the behavior of low upper-shelf material; the other involves thermal fatigue tests and pressurized thermal shock tests.

The behavior of low upper-shelf material is of interest for at least two reasons. The practical reason is that such material is in use in some reactor pressure vessels. Secondarily, a critical comparison of the theory of elastic-plastic fracture mechanics (EPFM) with experimental results from a test at upper-shelf temperatures of this material has not been carried out. Thus, there has been no experimental demonstration of how well, if at all, EPFM characterizes upper-shelf fracture behavior in the material of interest. A test vessel for this type of investigation might have a flaw implanted in a specially designed weld deposit in the cylindrical course of the vessel.

Thermally induced stresses are known to generate cracks, particularly in nozzle-corner regions. For this reason, as well as the fact that analysis of nozzle-corner cracks is still a developing art, a series of tests of nozzle-corner cracks under cyclic pressure or thermal loads is being considered.

Further work must be concluded before the feasibility of either concept can be determined.

1439 269

6. THERMAL SHOCK INVESTIGATIONS*

R. D. Cheverton

6.1 Introduction

During this report period for the Thermal Shock Program, a three-dimensional fracture mechanics analysis of TSE-2 was performed, final preparations were made for TSE-5, two thermal-hydraulic thermal shock experiments were conducted in the liquid nitrogen thermal shock test facility (LN$_2$-TSTF), development of the EB-weld flawing technique for TSE-5 was completed, and an appropriate tempering temperature for TSC-1 was determined.

6.2 Calculation of Stress-Intensity Factors for TSE-2 Intermediate and Final Crack Shapes

S. K. Iskander   D. G. Ball
R. S. Wallace

The flaws involved in TSE-2[1,2] were three-dimensional in nature and are being calculated by means of a three-dimensional finite-element (FE) analysis technique. The FE meshes for the TSE-2 intermediate and final crack shapes were presented in the previous quarterly progress report.[3] This report discusses preliminary FE analysis results for these crack shapes.

For the purpose of the FE analyses, the actual crack fronts for the initial, intermediate, and final crack shapes are represented by circular arcs. The initial flaw is semicircular and thus is represented by a single arc with its center on the inner surface of the test specimen. The intermediate and final crack shapes are not symmetrical, and, with the exception of one segment of the intermediate crack, they are not normal to the inner surface. Each of these crack shapes is represented by two different arcs tangent to each other at the deepest point of the crack and with their centers located off the surface of the test specimen, as shown in Fig. 6.1.

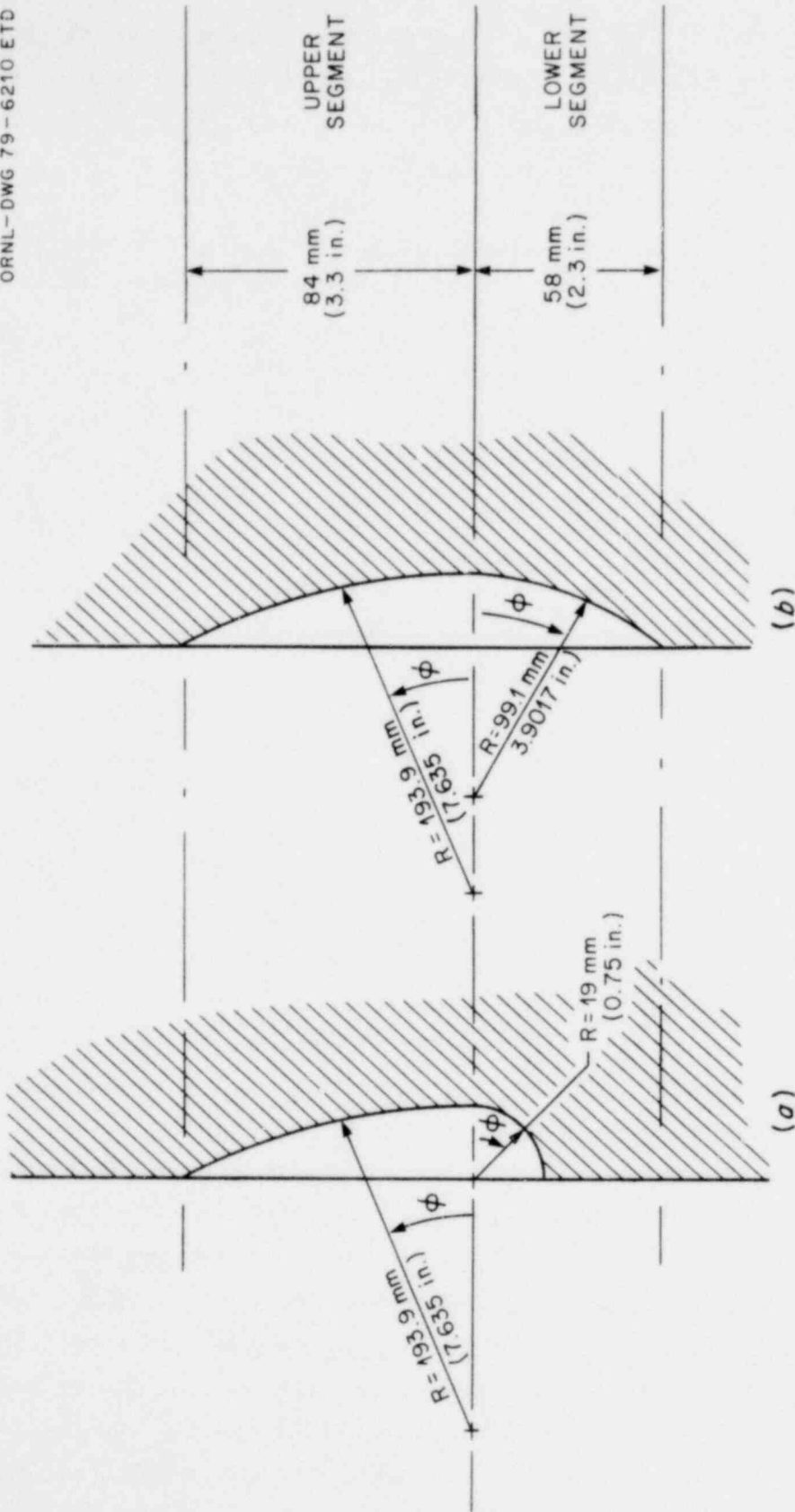*Conversions from SI to English units for all SI quantities are listed on a foldout page at the end of this report.

Fig. 6.1. Idealized crack shapes: (a) intermediate; (b) final.

The FE results for the intermediate crack shape at the instant this crack shape developed (30 sec) are given in Table 6.1. Some of these data are plotted in Fig. 6.2, which shows K_I as a function of position along the crack front.

Table 6.1. Stress-intensity factors and K_I/K_{Ic} for TSE-2 at 30 sec (KICTYP = 5)

Angle (ϕ)	Radius (mm)	Depth (mm)	a/W	Temperature (°C)	Tangential stress (MPa)	K_I (MPa√m)	K_{Ic} (MPa√m)	K_I/K_{Ic}
				Upper segment				
1.9	139.598	18.948	0.130	212.8	134.58	68.87	295.44	0.233
7.06	138.227	17.577	0.120	205.3	159.63	80.70	231.68	0.287
10.08	136.271	15.621	0.107	193.5	199.82	88.69	260.32	0.341
16.0	132.182	11.532	0.079	163.7	302.07	98.34	209.97	0.468
18.8	129.362	8.712	0.060	139.6	386.24	99.71	173.01	0.576
21.3	126.492	5.842	0.040	112.7	482.11	94.48	138.88	0.680
25.25	121.183	0.533	0.004	58.9	679.99	77.13	96.92	0.796
				Lower segment				
−3.3	139.675	19.025	0.130	213.2	133.27	52.07	296.18	0.176
−12.3	139.268	18.618	0.127	211.1	140.39	49.86	292.22	0.171
−18.8	138.684	18.034	0.123	207.9	151.01	50.41	286.38	0.176
−26.9	137.643	16.993	0.116	201.9	171.07	52.34	275.51	0.190
−33.2	136.576	15.926	0.109	195.4	193.20	55.36	263.78	0.210
−41.9	134.823	14.173	0.097	183.7	233.18	60.04	243.26	0.247
−48.1	133.375	12.725	0.087	173.0	269.68	65.29	225.29	0.290
−56.5	131.166	10.516	0.072	155.3	331.19	73.82	196.70	0.375
−63.1	129.261	8.611	0.059	138.7	389.46	82.09	171.69	0.478
−71.8	126.619	5.969	0.041	113.9	477.67	91.18	140.20	0.650
−78.1	124.587	3.937	0.027	93.8	550.58	101.64	121.25	0.838
−86.8	121.717	1.067	0.007	64.4	659.24	110.19	99.36	1.098

As shown in Fig. 6.2, the values of K_I are markedly different for each of the crack segments. For the arc segment with the smallest radius of curvature (lower segment), the K_I values decrease monotonically from the value at the surface to a minimum near the bottom. The upper segment of the crack has a maximum K_I about 8.9 mm below the surface. A similar shift in position of the maximum K_I value from the surface to below the surface as the crack shape changes from semicircular to semielliptical was previously obtained with an approximate technique for calculating K_I[4] and was reported in Ref. 1.
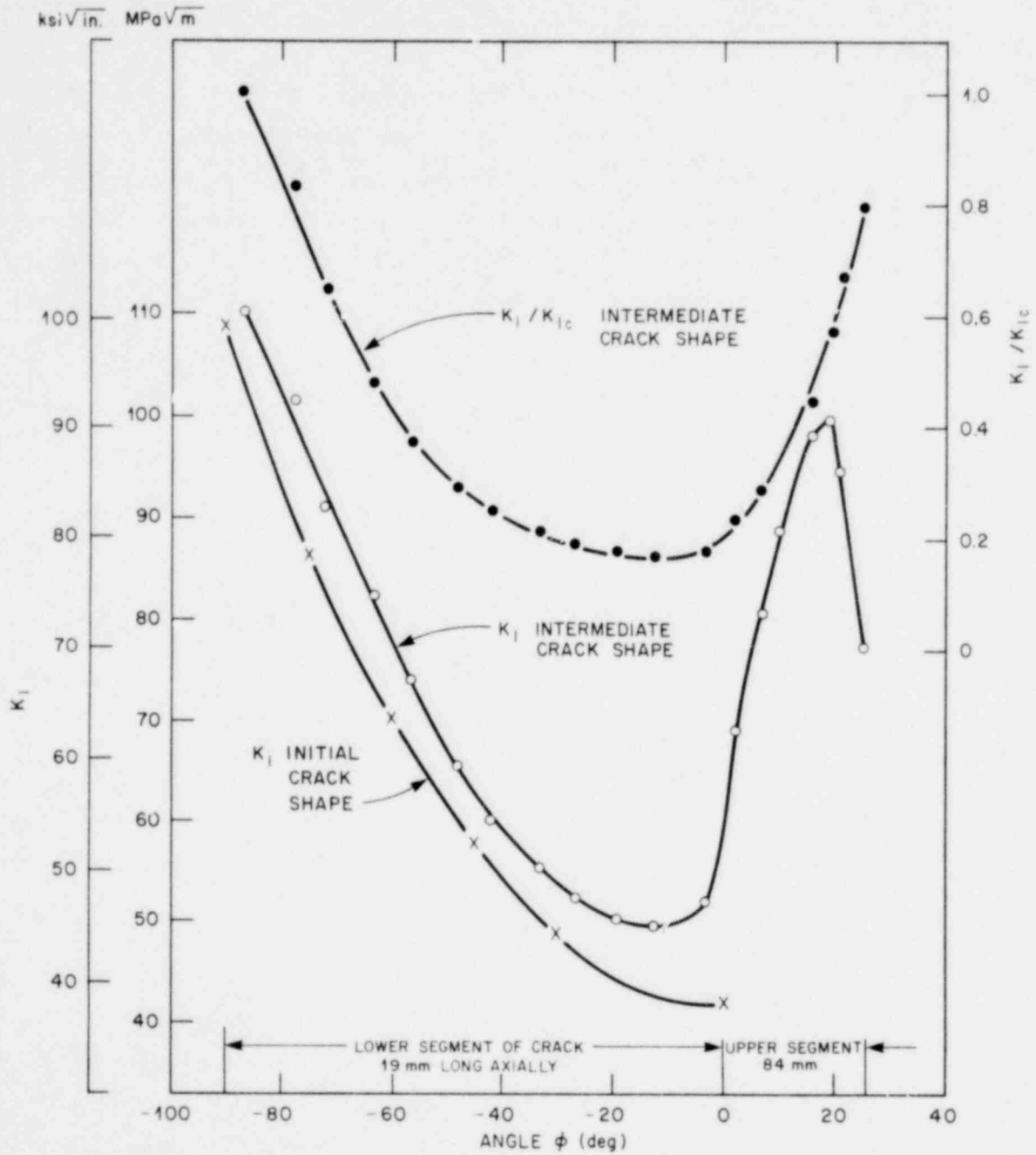
ORNL—DWG 79—6211 ETD

Fig. 6.2. K_I for initial and intermediate crack shapes and K_I/K_{Ic} for intermediate crack shape, all at time = 30 sec during TSE-2.

The K_I/K_{Ic} ratio* has also been plotted on Fig. 6.2. As indicated, essentially all of the crack front has K ratios of less than unity. This is reasonable, because, at this time in the transient, the crack has just arrested.

The final crack shape (Fig. 6.1) developed at ~1.5 min into the thermal transient and was analyzed for temperature distributions corresponding to times of 1, 1.5, 2, 3, 5, 8, and 15 min. The K_I values reached a maximum at ~3 min, and the variation of K_I with respect to the position on the crack front for this time is shown in Fig. 6.3. Plots for the other times

---

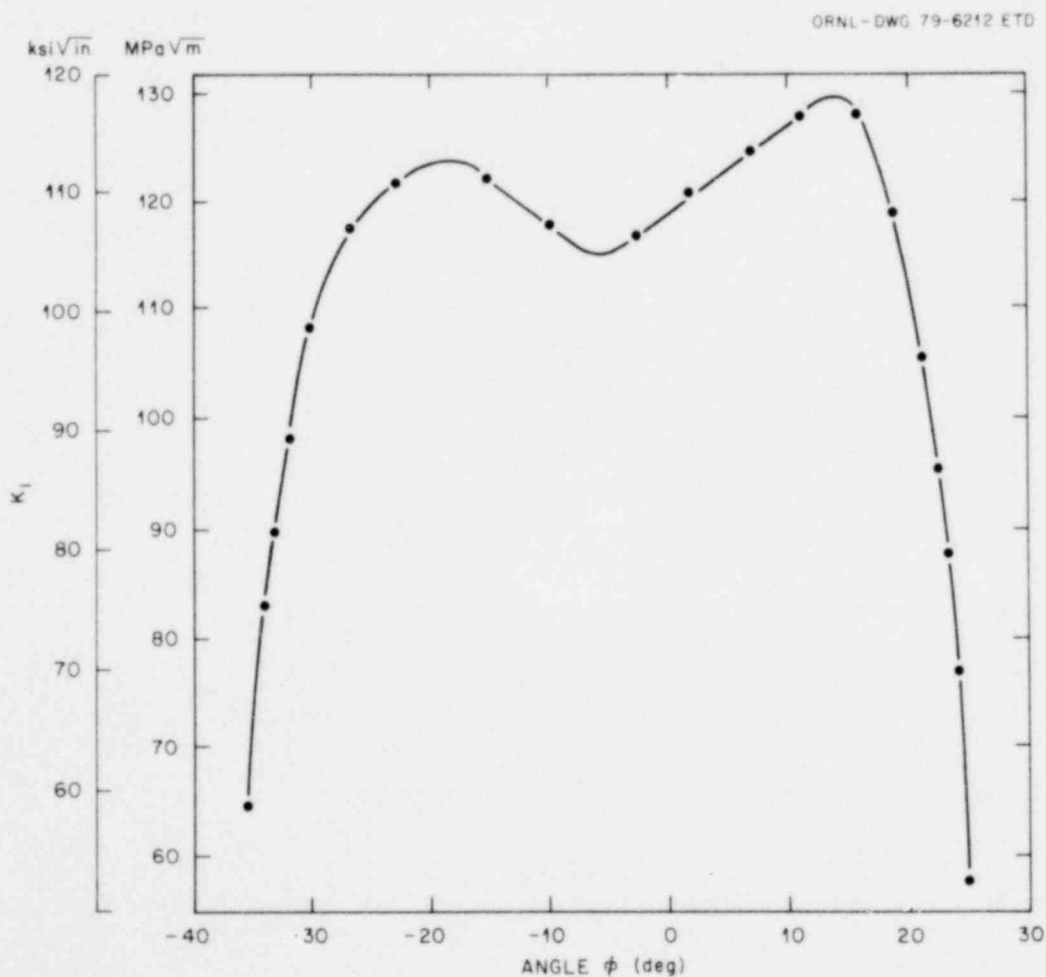*The values of K_{Ic} are from Ref. 5.

Fig. 6.3. K_I vs position along crack front (φ) for final crack shape at time = 180 sec during TSE-2.

1439 274

in the transient are similar in shape but are shifted vertically downward with respect to the one shown.

The variation of K_I and K_{Ic} with respect to time for two points ($\phi = 16.0$ and $1.9°$) on the upper segment of the final crack front is shown in Fig. 6.4. The point $\phi = 16.0°$ is ~11 mm below the surface and is the approximate location of $(K_I)_{max}$ for the times mentioned above (see Fig. 6.3); $\phi = 1.9°$ is near the deepest point of the crack (~19 mm). The K_I/K_{Ic} values for a point near the inside surface of the test specimen ($\phi = 25.25°$) were all less than 0.8.

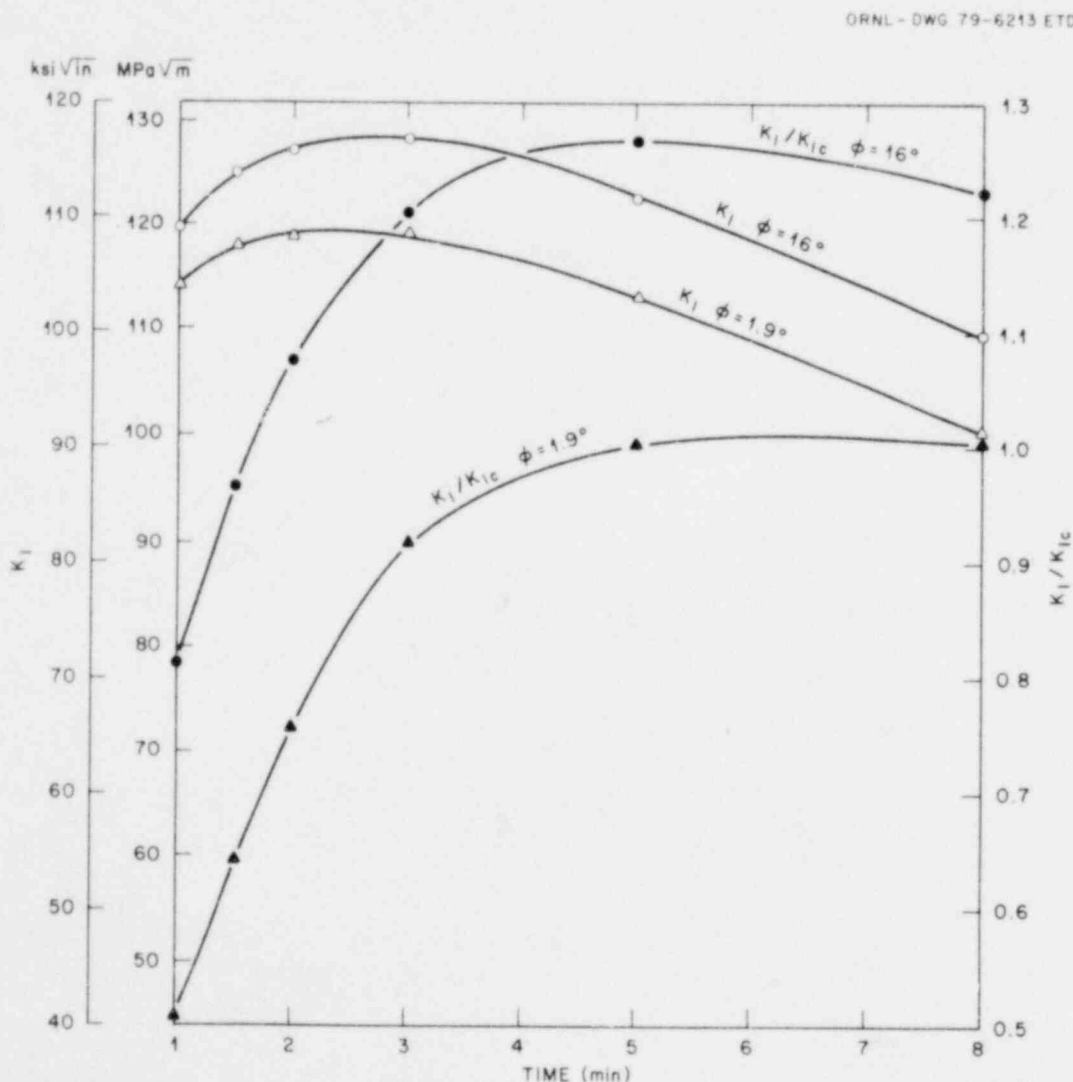ORNL-DWG 79-6213 ETD

Fig. 6.4. K_I and K_I/K_{Ic} as a function of time for two points, $\phi = 1.9$ and $16.0°$, on the upper portion of the crack front.

At the time the final crack shape first appeared (~1.5 min), the K
ratios along most of the crack front were less than unity, as indicated
by the data in Fig. 6.4. This would be expected, because the flaw had
just arrested. At later times, the K ratios over much of the crack front
became equal to and greater than unity; yet, reinitiation did not take
place. This may be because, by this time, K_I all along the crack front
was decreasing with time. However, because of the uncertainties in the
actual values of K_I and K_{Ic}, the possibility also exists that the actual
values of $(K_I/K_{Ic})_{max}$ were simply less than unity.

6.3 TSE-5 Design and Pretest Analysis

6.3.1 Purpose of TSE-5

Four thermal shock experiments have been conducted thus far as a part
of the ORNL HSST Thermal Shock Program. The purpose of these experiments
was to investigate the behavior of shallow surface flaws in thick-walled
steel cylinders under severe thermal shock conditions similar to those that
might be encountered in a pressurized-water reactor (PWR) during a loss-of-
coolant accident (LOCA). The tests were conducted on 533-mm-OD × 152-mm-
wall × 914-mm-long cylinders fabricated from A508 class 2 material (forg-
ing-grade LWR pressure vessel steel). A quench-only heat treatment was
used to achieve low toughness, simulating to some extent the radiation dam-
age in a PWR vessel after ~40 years of service. For three of the experi-
ments, the initial flaws were ~10 mm deep and extended the full length of
the cylinders, while for the remaining experiment, a semicircular flaw
with a radius of 19 mm was used; in all four tests, the flaws were on the
inner surface of the test cylinder. These experiments demonstrated initia-
tion and arrest of shallow flaws under severe thermal shock conditions and
indicated that, at least for shallow flaws, linear elastic fracture mechan-
ics (LEFM) is valid for these loading conditions. These experiments are
discussed in Refs. 1, 2, 5, and 6.

Analysis of the PWR loss-of-coolant accident followed by injection
of emergency core coolant (LOCA-ECC) (Refs. 1, 2, and 6) indicates that,
under some circumstances, a preexisting flaw on the inner surface of the

vessel could propagate deep into the wall and that the extent of propagation would be influenced by the vessel diameter-to-thickness ratio and also by warm prestressing (WPS). Neither of these effects could be investigated in the first four experiments because the test specimen diameter-to-thickness ratio was too small and because the toughness associated with the quench-only heat treatment was too low. Thus, additional experiments were in order.

The purpose of TSE-5 is once again to demonstrate initiation and arrest of an inner-surface flaw under severe thermal shock conditions but this time in tempered material and in a cylinder large enough to allow deep penetration as a result of a larger diameter-to-thickness ratio. A minimum wall thickness of ~150 mm, independent of diameter, was selected much earlier in the program[1] on the basis of heat transfer and fracture mechanics considerations. A secondary purpose is to demonstrate WPS.

6.3.2 Testing technique

Because tempered material is to be used for the TSE-5 test cylinder (designated TSC-1), the sink temperature must be much less than used previously for cracking to occur. Liquid nitrogen (−196°C) appeared to be an appropriate coolant, and three years of development effort[7] have culminated in techniques for overcoming film boiling and vapor binding problems associated with quenching in LN_2. For TSE-5, the inner surface of TSC-1 will be coated with a thin layer (~0.8 mm) of "rubber cement" (3M-NF34) to suppress film boiling, and the ends and outer surface will be well insulated. The thermal shock will be administered to the inner surface by first lowering TSC-1 into a container of LN_2 and then suddenly releasing a nitrogen-gas bubble from the interior cavity, allowing LN_2 to flood the cavity. Natural convection will provide circulation of liquid up through the central cavity and down over the insulation on the outside of the specimen. Nitrogen vapor will exit through the top of the tank containing the LN_2, and most of the entrained liquid will fall back into the tank. Makeup will be provided as necessary. A schematic of the test facility is shown in Fig. 6.5, and Fig. 6.6 is a photograph of the facility as TSC-1 is being lowered into the LN_2 tank during a preliminary thermal-hydraulic experiment.
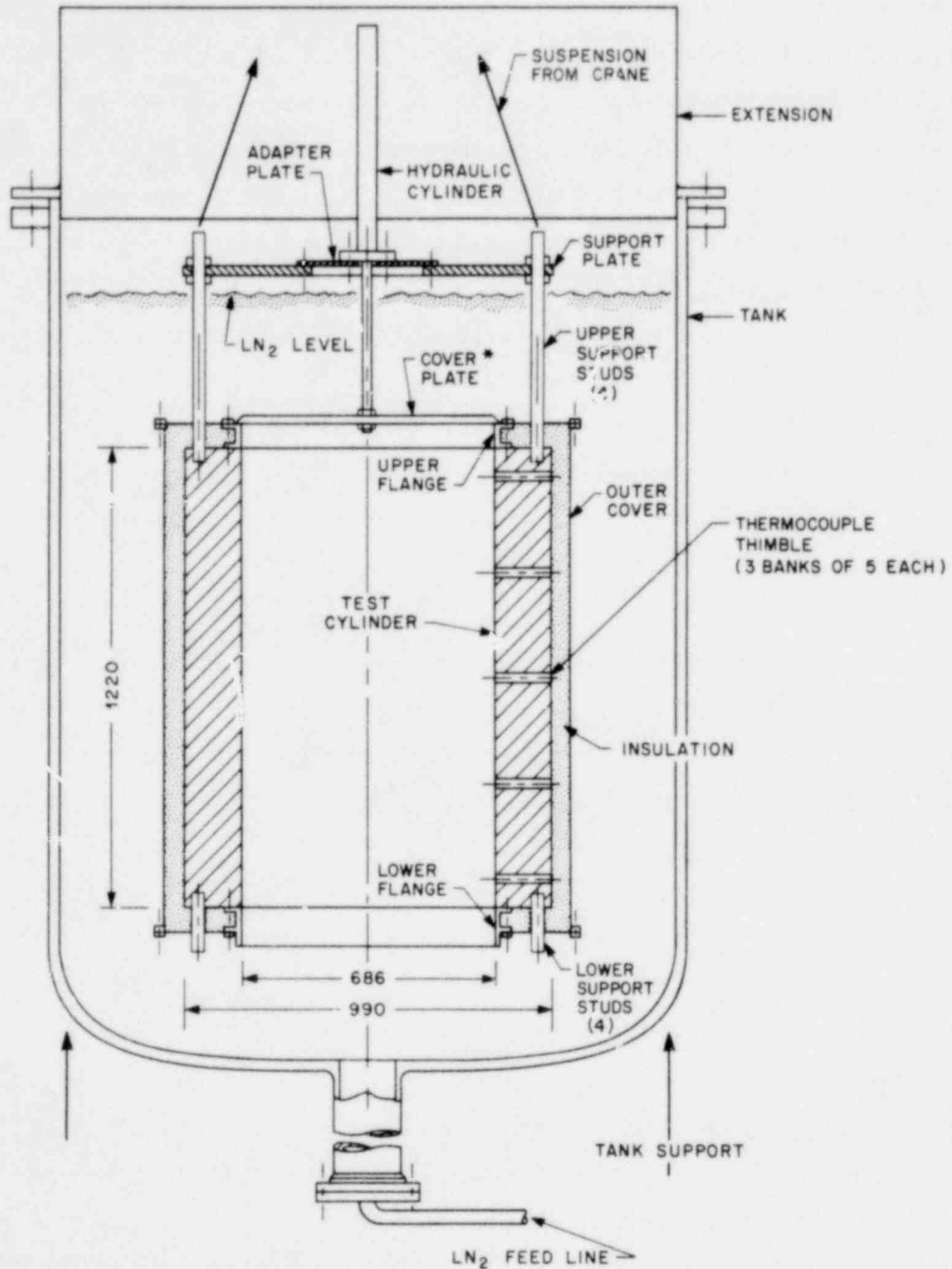
53

Fig. 6.5. Conceptual schematic design of the ORNL LN$_2$-TSTF for 990-mm-OD test cylinders.

ORNL PHOTO 7165—79
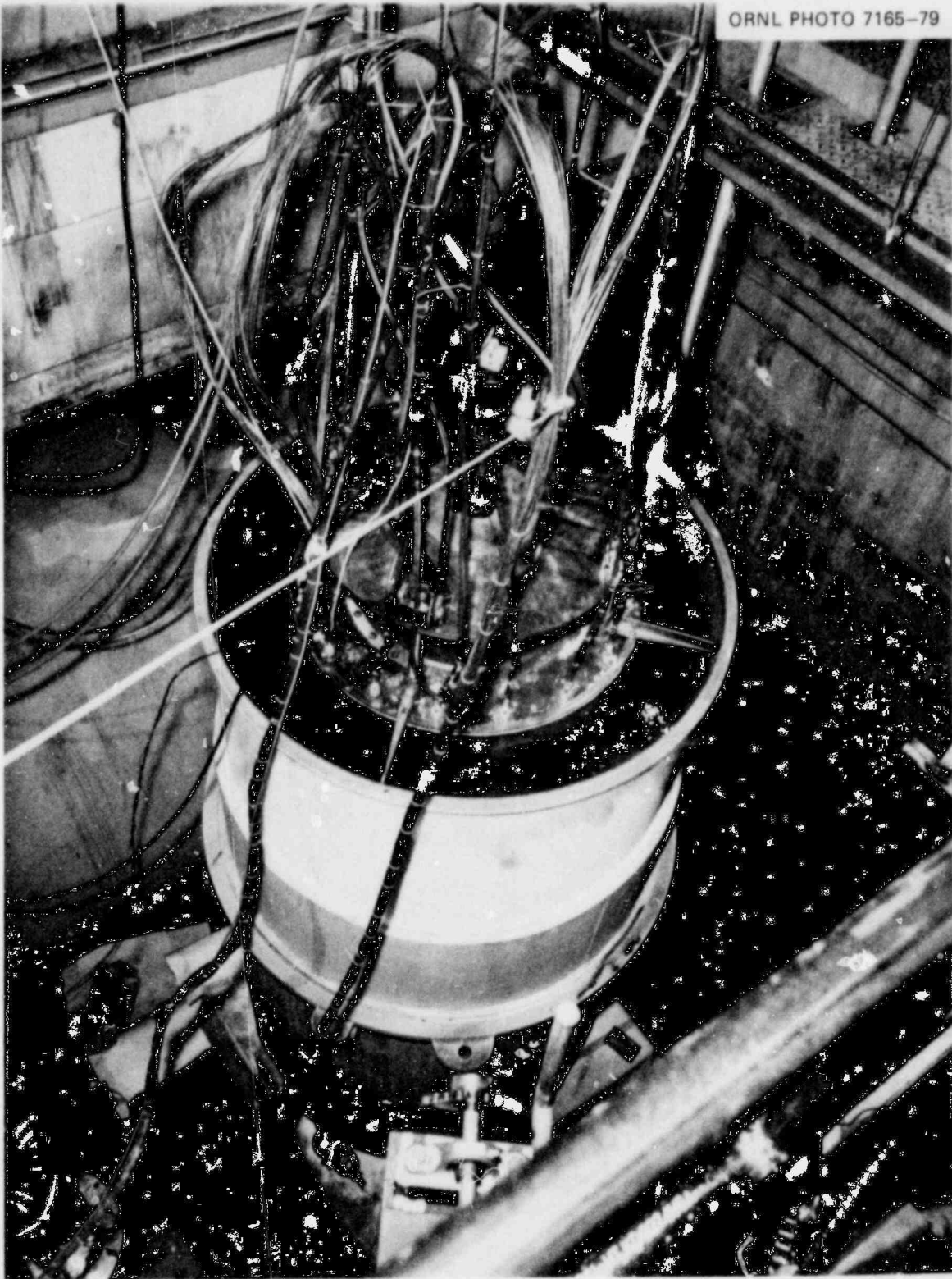
Fig. 6.6. TSC-1 being lowered into the LN$_2$ tank during a thermal-hydraulic experiment.

1439 279

Data retrieved from TSC-1 include indications of crack initiation
and arrest [crack-opening displacement (COD) gauges, acoustic emission,
ultrasonics]; and 12 thermocouples are used to measure the radial tem-
perature distributions in the wall as a function of time at 15 locations
around and along the length of the test specimen, as shown in Fig. 6.5.
These actual temperatures are used in the posttest fracture mechanics
analysis of the experiment.

The severity of the thermal shock and the tendency for vapor accumu-
lation to create axial asymmetry in quenching is controlled by the uni-
formity and thickness of the rubber cement coating on the inner surface.
There is an optimum thickness for maximum heat transfer rates, but this
high rate of heat removal can result in excessive vapor accumulation near
the upper end of the specimen and thus a reduced heat transfer rate in this
location. Minimizing the heat transfer coefficient and the length of the
test cylinder (consistent with other requirements) tends to alleviate the
situation. However, conflicting requirements for minimizing end effects
in the stress analysis[8] and achieving a sufficiently severe thermal shock
generally increase the required heat transfer coefficient and the length
of the specimen; even so, a reasonable compromise was possible. A coat-
ing thickness greater than optimum was used, and the length of the speci-
men was reduced to the minimum permissible.

Another limitation imposed by the particular testing technique is
the initial temperature of TSC-1. Early experiments[9] with the rubber
cement coating indicated a maximum permissible temperature of ~120°C as-
sociated with coating deterioration.

6.3.3 Proposed experiment (TSE-5)

The proposed TSE-5 thermal shock experiment is designed to demon-
strate initiation, arrest, and WPS of a long axial flaw on the inner sur-
face of a tempered, thick-walled steel cylinder having a sufficiently
large diameter that bending effects for fractional crack depths (a/W)
greater than 0.2 will have a substantial effect on the stress-intensity
factor. Two additional criteria for the experiment are that (1) calcu-
lated values of $(K_I/K_{Ic})_{max}$ for crack depths corresponding to initiation
and WPS events must be large enough to accommodate uncertainties in K_I

and K_{Ic} so that initiation prior to WPS is ensured and so that, if at an appropriate time in the transient reinitiation does not take place, this nonevent will be a clear indication that WPS was effective in preventing further propagation; and (2) the length of the test specimen must be sufficient to represent an infinitely long cylinder as far as crack behavior and analysis are concerned.

As shown in Fig. 6.7, the dimensions of TSC-1 are 991 mm OD × 152 mm wall × 1220 mm long. There are fifteen 25-mm-diam holes through the wall that accommodate the thermocouple thimbles shown in Fig. 6.8. The flaw

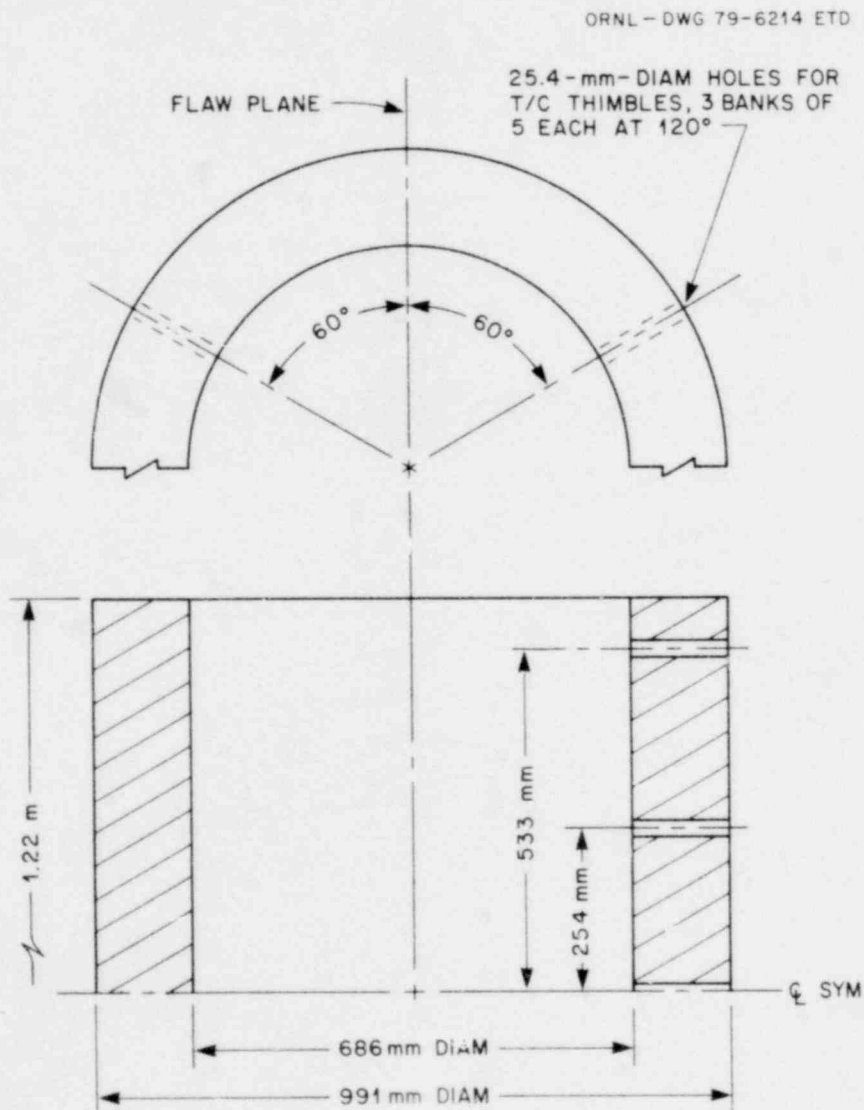ORNL-DWG 79-6214 ETD

Fig. 6.7. Detailed design of TSC-1.
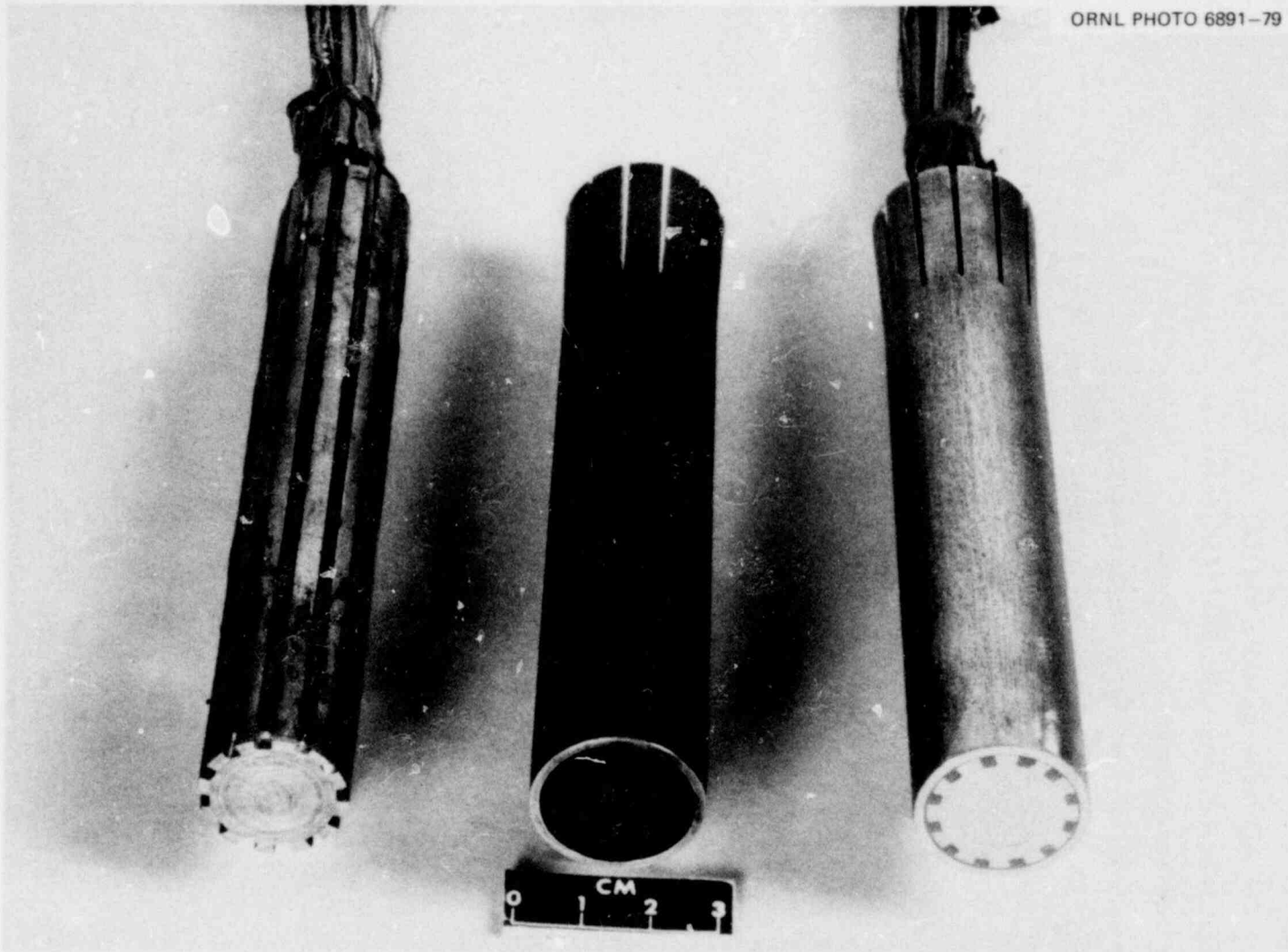
Fig. 6.8. TSE-5 thermocouple thimble components and assembly.

1439 282

is located on the inner surface of the cylinder halfway between two of the three equally spaced banks of thimble holes and is 15 to 18 mm deep. The actual depth of the initial flaw will be determined posttest by destructive means.

The material for TSC-1 is A508 class 2 that has been tempered at an appropriate temperature (613°C) for achieving fracture toughness properties similar to those for HSST Plate 02.[10]

The thickness of the rubber cement coating on the inner surface of TSC-1 will be ~0.8 mm, and the initial temperature of the specimen will be 93°C. Conditions for TSE-5 are summarized in Table 6.2.

Table 6.2. Test conditions for TSE-5

Test specimen	TSC-1
Test specimen dimensions, m	
OD	0.991
ID	0.896
Length	1.22
Test specimen material	A508 Class 2
Test specimen heat treatment	Tempered at 613 C for 4 hr
K_{Ic} vs temperature curve specified	HSST Plate 02 (Ref. 10)
K_{Ic} and K_{Ia} curves used in final analysis	ASME Section XI, Appendix A (Refs. 11 and 12) $RT_{NDT} = -34°C$
Flaw	Long axial sharp crack, a = 15 mm
Temperatures, °C	
Wall (initial)	93
Sink	−196
Coolant	LN_2
Flow rate	Natural convection loop
Coating on quenched surface	Rubber cement (3M-NF34)
Coating thickness, mm	0.76

6.3.4 Fracture mechanics characteristics of TSE-5 (pretest)

During the design phase of TSE-5, calculations were made for different heat transfer and material property conditions, and, finally, the test conditions specified in Table 6.2 were selected. As indicated in

1439 283

this table, the static fracture toughness and arrest toughness curves used
in the final analysis are those in Section XI of the ASME Code[11],[12] with
$RT_{NDT} = -34°C$; these curves are shown in Fig. 6.9. The static fracture
toughness curve obtained in this manner duplicates the nominal HSST Plate
02 data[10] in the temperature range of interest (−46 to +10°C). Early
studies had indicated that the HSST Plate 02 data would be appropriate
for TSE-5.

Results of the analysis corresponding to the conditions in Table
6.2 are presented in Figs. 6.10 and 6.11. Figure 6.10 is the critical-
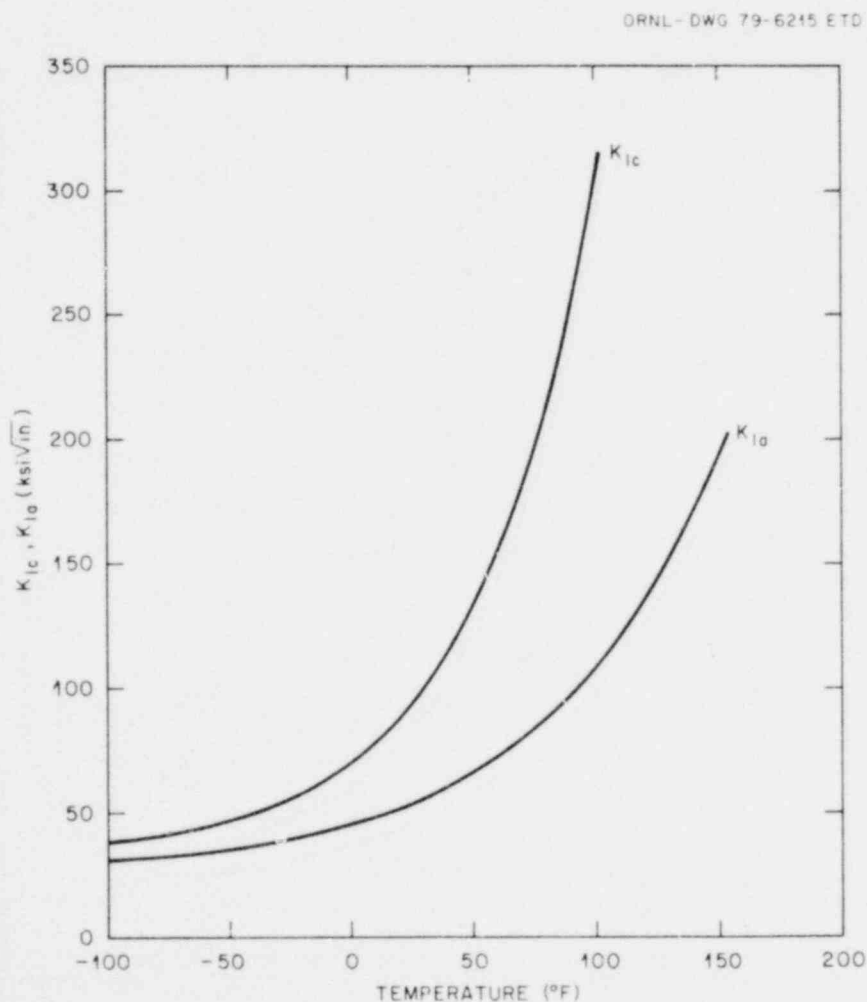crack-depth set of curves showing crack depths vs time corresponding to

ORNL-DWG 79-6215 ETD

Fig. 6.9. Static fracture and arrest toughness curves used in pre-
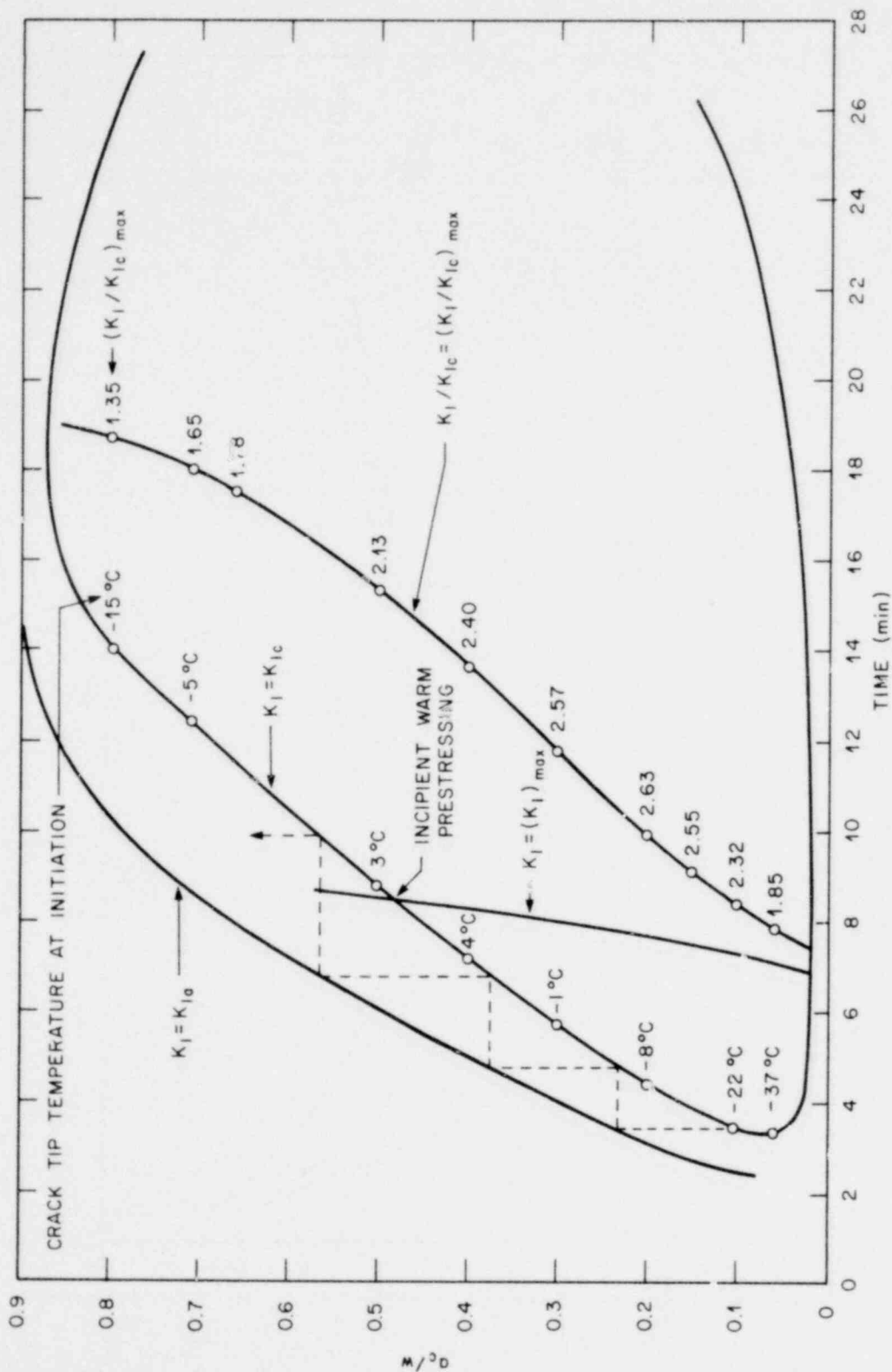test analysis of TSE-5 [ASME Section XI, Appendix A, $RT_{NDT} = -34°C$
(−30°F)].

1439 284

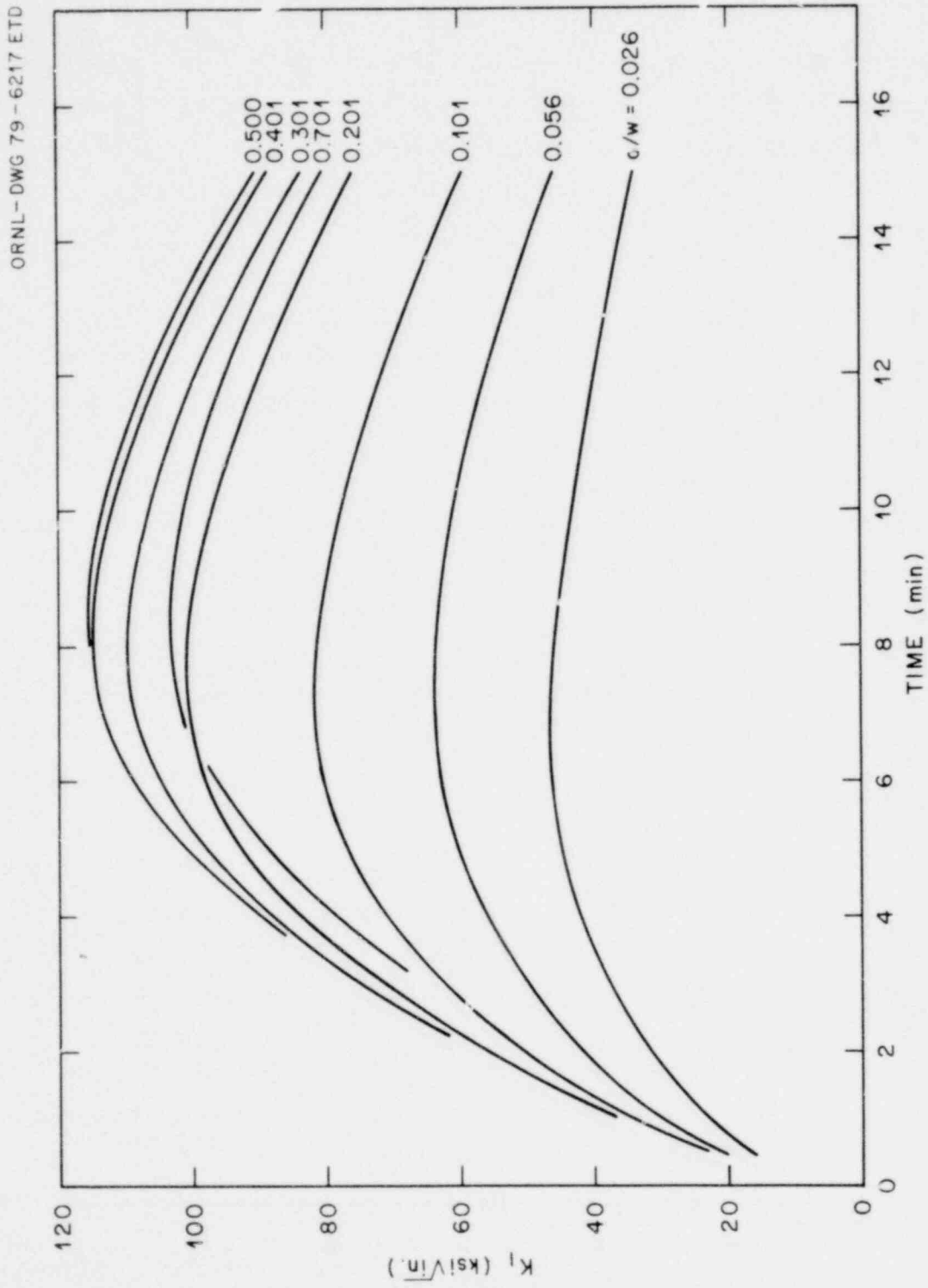Fig. 6.10. Critical-crack-depth curves for pretest analysis of TSE-5.

Fig. 6.11. Stress-intensity factor as a function of time for several crack depths. Pretest TSE-5 analysis.

initiation ($K_I = K_{Ic}$), arrest ($K_I = K_{Ia}$), $K_I = (K_I)_{max}$, and $K_I/K_{Ic} = (K_I/K_{Ic})_{max}$. The crack-tip temperatures corresponding to initiation events and specific values of $(K_I/K_{Ic})_{max}$ are also shown in Fig. 6.10. The dashed line in Fig. 6.10 indicates the possible behavior of the long axial flaw, assuming that the initial fractional flaw depth (a/W) is 0.10. As indicated, the crack front advances in a series of initiation-arrest events, and, if WPS is effective, the final arrested crack depth will be at a/W ~0.56.

Incipient warm prestressing (IWPS) for sharp flaws occurs at a/W ≅ 0.48; if a flaw of this depth initiated, it would arrest at a/W ≅ 0.70. This is the maximum depth to which a flaw could extend, because flaws with depths greater than 0.48 could not initiate, assuming WPS to be effective. The calculations indicate that if WPS is not effective the flaw will extend nearly all the way through the wall.

The crack-tip temperature for the first initiation event is approximately −22°C, and the maximum associated with a subsequent initiation event is 4°C and corresponds to a fractional crack depth of 0.4. As indicated by the curves in Fig. 6.9, this temperature range corresponds to the lower transition region of the fracture toughness curve. Values of K_I (or K_{Ic}) at the times of initiation can be obtained from Figs. 6.9 and 6.11. The maximum value, which corresponds to an initiation temperature of 4°C, is ~127 MN·m$^{-3/2}$.

The requirement that $(K_I/K_{Ic})_{max}$ be sufficiently greater than unity to ensure initiation for a/W < $(a/W)_{IWPS}$ and that it leave no doubt regarding the effectiveness of WPS, should initiation not take place for a/W ≥ $(a/W)_{IWPS}$, is satisfied. For the initial crack depth, $(K_I/K_{Ic})_{max}$ ≅ 2.3, and for the maximum arrested crack depth (a/W = 0.7), $(K_I/K_{Ic})_{max}$ ≅ 1.7.

The actual performance of TSE-5 will depend on how well the assumed heat transfer rate is duplicated and how closely the actual K_{Ic} and K_{Ia} data match the data specified and used in the pretest calculations. Preliminary heat transfer and fracture toughness data obtained specifically for TSE-5 are discussed in the following sections.

6.4 Thermal-Hydraulic Experiments with
TSC-1 in LN₂-TSTF

6.4.1 General

Two thermal-hydraulic experiments were conducted in the LN_2-TSTF with the test specimen (TSC-i) to be used for TSE-5. The purpose of these tests was to shake down equipment, check operational procedures, and investigate further the heat transfer characteristics of the LN_2 quench. The continuing concern over heat transfer is associated with a tendency for axial asymmetry in quenching. Earlier experiments[9] with smaller test specimens and a qualitative analysis[13] indicated that a satisfactory degree of symmetry could be achieved with the TSE-5 test facility and test specimen, but testing with the actual equipment and procedures was necessary for confirmation.

For these first two experiments, TSC-1 did not contain a detectable flaw. Further, the material was in the quench-only (high-strength) condition so that the thermal shock would not result in stresses greater than the yield strength and thus in residual stresses.

6.4.2 First thermal-hydraulic test (LN₂-TSE-TH-1)

In preparation for this experiment, the inner surface of TSC-1 was spray coated with ~0.86 mm of rubber cement (NF-34) in five separate applications. The spray apparatus performed satisfactorily, and the coating was uniform in thickness and surface appearance. Heating of the test cylinder to the desired initial temperature of 93°C was started ~24 hr before the test. At test time, there was a linear axial gradient in temperature from 82°C at the bottom end to 93°C at the top.

The test took place on April 19, 1979, without difficulty, although some modifications in equipment and procedures were indicated and were made posttest in preparation for the second test. A photograph of the test specimen being lowered into the LN_2 tank during LN_2-TSE-TH-1 is shown in Fig. 6.6.

Results from the experiment indicate that the degree of axial symmetry was very good. This is illustrated in Fig. 6.12, which shows the temperature at the innermost thermocouple location (1.27 mm from inner
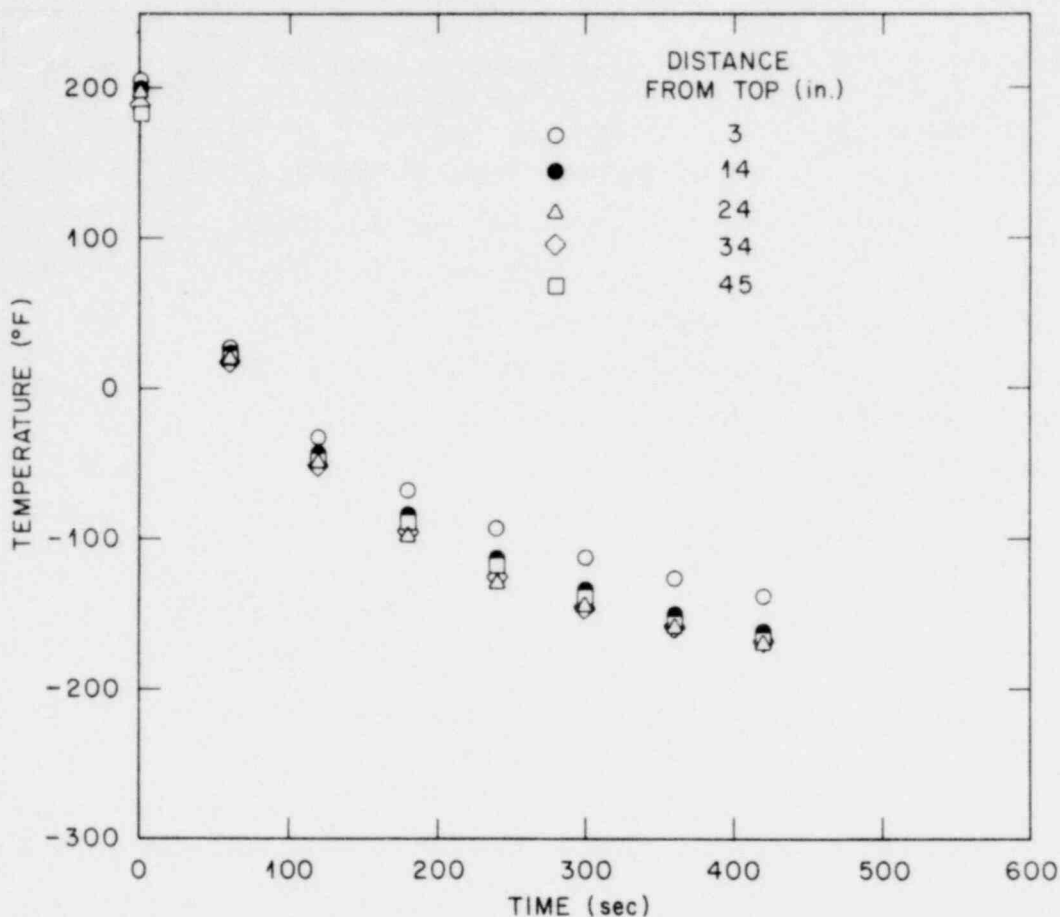
ORNL−DWG 79−6218 ETD

Fig. 6.12. Temperature vs time for points 1.27 mm from the inner surface during LN$_2$-TSE-TH-1.

surface) for the five thimbles in one bank of thermocouple thimbles as a function of time. The upper-thimble temperature lags ~17 K behind the average of those for the other four axial locations, and temperatures at these four locations are grouped within a 6 K range. Part of the 17 K lag is due to the initial 11 K axial gradient. The largest difference circumferentially during the transient was only 8 K.

Figure 6.13 shows a comparison of the surface-temperature transient measured during the experiment with that assumed for the pretest TSE-5 analysis. The measured temperature initially drops off more rapidly than the calculated value but later decreases more slowly. The conclusion is that the measured quench rate will be satisfactory for TSE-5.
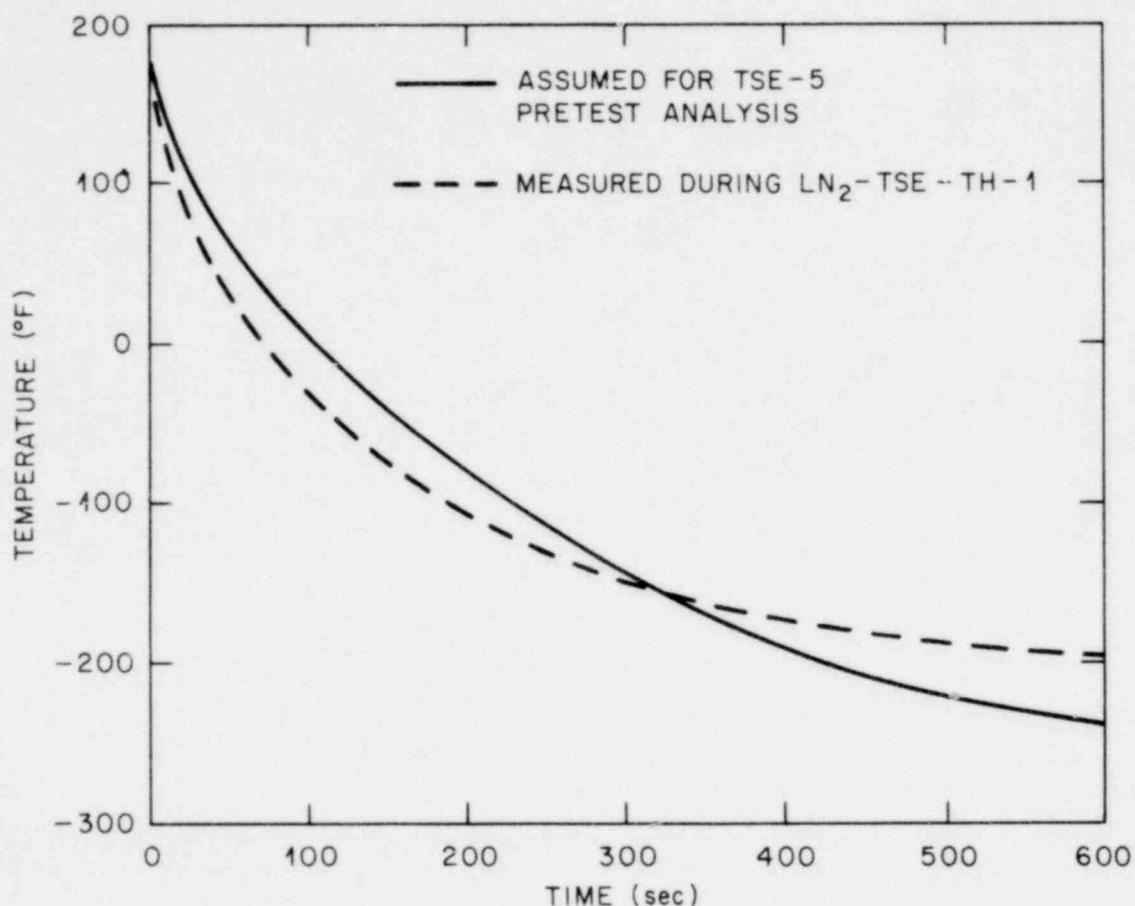
1439 289

ORNL- DWG 79-6219 ETD

Fig. 6.13. Comparison of LN$_2$-TSE-TH-1 and TSE-5 assumed surface-temperature transients.

6.4.3 Second thermal-hydraulic test (LN$_2$-TSE-TH-2)

For this experiment, a higher heat transfer rate was desired so that there would be a greater tendency for vapor binding in the upper portion of the cylinder and thus a greater degree of asymmetry in quenching. This was accomplished by using a more nearly optimum thickness (~0.48 mm) of the rubber cement coating; otherwise, test conditions were the same as before. The experiment was conducted on May 17, 1979.

As shown in Fig. 6.14, the quench rate was indeed greater than before, and, as shown in Fig. 6.15, the degree of axial asymmetry was considerably greater. Again, innermost temperatures at the lower four thermocouple thimble locations were within 6 K; however, the temperature
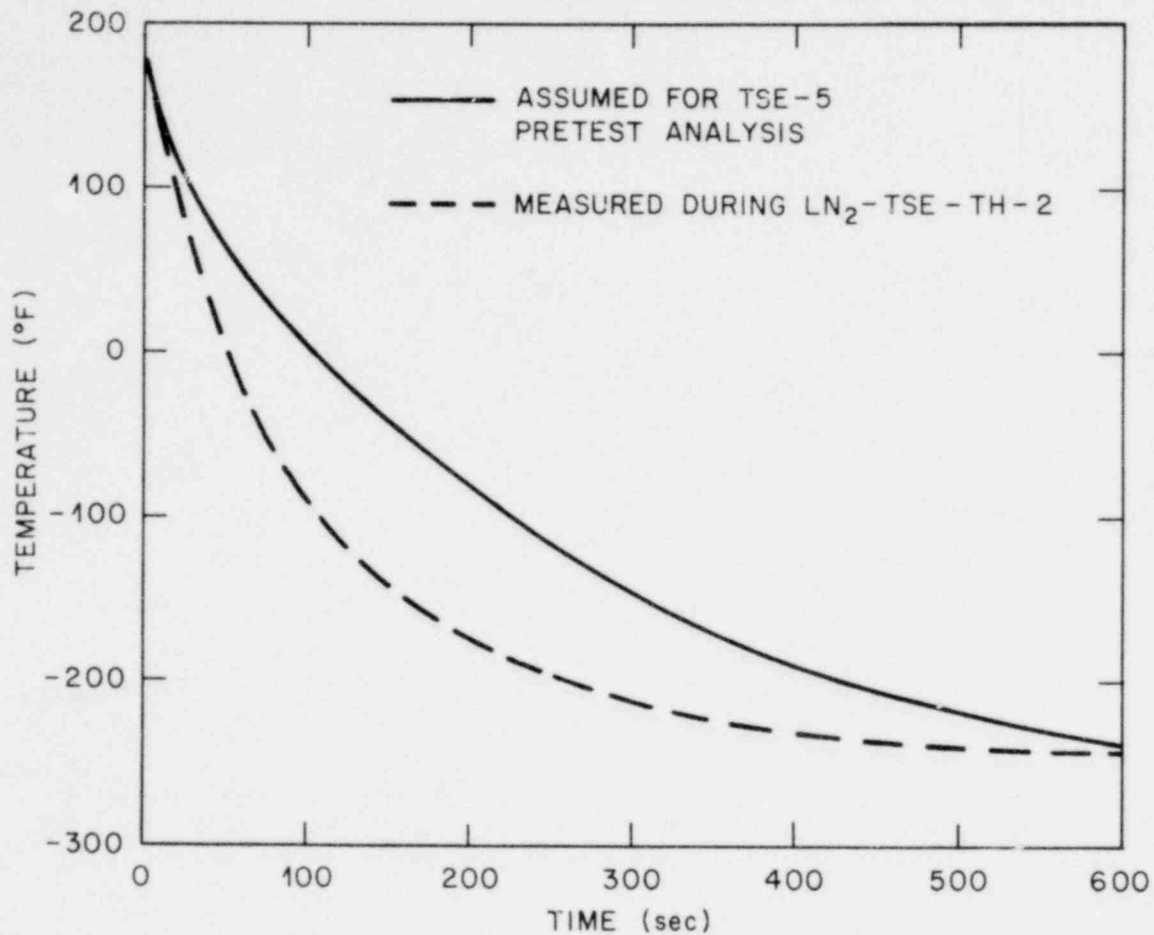
Fig. 6.14. Comparison of LN_2-TSE-TH-2 and TSE-5 assumed surface—temperature transients.

at the upper thimble lagged behind the others by as much as 44 K, even though the initial axial temperature gradient was less than before. These results indicate a rather abrupt change in heat transfer coefficient with increasing vapor fraction. From a heat transfer point of view, a solution to the problem would be to reduce the length of the cylinder. However, to avoid the necessity for a three-dimensional fracture mechanics analysis, the length cannot be reduced. Thus, even though thermal shocks more severe than those required for TSE-5 are attainable, they may not be permissible in future experiments because of excessive axial asymmetry in quenching.
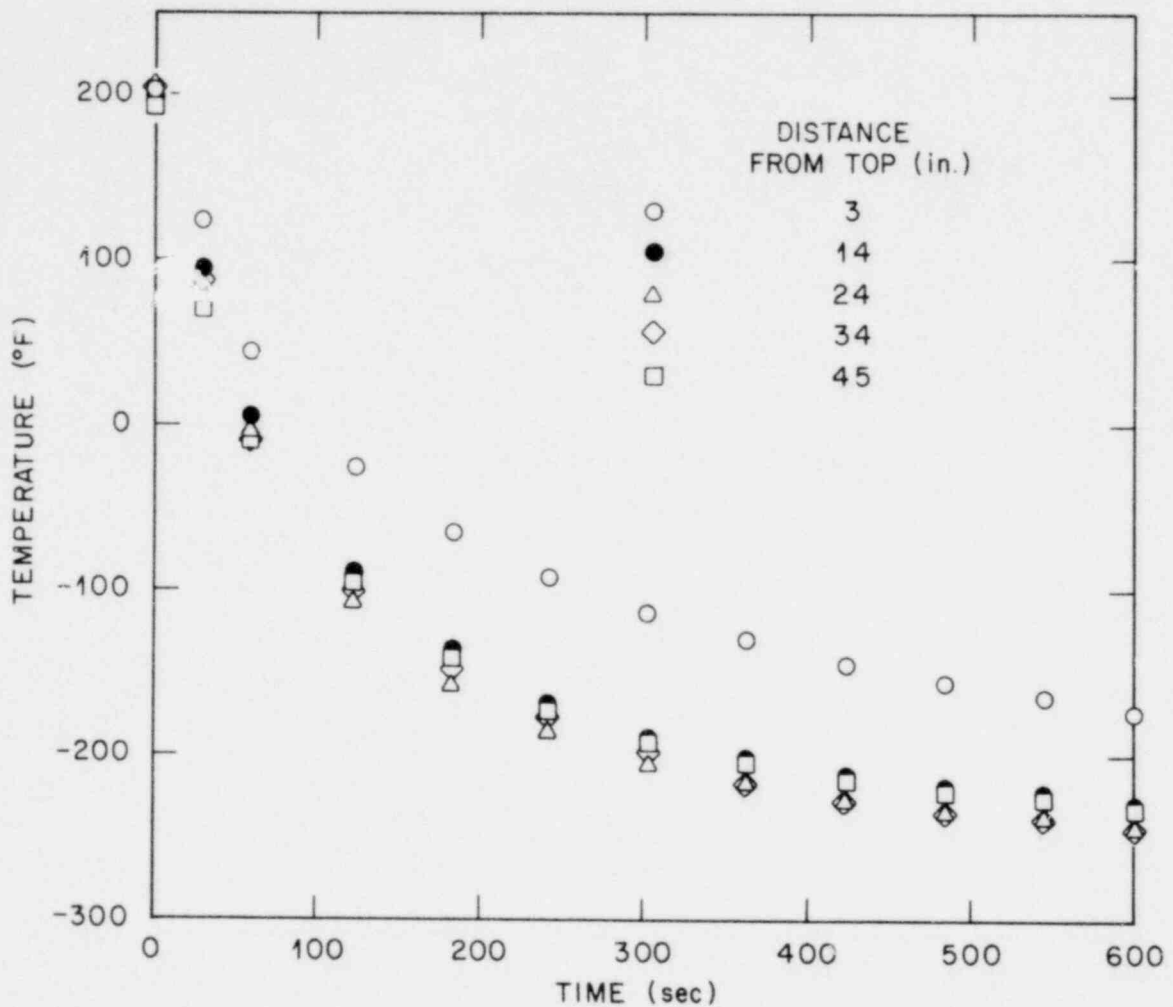
ORNL-DWG 79-6221 FTD

Fig. 6.15. Temperature vs time for points 1.27 mm from the inner surface during LN$_2$-TSE-TH-2.

6.5 TSC-1 Flawing Development

P. P. Holz

Development efforts for achieving a long axial flaw of appropriate depth in TSC-1 by means of the EB-weld technique have been completed. The final test weld was made in the TSC-1 prolongation. Cracking of this weld by means of hydrogen charging was completed, and a typical fracture surface from this weld is shown in Fig. 6.16. Figure 6.17 shows the TSC-1 prolongation in the weld box just prior to the welding

EB—WELD FRACTURE

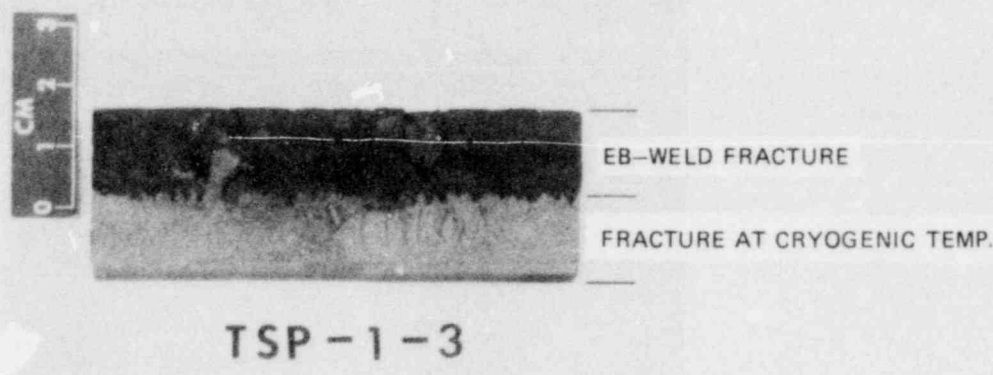FRACTURE AT CRYOGENIC TEMP.

TSP-1-3

Fig. 6.16. EB-weld fracture surface from test weld in TSC-1 prolongation.

ope. tion, and Fig. 6.18 shows the prolongation during hydrogen charging of the EB weld.

Weld parameters for the TSC-1 prolongation EB weld were as follows: 55.2 kV, 218 mA, 60% filament dial setting, focus sharp + 14, and a travel speed of 35 mm/sec.

6.6 Thermal Shock—Temper Study

D. A. Canonico   W. J. Stelzman

We are continuing the evaluation of the effect of tempering temperature on the fracture toughness properties of the SA508 Class 2 steel forgings that will be used in the next series of thermal shock experiments. During this quarter, we completed the testing of CT-oriented 1T CS and determined the tempering temperature for test cylinder TSC-1. The test material was obtained from a prolongation of TSC-1, which was normalized at 927°C for 8 hr, austenitized at 860°C for 9 hr, and quenched in water. Radial segments were removed from the prolongation and were used to investigate the effect of tempering temperature on toughness and tensile properties. Tempering was done for 4 hr at 705, 675, 650, 595, 450, and 370°C. The test results obtained from these materials were presented in previous reports.[14,15]

ORNL PHOTO 7352—79R

CARRIAGE TRACK
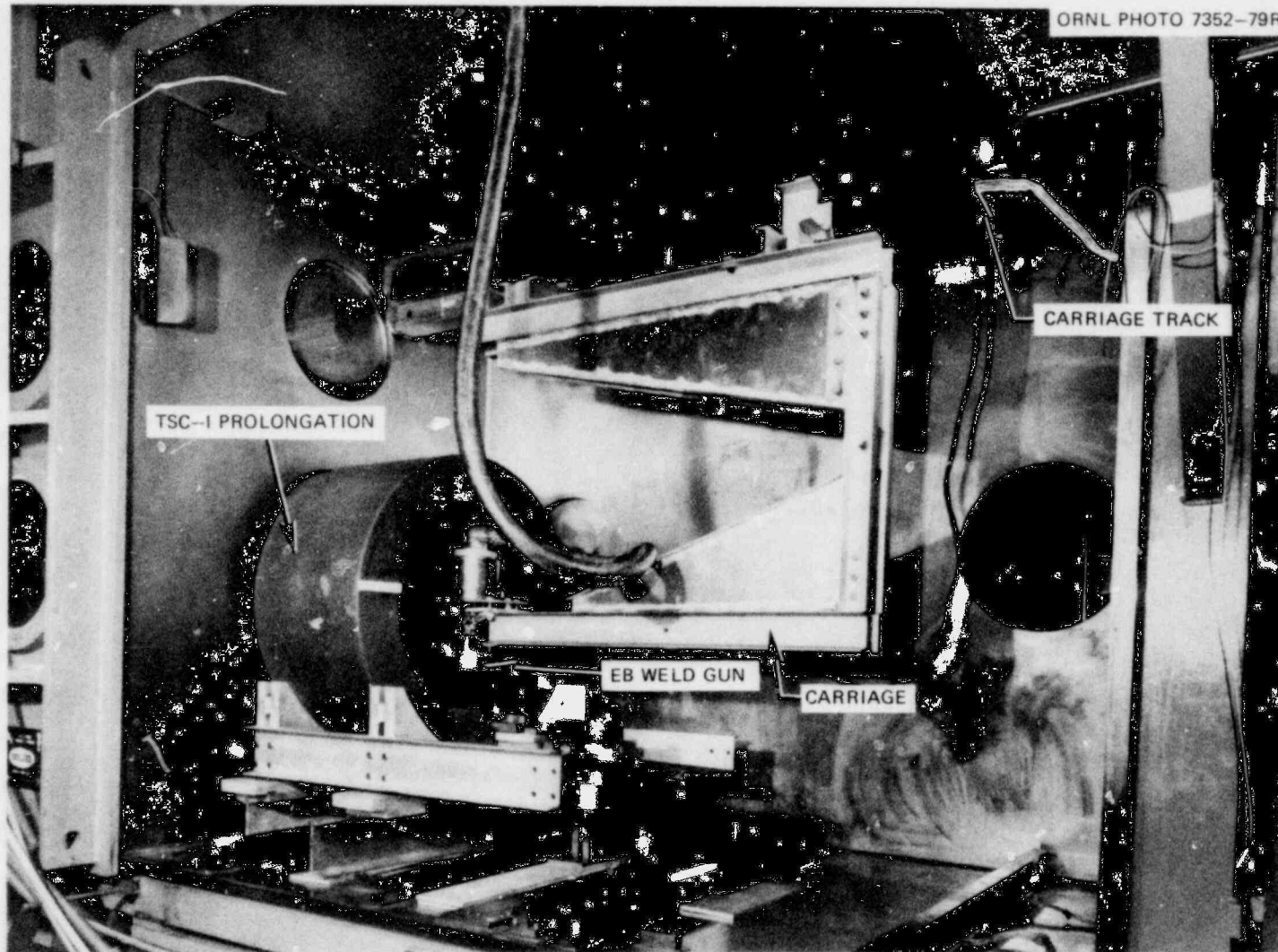
TSC—1 PROLONGATION

EB WELD GUN

CARRIAGE

Fig. 6.17. View of interior of EB-weld box prior to making EB weld in TSC-1 prolongation.

69

1439 294

70

1439 295

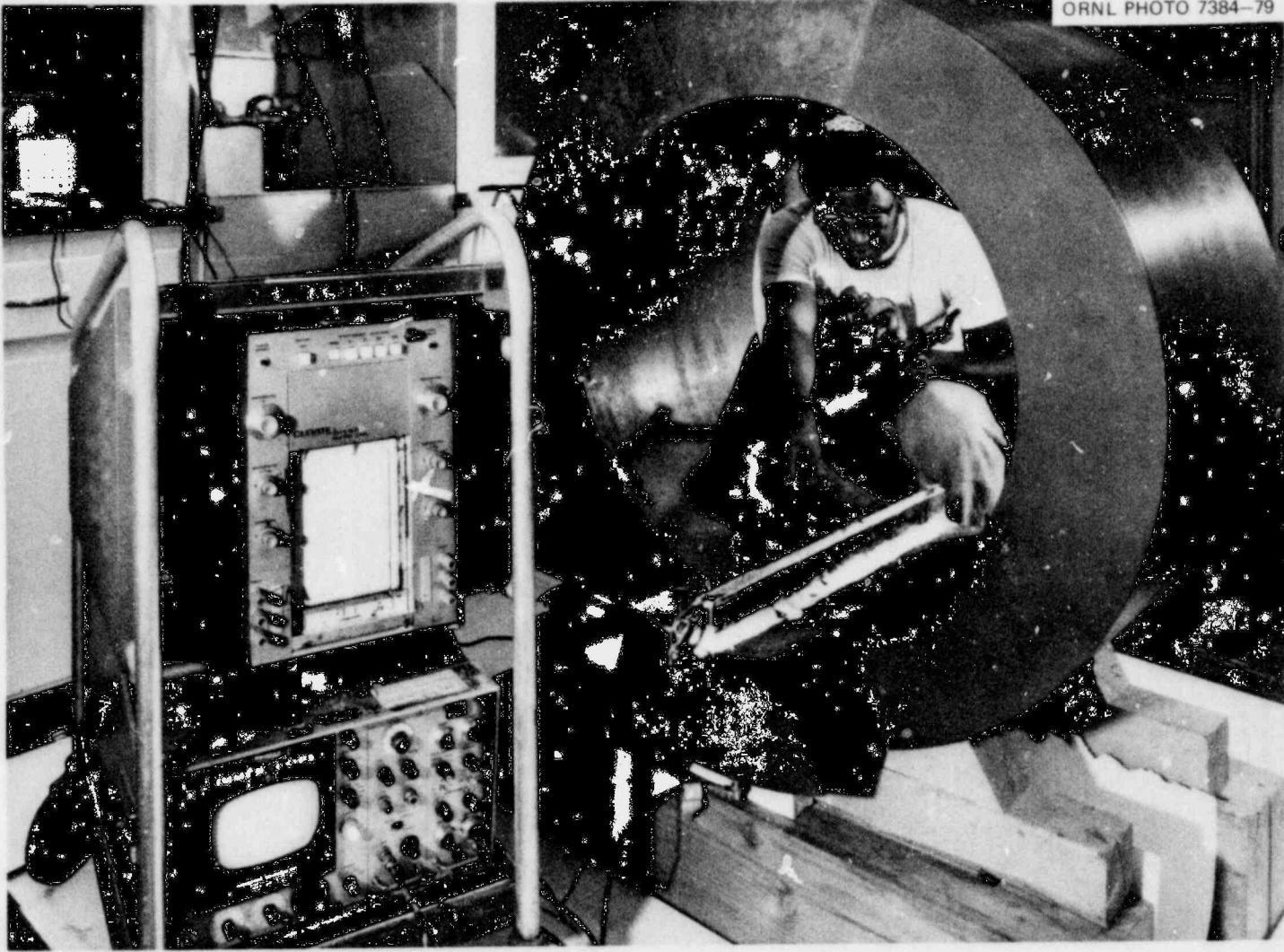Fig. 6.18. Hydrogen charging of EB test weld in TSC-1 prolongation.

The conditions for the thermal shock experiment are based on the K_{Ic} curve shown in Fig. 6.9, which is based on data reported for A533 Grade B Class 1 steel. The fracture toughness results of the 595 and 650°C tempers bracketed the values desired for the test. Therefore, additional radial segments from the TSC-1 prolongation were tempered at 600°C for 4 hr to define more accurately the toughness relative to the desired values. All of the compact specimens were machined adjacent to the inside surface of the prolongation with the fatigue crack tip close to the proposed crack-tip site in the test section. The results from CT-oriented 1T CS are given in Table 6.3 and plotted in Fig. 6.19. Included in Fig. 6.19 are the 595 and 650°C 1T CS results previously reported[15] and the

Table 6.3. Static fracture toughness (K_{Icd}) from 1T compact specimens[a] of quenched prolongation TSC-1 after tempering at 595, 600, and 650°C

Temper[b] temperature [°C (°F)]	Test temperature [°C (°F)]	Static fracture toughness, K_{Icd} [MN·m$^{-3/2}$ (ksi $\sqrt{in.}$)]
595 (1100)	−46 (−50)	39 (36)
	−18 (0)	83 (75)
	−18 (0)	84 (77)
	10 (50)	105 (95)
600 (1110)	−46 (−50)	41 (37)
	−46 (−50)	57 (52)
	−46 (−50)	83 (76)
	−18 (0)	101 (92)
	−18 (0)	66 (60)
	−18 (0)	104 (94)
	−18 (0)	65 (60)
	10 (50)	92 (84)
	10 (50)	67 (61)
	10 (50)	106 (96)
	10 (50)	69 (62)
	10 (50)	160 (145)[c]
	38 (100)	208 (189)[c]
	38 (100)	186 (169)[c]
	38 (100)	98 (89)
	38 (100)	217 (197)[c]
650 (1200)	−46 (−50)	113 (103)
	−18 (0)	119 (109)[c]
	−18 (0)	114 (103)[c]
	10 (50)	162 (148)[c]

[a] CT-oriented.

[b] Tempered for 4 hr, air cooled.

[c] Nonvalid per ASTM E399.

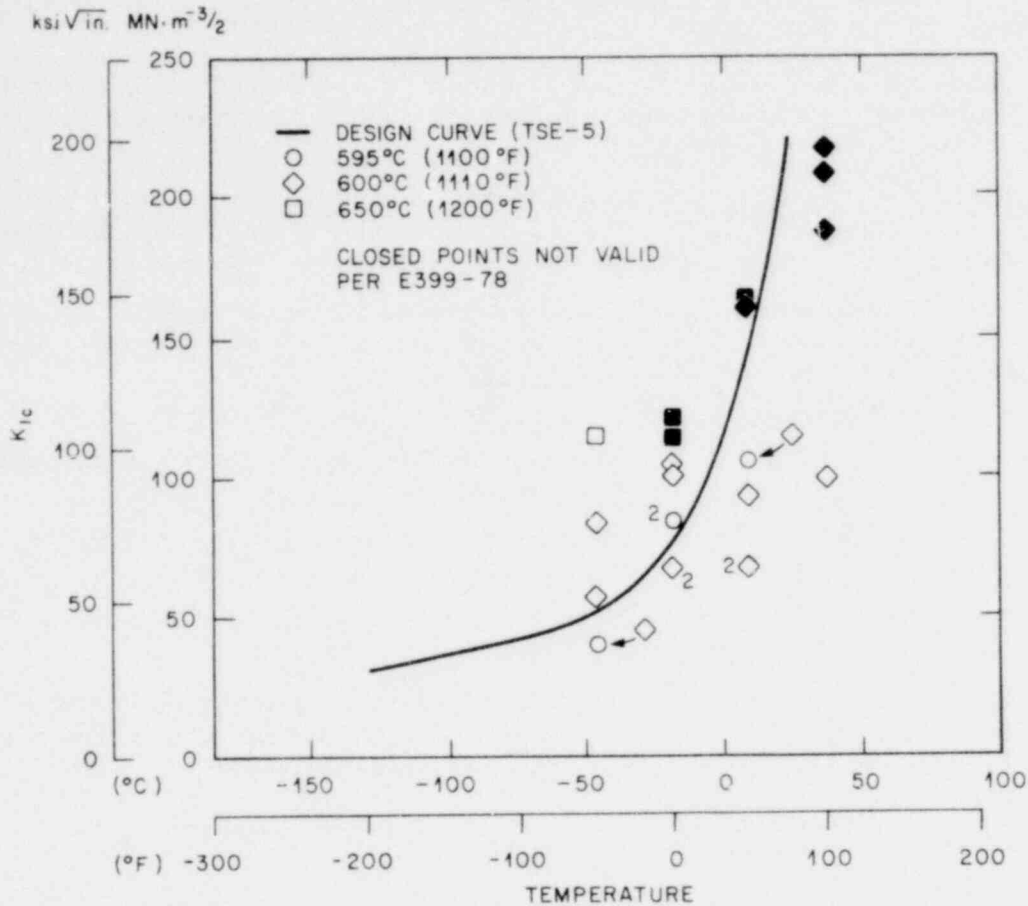1439 296

ORNL-DWG 79-6222 ETD

Fig. 6.19. Effect of temperature on static fracture toughness of quenched TSC-1 prolongation after tempering at 595, 600, and 650°C: CT-oriented 1T CS.

K_{Ic} curve from Fig. 6.9. From these results, the conclusion was that tempering on the TSC-1 material at 610°C for 4 hr followed by an air cool should provide the desired toughness properties.

References

1. R. D. Cheverton, *Pressure Vessel Fracture Studies Pertaining to a PWR-LOCA-ECC Thermal Shock: Experiments TSE-1 and TSE-2*, ORNL/NUREG/ TM-31 (September 1976).

2. R. D. Cheverton and S. E. Bolt, *Pressure Vessel Fracture Studies Pertaining to a PWR-LOCA-ECC Thermal Shock: Experiments TSE-3 and TSE-4 and Update of TSE-1 and TSE-2 Analysis*, ORNL/NUREG-22 (December 1977).

1439 297

3. R. D. Cheverton and S. E. Bolt, "Thermal Shock Investigations," *Heavy-Section Steel Technology Program Quart. Prog. Rep. January—March 1979*, ORNL/NUREG/TM-324, pp. 90—111.

4. J. G. Merkle, *Quarterly Progress Report on Reactor Safety Programs Sponsored by the Division of Reactor Safety Research for July—September 1974*, ORNL/TM-4729, Vol. II, pp. 3—22.

5. R. D. Cheverton and S. K. Iskander, *Application of Static and Dynamic Crack Arrest Theory to Thermal Shock Experiment TSE-4*, ORNL/NUREG-57 (June 1979), Fig. 4, p. 9.

6. R. D. Cheverton, S. K. Iskander, and S. E. Bolt, *Applicability of LEFM to the Analysis of PWR Vessels Under LOCA-ECC Thermal Shock Conditions*, ORNL/NUREG-40 (October 1978).

7. G. D. Whitman, *Heavy-Section Steel Technology Program Quart. Prog. Rep. January—March 1977*, ORNL/NUREG/TM-120, pp. 88—97 (and subsequent quarterly reports through 1979).

8. R. D. Cheverton, *Heavy-Section Steel Technology Program Quart. Prog. Rep. July—September 1978*, ORNL/NUREG/TM-275, pp. 81—82.

9. R. D. Cheverton, *Heavy-Section Steel Technology Program Quart. Prog. Rep. April—June 1977*, ORNL/NUREG/TM-147, pp. 75—77.

10. W. O. Shabbits et al., *Heavy-Section Steel Technology Program Technical Report No. 6 — Heavy-Section Fracture Toughness Properties of A533 Grade B Class 1 Plate and Submerged-Arc Weldment*, WCAP-7414 (December 1969).

11. ASME Boiler and Pressure Vessel Code, Section XI, Appendix A.

12. *Flaw Evaluation Procedures: ASME Section XI*, EPRI NP-719-SR, p. 0—2 (August 1978).

13. R. D. Cheverton, *Heavy-Section Steel Technology Program Quart. Prog. Rep. April—June 1978*, ORNL/NUREG/TM-239, pp. 50—56.

14. W. J. Stelzman and D. A. Canonico, "Thermal Shock—Temper Study," *Heavy-Section Steel Technology Program Quart. Prog. Rep. October—December 1978*, ORNL/NUREG/TM-298, pp. 57—61.

15. W. J. Stelzman and D. A. Canonico, "Thermal Shock—Temper Study," *Heavy-Section Steel Technology Program Quart. Prog. Rep. January—March 1979*, ORNL/NUREG/TM-324, pp. 104—111.

CONVERSION FACTORS[a]

SI unit	English unit	Factor
mm	in.	0.0393701
cm	in.	0.393701
m	ft	3.28084
m/s	ft/s	3.28084
kN	lb_f	224.809
kPa	psi	0.145038
MPa	ksi	0.145038
$MN \cdot m^{-3/2}$ ($MPa \cdot \sqrt{m}$)	ksi $\sqrt{in.}$	0.910048
J	ft-lb	0.737562
K	°F or °R	1.8
kJ/m^2	in.-lb/in.^{2}	5.71015
$W \cdot m^{-2} \cdot K^{-1}$	Btu/hr-ft^2-°F	0.176110
$T(°F) = 1.8 \, T(°C) + 32$		

[a]Multiply SI quantity by given factor to obtain English quantity.

1439 300

Internal Distribution

1.	R. G. Berggren	17.	S. E. Moore
2.	S. E. Bolt	18.	F. R. Mynatt
3.	R. H. Bryan	19.	D. J. Naus
4.	J. W. Bryson	20.	F. H. Neill
5.	D. A. Canonico	21.	J. L. Rich
6.	R. D. Cheverton	22.	G. C. Robinson
7.	J. M. Corum	23.	G. M. Slaughter
8.	W. B. Cottrell	24.	J. E. Smith
9.	W. L. Greenstreet	25.	W. J. Stelzman
10.	R. C. Gwaltney	26.	H. E. Trammell
11.	P. P. Holz	27-42.	G. D. Whitman
12.	S. K. Iskander	43.	Patent Office
13.	K. K. Klindt	44-45.	Central Research Library
14.	Milton Levenson	46.	Document Reference Section
15.	J. G. Merkle	47.	Laboratory Records Department
16.	C. A. Mills	48.	Laboratory Records (RC)

External Distribution

49. C. Z. Serpan, RSR, Nuclear Regulatory Commission, Washington, DC 20555

50. Office of Assistant Manager, Energy Research and Development, DOE, ORO

51-52. Technical Information Center, DOE

53-422. Given distribution as shown in category RF (NTIS — 10)

1439 301